FLAME STABILIZATION BY A PLASMA DRIVEN RADICAL JET IN A HIGH SPEED FLOW

A Thesis
Presented to
The Academic Faculty

by

Woong-Sik Choi

In Partial Fulfillment
of the Requirements for the Degree
Doctor of Philosophy in the
George W. Woodruff School of Mechanical Engineering

Georgia Institute of Technology
May 2009

FLAME STABILIZATION BY A PLASMA DRIVEN RADICAL JET IN A HIGH SPEED FLOW

Approved by:

Dr. Ben T. Zinn, Advisor
George W. Woodruff School of
Mechanical Engineering
Georgia Institute of Technology

Dr. Jeff Jagoda, Co-Advisor
Daniel Guggenheim School of Aerospace
Engineering
Georgia Institute of Technology

Dr. Ari Glezer
George W. Woodruff School of
Mechanical Engineering
Georgia Institute of Technology

Dr. Sheldon Jeter
George W. Woodruff School of
Mechanical Engineering
Georgia Institute of Technology

Dr. Yedida Neumeier
Daniel Guggenheim School of Aerospace
Engineering
Georgia Institute of Technology

Date Approved: 15 May 2009

To my parents and wife,

ACKNOWLEDGEMENTS

I would like to acknowledge the support and help of mentors, friends, and family without whom this thesis would not have been possible.

First of all, I would like to express my sincere appreciation to Co-advisor, Dr. Jeff Jagoda, for his guidance, patience, encouragement and support. I also thank advisor, Dr. Ben T. Zinn, for his support and help. I also thank my thesis reading committee: Dr. Ari Glezer and Dr. Sheldon Jeter for their valuable suggestions and feedbacks on this thesis. I would like to make special thanks to Dr. Yedida Neumeier for serving on my thesis committee and his valuable advice and guidance on my research.

I would like to thank current and old colleagues in Combustion Lab., Jaeyeon, Juhyung, Murgi, Shai, Yongjae, Venkata, Dong-hyuk, Insu, Chiluwata, and research engineer, David Scarboough, for their technical support, valuable discussions and friendship. Especially, thanks to Jaecheol Kim for his help, support and friendship. I also thank my friends in AE and ME departments for their supporting and encouraging me. I never forget their friendship in my life.

My special thanks to my parents and wife, Chowoon Lee for their endless love and support.

The financial support of the NASA GLENN R.C and the U.S. Air Force under the URETI(University Research Education Technology Institute) for Aero Propulsion and Power Technology is gratefully acknowledged.

TABLE OF CONTENTS

LIST OF TABLES

LIST OF FIGURES

NOMENCLATURE

a_T	Tangential strain rate
A	Flame contacting area on the flame detector, or arbitrary constant
A_m	Cross section area of a main combustor
A_{RJG}	Cross section area of a radical jet generator
A_{jet}	Cross section area of a radical jet, $(= A_{RJG})$
c_p	Constant pressure specific heat
d	Distance, dimension of stabilizer, or electrode gap distance
d_g	Electrode gap distance
D_r	Exit diameter of a radical jet generator
D_s	Maximum spark convection distance
Da	Damköhler number, the ratio of characteristic ignition time to the characteristic flow time
E_{min}	Minimum ignition energy, J
$E_{s,max}$	Maximum energy accumulation by the spark discharge in a single flame kernel
h	Plank constant, $6.626\ 075\ 5(40)\cdot 10^{-34}$ J-s/molecule
H	Heaviside step function
$I_{\mathrm{CH}^*,\phi}$	PMT output voltage when CH* chemiluminescent intensity are measured from a radical jet with equivalence ratio, ϕ
$I_{\mathrm{CH}^*,L}$	PMT output voltage when CH* chemiluminescent intensity are measured from a premixed laminar flame with known flame surface
k	Reaction rate coefficient, $AT^b \exp\left(-E_a/R_uT\right)$

ℓ	Turbulent integral length scale
L	Maximum length of the recirculation zone
L_{ig}	Ignition distance
$L_{j,\phi}$	Length of jet with equivalence ratio, ϕ
L_{jet}	Length of radical jet, (= L_j)
M	Momentum flux ratio
MW_{mix}	Molecular weight of mixture
N_{AV}	Avogadro number, 6.022 136 7(36) $\cdot 10^{23}$ molecules/mol
N	Number density, m^{-3}
	Number of sample to detect a flame
	Number of sample to measure a total pressure
p	Pressure
Q_m	Volume flow rate of a main flow
r_u	velocity ratio of outer flow to inner jet
R_g	Electrical resistance between the gap, Ω
R_1	Resistance in a flame detector, Ω
S_d	Flame displacement speed
S_L	Laminar flame speed
T	Temperature
T_{f}	Adiabatic flame temperature
T_m	Main flow temperature
T_{mix}	Radical jet temperature measured at the RJG exit
u'	Turbulent intensity
U	Flow velocity
U_{BO}	Blow off velocity in conventional flame stabilization

U_c	Flow speed at the edge of mixing zone
U_{in}	Inlet velocity in a RJG
U_m	Inlet velocity in a main combustor
U_{max}	Maximum flame stabilization velocity in a radical jet flame stabilization
U_{mc}	Velocity of cold main flow passing beside a radical jet
$U_{RJG,cold}$	Characteristic radical jet velocity calculated using cold flow and RJG diameter, U_{rc}
$U_{RJG,hot}$	Radical jet exit velocity approximately estimated by inlet flow rate and exit temperature, U_{rh}
V_B	Breakdown voltage of electrical discharge
V_{cr}	Critical output voltage from the flame detector to distinguish the presence of the flame
V_{jet}	Radical jet volume
V_0	Applied voltage on the flame detector
V_1	Voltage across the resistor in the flame detector
$[\mathrm{X_i}]$	Molar concentration of species i, mol/cm^3
α	Thermal diffusivity, m^2/s
γ	Ratio of discharge power consumption to the rate of combustion heat release
	Length ratio of burnt gas to the unburned gas mixture
δ	Laminar flame thickness
	Mixing layer thickness
η	Similarity variable, $y/\delta(x)$
κ	PMT output voltage per unit mole of CH*
λ	Taylor microscale

ν	Radiation frequency, Hz
ξ	Flammability determined by the flame detector, the time fraction that the detector senses the flame for a given time period
ρ	Density
σ	Electrical conductivity of a flame, mhos/m
σ_s	R.M.S stretch rate in a turbulent combustion
τ_c	Characteristic chemial time
τ_{ig}	Ignition delay time
τ_s	A single spark duration
τ_f	Characteristic flow time
ϕ	Equivalence ratio
ψ	Flame surface area per unit volume of radical jet
χ_i	Mole fraction of species i

SUMMARY

In current afterburners combustion is stabilized by the high temperature, recirculating region behind bluff body flame holders, such as V-gutters. Blocking the high speed flow with bluff bodies causes a significant pressure drop, and heating the flame holder by the hot combustion product causes a thermal signature, which is a critical problem in a military jet. To reduce these problems, ignition methods using a high frequency (HF) spark discharge, or a radical jet generator (RJG) were developed. The HF discharge ignited and stabilized a flame successfully in a premixed methane-air flow. The electrical power consumption was very small compared to the combustion heat release, as long as the operating velocity was relatively low. However, a theoretical study showed that the ratio of the electrical power consumption to the heat generation by the stabilized flame increases rapidly with increasing flow velocity. For flame stabilization in a high velocity flow, the developed RJG showed much better performance than direct exposure to a plasma. The present study investigated the characteristics of a radical jet produced in a RJG and injected into a main combustor. The limits of flame stabilization by this jet was measured experimentally, and compared to those of bluff body flame holders. The flame holding performance of the radical jet was also experimentally compared to that of a thermal jet. The effect of radicals on flame stabilization was examined using CHEMKIN, and the limit of flame stabilization by the radical jet was estimated for a simple flow configuration using an approximate solution. The results suggest that the reduction of local spontaneous ignition delay time by active species in the radical jet and the longer length of a typical radical jet compared to the dimension of the recirculation zone behind a bluff body increases the maximum velocity at which a flame can be stabilized.

CHAPTER I

INTRODUCTION

1.1 Background

Generally in an aircraft afterburner the flow speed is much higher than the turbulent flame speed. Thus ignition and flame stabilization are achieved by the creating a recirculation zone. Because the residence time of the flow in the recirculation zone is much longer than the chemical time of typical hydrocarbon fuel air mixtures, chemical reactions in that region are almost completed. Therefore, the temperature there is very high. These recirculation zones provide heat to an incoming combustible flow, and generate a continuous ignition source

Recirculation zones are produced by blocking a part of inlet fuel-air mixture streams with bluff bodies, using wall cavities, or injecting secondary jets in different directions to the flow [36, 41, 82, 138]. Among those, bluff body flame holders like V-gutters may be the most widely used flame stabilization systems in the aircraft engines because of their simplicity.

Typically the performance of the flame stabilizer is represented by the maximum velocity at which a flame can be stabilized in a combustor. In a flame stabilized by a bluff bodies, operating flow velocity, i.e., a flame holding performance, can be improved by increasing wake area behind the holder. This results in a longer residence time of unburned fuel-air mixture in a mixing region [47, 138]. Increasing the wake area is achieved by increasing size of the flame holders. However, this also increases a pressure loss across the flame holder, which reduces the efficiency of the combustor [64, 82]. Another practical problem in military jets, is thermal signature that is generated by the hot flame holder.

Since running an afterburner is typically required only for a very short time, the existence of these non removable flame holders reduces the overall engine performance. Reducing this pressure loss and, at the same time, the increasing flame stabilization limits are required in advanced flame holding systems. Recently, flame stabilization by plasma have been studied since these technics are expected to broaden flammability limits without unnecessary total pressure and heat loss. The present study investigates the use of a flame stabilization system based on a plasma and a plasma driven radical jet. Its mechanism of operation and the limitations are discussed.

1.2 Literature reveiw

1.2.1 Flame stabilization by bluff bodies

The mechanism by which a bluff body stabilizes a flame in a high velocity flow have been investigated by many researchers. The flammability limit curves for various fuels, and for various fuel to air ratios, have been measured [34, 37, 77, 130, 132, 136], see Fig. 1. The effects of the recirculation zone lengths [93] and blockage of the stabilizer in a combustor [131] on the flammability limits have been also investigated. Early studies suggested criteria which limit the operating range of the combustor from parametric studies. In the following, several results and suggested theories are introduced.

The study of the chemiluminescence near bluff body flame holder showed that the chemical reaction in a recirculation zone behind the flame holder is completed, and the flame is stabilized in a mixing zone between the recirculating flow. Incoming combustible flow is then ignited by heat transfer from the recirculation zone [41, 136]. Early theories are all essentially based on this physical concepts [76, 106, 136].

Spalding [106] supposed that the flame can be stabilized only when the amount of combustible flowing through the jet per unit time is less than the amount of combustible mixture

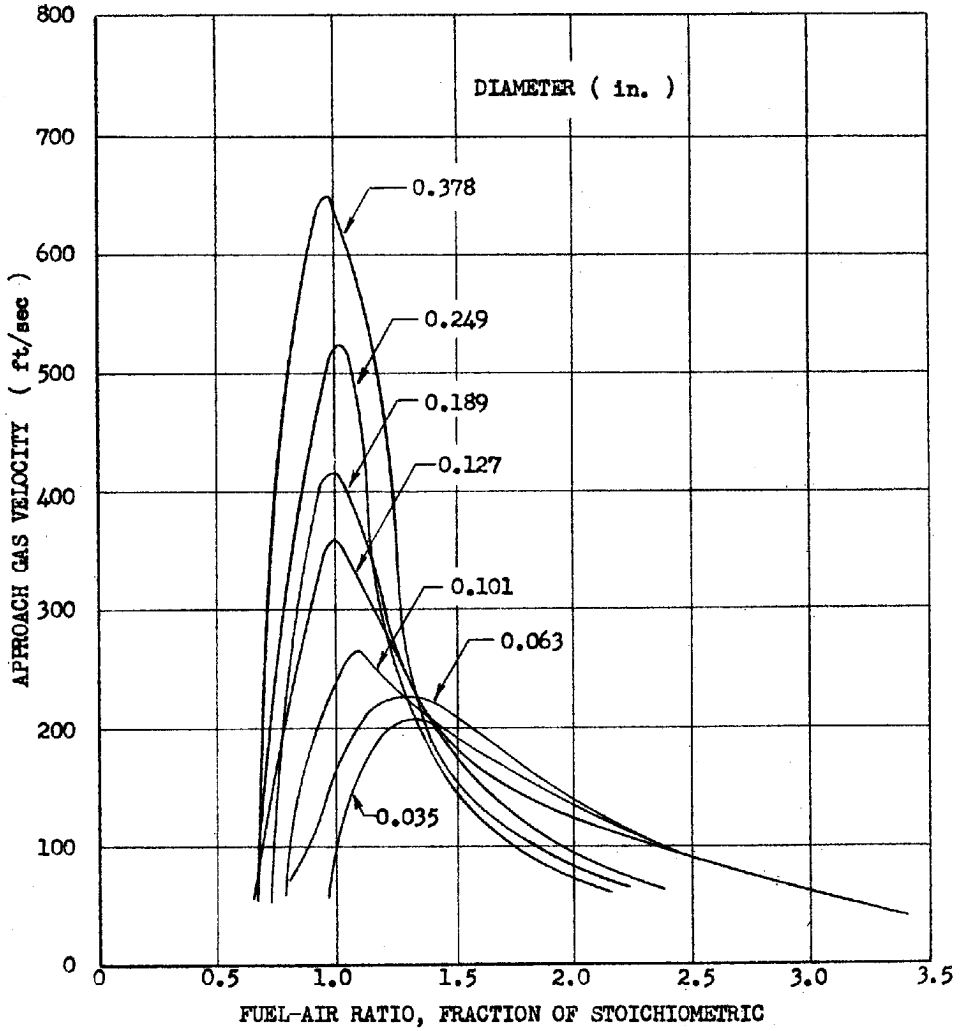

Figure 1: Flammability limit curve of pre-heated gasoline-air flow for cylindrical rod flame holders with various size. Picture reproduced from Zukoski [136].

that can react per unit time. He suggested that the blow off velocity, U_{BO}, is determined by

$$\frac{U_{BO}}{dpS_u{}^2} = \text{const.} \tag{1}$$

where d, p, and S_u are a dimension of the stabilizer, pressure, and the laminar flame speed, respectively.

Similarly, Longwell *et al.* [76] assumed that a homogeneous chemical reactions occurs

in the recirculation zone behind the bluff bodies, i.e., the region was assumed to be a perfectly stirred reactor. They suggested a functional dependency between the parameters, as

$$\frac{\dot{m}}{VP^2} \sim \frac{UD^c}{p} \tag{2}$$

where $\dot{m}$ is the mass flow rate of air entering the reactor with volume V, U is the stream velocity, D is a characteristic dimension of the bluff bodies, c is an empirical exponent, and p is a static pressure.

Zukoski and Marble [136, 137] suggested that the flame is only stabilized when the characteristic flow time of the combustible mixture become comparable to a characteristic time period required for ignition. According to this theory, the flame blow off criterion was represented by

$$\left(\frac{U_c \tau_c}{L}\right)_{BO} = 1. \tag{3}$$

where U_c are flow speed at the edge of the mixing zone, τ_c is a characteristic ignition time and L is the maximum length of the recirculation zone. This criterion represented the flame stabilization limits very simply with two independent parameters, the characteristic chemical time and the recirculation zone length. However, in this case the value of τ_c must be known. Furthermore, because τ_c is a characteristic value, which depends on many chemical parameters, it must be measured experimentally.

All these parametric studies resulted in a correlation among the blow off velocity, dimension of bluff bodies, and chemical reaction rate, which is usually represented by the laminar flame speed. A valuable analytical study was performed by Marble and Adamson [80]. They modeled the flame stabilization by the bluff body flame holders as an ignition occurring in a mixing layer between a hot non-reactive gas jet and a combustible outer flow, and found a ignition distance from start of a mixing layer. Temperature of the inner jet was assumed as slightly lower than the flame temperature of the outer gas mixture, and the ignition distance was determined as the distance from the inner jet nozzle to a location where the first local temperature peak appeared. They found the location of the ignition distance

in a laminar flow. Cheng and Kovitz [24] solved the same problem with different boundary conditions where the velocity profiles was a Blasius profiles at the end of a flat plate of finite length while Marble and Adamson idealized the velocity profiles as a step function. The results are very sensitive to the methods of calculation. Indeed, ignition distances obtained in the latter were smaller than the values reported by the former by a factor of 15. Although the obtained values are highly dependent on the solution used, the underlying physics is very simple. Williams [129] hypothesized that the ignition distance is equal to the product of chemical reaction time and the mean convective velocity, and roughly determined it by

$$L_{ig} = (u_1 + u_2)\rho_1 Y_{F,1}/[2W_F(\nu'_F - \nu''_F)\omega]. \tag{4}$$

where u_1 and u_2 are cold and hot stream velocities, respectively. This equation is further simplfied by assuming, a reaction rate, ω, using a single step, unimolecular reaction from reactant to product. Then Eqn. (4) becomes

$$L_{ig} = \left(\frac{u_1 + u_2}{2}\right)\left(\frac{T_2}{T_1}\right)A^{-1}e^{E_1/R_u T_2}. \tag{5}$$

From the equation above, it appears that the blow off velocity is determined by limiting L_{ig} to the recirculation zone length. Williams showed that this approximate criterion can be reduced to the same correlation as given in Eqn. (1).

1.2.2 Flame stabilization by electrical discharges

Spark discharges have also been used as an effective ignition source in many combustors because of their simplicity and reliability. During ignition by a spark discharge, a spark kernel is initially created. It then expands to a critical size where the rate of heat generation by the combustion reaction is greater than the rate of heat loss. Researchers have focused on the measurement of minimum spark energies and ignition kernel sizes required for successful ignition in various mixture conditions consisting of different fuel types, fuel-air ratios, and flow velocities [8, 63, 70]. They have also developed simple theories to estimate

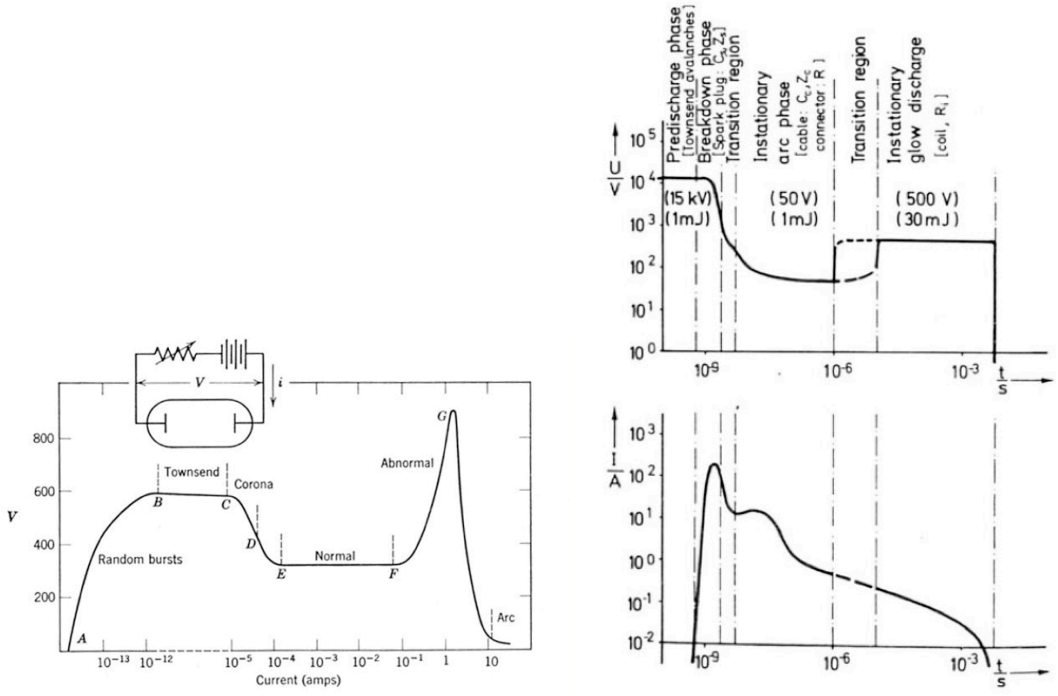

(a) (b)

Figure 2: a) voltage / current properties of corona, glow, and arc discharge in [18], b) schematic diagram of voltage and current variations with time in a spark discharge in [79]

these values [8, 95, 108]. In such theories, a spark kernel is modeled as a pocket of high temperature (>10,000K), homogeneous, non-reacting gas, corresponding to the very high temperatures observed in electrical discharges.

Another important issue concerning spark ignition is the ignition delay time. With ignition by a spark discharge, ignition delays can be reduced by faster ignition kernel growth caused by, for example, high breakdown energy [79] or long discharge duration [8, 99]. The former effect was discovered by Maly and Vogel (1978). They compared the effectiveness of energy transfer from the plasma to the surroundings by measuring ignition delay times for different discharge phases in a spark discharge.

Electrical discharges are commonly divided into three different discharge types according to their voltage-current characteristics: corona (high voltage, low current), arc (low voltage, high current), and glow [19](see Fig. 2(a)). According to Maly and Vogel a spark can be divided into four consecutive phases, the corona phase, the breakdown, the arc phase,

and, finally, the glow phase (see Fig. 2(b)). Among the four discharge phases, it was shown that the phase consisting of the corona and the breakdown resulted in the fastest ignition of a combustible mixture and caused the highest flame kernel propagating velocity when compared to the arc and glow phases [79].

Recently various methods to generate pure corona or breakdown phase discharges were developed. Such discharges were used as igniters to reduce ignition delay time and increase the flammability limit. For example, the performance of corona discharge [73, 74], nanosecond pulsed barrier discharge [6, 14, 15, 16, 84, 85], and RF plasma [26] were investigated relative to the ignition in internal combustion engines and flame stabilization in a combustible channel flow. It was shown that the ignition delay times using corona and the barrier discharges, in which arc formation is prevented by a dielectric cover, was shorter than for flames ignited by a conventional spark discharge with the same energy. It was explained that shorter delay times in the corona ignition are attributed to the wider special distribution caused by their characteristic multi-site discharges and their higher electron energy. However, for the same reason (i.e., multi-channel discharges) their electrical energy is more dispersed and thus, the minimum ignition energy of a corona discharge is higher than that of a spark [73].

1.2.3 Flame stabilization by active radical jets

More recently, plasmas have been used as flame holders under difficult operating conditions, such as combustion in high velocity flows or for mixtures near or beyond the flammability limit [26, 27, 60, 69, 124]. However, if a direct spark is used for ignition, the effect of the plasma is extremely localized and the electrical power required to hold a flame increases with increasing flow velocity. Therefore, a form of plasma jet called a plasma torch or active radical jet was developed. Here the plasma itself is shielded from the main flow and the resulting turbulent mixing between the hot, radical laden, injected plasma jet and

the unburnt main gas flow can increase the volume of ignition and, therefore, the efficiency of the process.

Depending on the role that the discharge plays in the radical generating system, these devices can be further classified. In one, an inert gas carries the radicals produced by a strong discharge such as an arc. In the other, radicals initially generated by a relatively weak discharge are later multiplied by chemical reactions of a combustible feedstock gas. Clearly, the former case requires more electrical energy than the latter.

For several decades, it has been known that combustion generated by spark ignition of rich mixtures in a pre-chamber and then injected into a main chamber, ignites the fuel-air mixture in the latter more effectively than a conventional, direct spark ignition system. Such a "pre-chamber torch" decreases the ignition delay and the combustion duration in a fixed volume chamber by factors of 5-7 and 3-4 respectively [46]. Weinberg (1978) developed a plasma jet igniter that can be installed in an internal combustion engine instead of a conventional spark plug. However, this plasma jet igniter uses relatively strong DC arc discharges to form plasma jets. The same plasma jet system was also tested to support a flame in a combustible gas stream for various feedstock gases ranging from rich hydrocarbon fuel/air mixtures to inert gases. He found that N_2 and H_2 based plasma jets effectively increases the burning rate in the main stream since N atoms produced by arc discharges have a relatively long lifetime in a jet and hydrogen atoms have a high diffusivity [49, 126, 127]. A mechanism by which N or H atoms increase burning velocity was suggested by Shebeko (1982). He suggested that the electric field associated with the discharge could affect the kinetics of combustion and that flame velocity can be changed by accelerating a reaction such as $H + O_2 \rightarrow OH + O$. He suggested that N_2, vibrationally excited by the electric field, collides with O_2 molecules and transfers its energy to vibrationally excite the latter. Vibrationally excited O_2 is more likely to dissociate, which favor the forward reaction. However, Mintoussov et. al.(2004) suggested that discharge induced electronic excitation rather than

vibrational excitation causes the increase in propagating velocity since the rate of the vibrational relaxation process is high compared to the vibrational excitation process of N_2 and O_2 in a typical hydrocarbon fuel-air mixture [85]. Zhang et al. suggested that the radical effect on the combustion process is more significant in much leaner mixtures than under stoichiometric condition since sufficient radicals already existed in the latter [62, 135]. These results suggest that although the detailed mechanism by which the radicals from plasma jets affect the combustion process is not yet fully understood, it appears that the radicals initiate chain reactions that increase the propagating velocity [85].

Besides the effect of active radicals, it has been suggested that turbulence and UV radiation generated by the plasma or the plasma jet affect the combustion process. It is well known that an increase of turbulence intensity can increase burning velocity [2, 3, 90]. Cetegen et al. (1980) showed that a dominant effect of the plasma jet on the enhancement of a combustion process is plasma jet induced turbulence [22]. Turbulent velocity and mixing patterns produced by plasma jets in the ambient gas were studied by Schlieren and shadow method [55, 117]. On the other hand, Orrin et al. (1980) demonstrated that UV radiation, at the energy levels of interest in internal combustion engines, has little effect on flame initiation. They demonstrated this by separating the plasma jet igniter from a methane-air or ethylene-air mixtures by a lithium fluoride window, which transmits ultraviolet radiation more efficiently than any other solid substance [88].

Recently, plasma jet igniters have also been used to stabilize supersonic combustion. It was shown that plasma torch ignition reduced ignition delay times through the effect of additional radicals like O and H. Furthermore, the dependence of the ignition limit on fuel types and plasma jet properties in supersonic flows were investigated [109, 110].

1.3 Overview of present work

The present study deals with flame ignition and stabilization in a high speed combustible mixture flow by a radical jet. Plasma in the form of a high frequency spark discharge generates it by igniting a premixed methane-air mixture with relatively low flowrate and holding its flame. Chapter 2 introduces high frequency spark discharge and the radical jet generator (RJG). This chapter also describes measurement tools used in this study. In chapter 3, the methodology by which the plasma generates a radical rich flame and its operating limits are discussed. Major focus of this research is the role that radicals produced in the plasma supported flame, play in the ignition and flame stabilization of a large combustible flow. This is difficult because effect of radicals and heat are rarely separable. However, in this study these effects were investigated experimentally by comparing flammability and the local level of radicals for a radical jet and hot product jet. Chapter 4 also reports the limits of the flame stabilization by a radical jet, and the characteristic chemical times as calculated using similar techniques as the early studies. Ignition distances are also measured experimentally. In Chapter 5, CHEMKIN is used to understand the role of radicals on the flame stabilization limits, and to approximate the level of radicals in a radical jet. A simple theoretical approach is used to predict the limit of flame stabilization by a radical jet. Finally Chapter 6 focuses on the conclusions and recommendations.

CHAPTER II

FACILITIES AND MEASUREMENT TOOLS

2.1 High frequency spark discharge

A spark discharge between two electrodes occurs when the electric field in the gap is so large that a breakdown can occur. In general, breakdown is defined as the fast formation of a strongly ionized conductive channel between two electrodes caused by an applied electric or electromagnetic field. Thus when a breakdown occurs, a large current can pass through a normally insulating material [11]. The minimum applied voltage at which breakdown occurs is called the "breakdown voltage," V_B. Paschen's Law [89] predicts the breakdown voltage as $V_B = f(p \cdot d)$, where p is the gas pressure and d is the electrode gap distance: I.e., the breakdown voltage between two electrodes of given shapes and material in a given gas is proportional to the gap distance times gas pressure. The breakdown voltages also vary with the type of voltage source [19, 94]. For sparks caused by a DC source in a uniform field, the breakdown voltage in volt is given by the following equation [31, 94]

$$V_B = 1.36 \times 10^{-8} \left(\sqrt{Nd}\right) + 9.96 \times 10^{-20} Nd \tag{6}$$

where N is the number density of molecules per m^3, and d is the electrode gap distance in m. For a breakdown caused by an AC source the following empirical reationship is provided [94]:

$$V_B = 25 + 4.55d \qquad \text{for rod-plane gap} \tag{7}$$

$$V_B = 10 + 5.25d \qquad \text{for rod-rod gap} \tag{8}$$

where V_B is in kV and d, the gap distance, is in cm.

The present study uses 5 to 10 mm electrode gap distances, and, therefore, requires an AC power supply of about 15kV . A low voltage (5 V) square wave output from a function

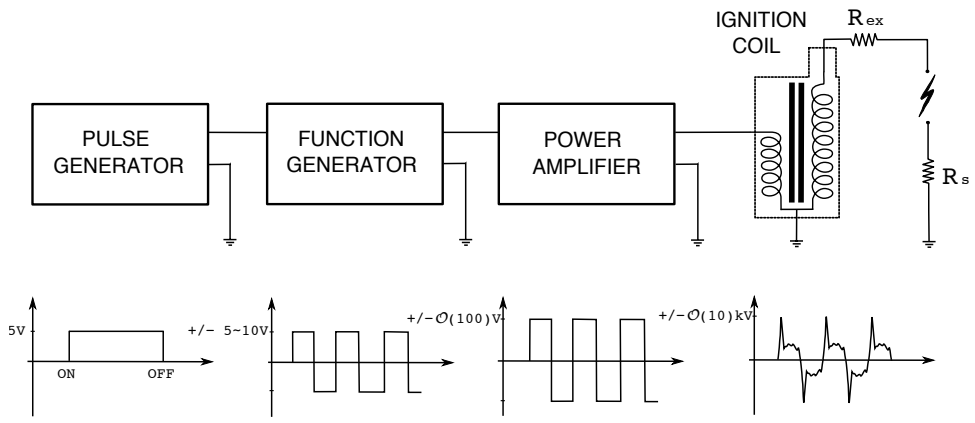

Figure 3: Schematic of the high frequency spark discharge generator set-up

generator (B&K Precision Corporation, Model 4040A) is amplified by a power amplifier (Crown, Macro-Tech 1200) by a factor of 20. This output, in turn, is amplified by a power transformer, an automotive ignition coil with a ratio of secondary to primary winding of about 100, which generates a high voltage that is sufficient in breaking down the gas between two electrodes. The frequency of the driving square wave used in this study was typically 5kHz. Since a pair of sparks with opposite polarities is produced in each cycle, the frequency of the resulting spark discharge is 10 kHz. Discharge voltage and current are measured using a high voltage probe (Tektronix P6015A) and a shunt resistor, respectively. Both values are monitored and recorded by a digital oscilloscope (Tektronix TDS 3012B). These instantaneous values are then multiplied and integrated over the duration of the discharge to determine the nominal power of each spark.

2.2 Radical jet generator (RJG)

A Radical Jet Generator (RJG) was developed to act as a flame holder instead of the conventional bluff body. It is a simple, small pipe combustor, in which a high frequency spark discharge ignites and stabilizes a premixed flame. Figure 4 shows different designs of the RJG. Generally it has an inlet and an outlet for the gas stream. The electrical discharge inside the RJG is generated by one or two thin tungsten or steel electrodes installed in the

combustor. If a single electrode is used, the discharge occurs between the cathode and a random point on the wall of the RJG. The electrode is mounted so that one end is located at the center of the flow, while the other end is connected to the high voltage spark source. The electrode is electrically insulated by a ceramic tube shield to prevent shorting it to the combustor, which is electrically grounded. The ceramic tube thus maintains the location of spark discharge downstream, where the electrode is exposed. A thick plastic tube also can be used for the insulation. In this case, a ceramic honeycomb separates the tube from the combustion zone, see Fig. 4(c). The spark channel, which is continuously re-generated at the rate of 10kHz, between the electrodes or between the center electrode and the combustor wall ignites the premixed combustible gas, and anchors the flame. The interaction between the spark channel in the RJG and the flow will be described in the next chapter.

Each RJG shown in Fig. 4 was designed for specific experimental purposes. The simplest one is the quartz tube RJG in Fig. 4(a). The shape of plasma assisted flame inside the RJG can be observed through the quartz tube, and the results are discussed in Chapter 3. The electrode configuration in the quartz tube RJG was pin-to-pin, so that the spark channel, which supports the flame, was centered in the tube. As a result the structure of the flame was simpler than that in center-to-wall configurations in other RJGs, where the flame location is biased towards one side.

Type (b) was designed to increase flow residence time while keeping the high exhaust jet velocity in the main flow, using a larger diameter combustion chamber and a smaller diameter nozzle. This type of RJG has a step in the wall near the electrode tip. This step could also act as a flame holder for low speed flows. Therefore, the premixed inlet flowrate and fuel-air ratio determine whether the flame is attached at the discharge channel or at the step. If the flame anchors at the step and combustion is completed whthin the RJG, then the number of radicals ejected out of the RJG significantly decreases; in other words, a jet of only hot products is produced. To differentiate it from the radical jet, this hot gas jet will be

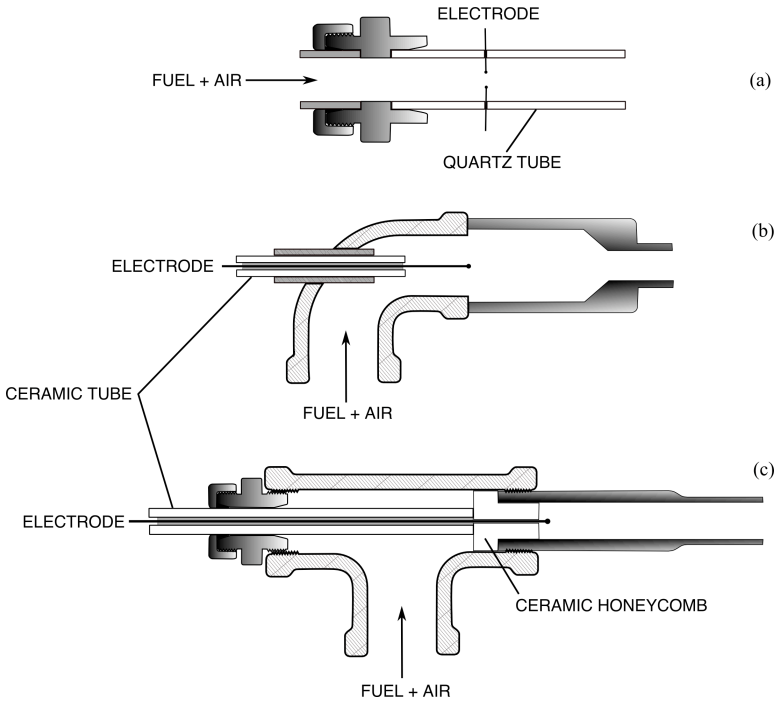

Figure 4: Three types of the radical jet generators, (a) quartz tube RJG with pin to pin electrodes, (b) RJG with a area reduced combustion chamber, (c) RJG with a constant area combustion chamber

referred to as a thermal jet. Ignition by such thermal jets have been investigated in previous studies, which investigated to understand the ignition mechanism in a laminar mixing zone [80], and the mechanism of the flame stabilization by hot recirculating flow [129]. Flame stabilizations in the main flow with both thermal and radical jets was investigated using this RJG and the results are reported in Chapter 4.

The RJG shown in Fig. 4(c) was designed to maximize the generation of radicals. The RJG was generally operated with the plasma in a sufficiently high speed flow, so that a flame could anchor only at the spark channel. Unlike in type (b) there are no steps in the flow stream, either at the inlet or outlet, where a flame could be stabilized without the plasma, This RJG was tested for the ability to stabilize combustion in a main flow in both a cross flow and a coaxial flow configuration. Thus, the majorities of measurements reported here were performed with this type of RJG.

2.3 Main combustor

The ability of the RJG to stabilize a flame was compared to that of a conventional flame holders by measuring the blow off velocity as a function of the fuel-air ratio in the main combustor. For these tests, a simple straight pipe without bluff body flame holders was used as a main combustor. The cross sectional areas of the main combustors are significantly larger than those of RJGs. Two different main combustor configurations were used, see Fig. 5. In one, the radical jet was injected into a main flow perpendicular to, and the other, the jet was injected coaxially with a main flow.

In the cross flow configuration(see Fig. 5, LHS), the RJG was mounted through one side wall of the main combustor, which is a rectangular tube. In order to see inside combustion zone, a quartz window was installed in the wall. The distance between the exit of the RJG and the opposite wall of the main combustor has to be large enough so that the radical jet cannot reach the opposite wall. Otherwise considerable energy of the radical jet may be wasted by heating the main combustor wall. The cross section of the left combustor in Fig. 5 is 3.81 by 3.81 cm (1.5 $\times$ 1.5 inches), which is large enough to prevent wall heating for reasonable main flow velocities. For the coaxial configuration, the RJG was mounted inside the main combustor (see Fig. 5, RHS), which is a circular tube. This required a large diameter that can enclose the RJG. It was connected to the relatively smaller diameter quartz tube via a diameter reduced coupling to achieve the high speed flow where the flame is to be stabilized. Optical access was provided to observe the mixing region between the radical jet and the cold, main flow, and to measure the level of radical through the quartz tube.

2.4 Chemiluminescence measurements

During the combustion processes, chemical reactions generate electronically excited species [39]. Chemiluminescence is the emission of light when such excited molecules return to

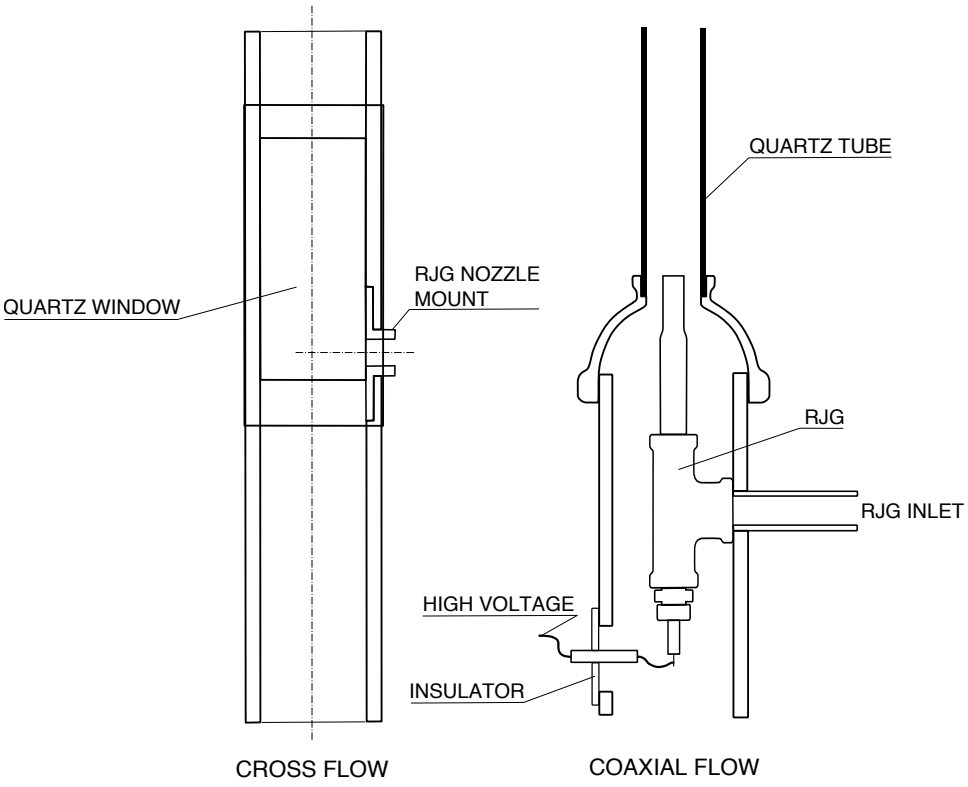

Figure 5: Configuration of main combustors

their ground state. In flames, CH (methylidyne) radicals and OH (hydroxyl) radicals produce strong chemiluminescence intensities. It is well known that the electronically excited species are formed by the reactions [33, 44, 51, 56, 92],

$$\mathrm{O+H+M} \rightarrow \mathrm{OH^{*}+M} \quad (R1)$$

$$\mathrm{CH+O_2} \rightarrow \mathrm{CO+OH^{*}} \quad (R2)$$

$$\mathrm{C_2H+O} \rightarrow \mathrm{CO+CH^{*}} \quad (R3)$$

$$\mathrm{C+H+M} \rightarrow \mathrm{CH^{*}+M} \quad (R4)$$

$$\mathrm{C_2H+O_2} \rightarrow \mathrm{CO_2+CH^{*}} \quad (R5)$$

$$\mathrm{C_2+OH} \rightarrow \mathrm{CO+CH^{*}} \quad (R6)$$

where the asterisk (*) denotes the electrically exited state. Then CH* and OH* may be quenched by collision with third bodies,

$$\mathrm{A^{*}+M} \rightarrow \mathrm{A+M} \quad (9)$$

or emit chemiluminescent light when returning to the ground state,

$$A^* \rightarrow A + h\nu \tag{10}$$

where h is the Plank's constant, 6.626 068 96 $\times 10^{34}\, J \cdot s$ [87] and ν is the frequency of light emitted.

The level of radicals in the exhaust of the RJG may be evaluated by the intensities of the chemiluminescence. The wavelengths corresponding to the OH ($A^2\Sigma^+ - X^2\Pi$) and CH ($A^2\Delta - X^2\Pi$) transition are 309 nm and 431nm, respectively [39, 68].

A photomultiplier and narrow bandpass interference filters were used to measure the relative chemiluminescent intensities. Center wavelengths of the filters are 430 nm and 310 nm with a full width-half maximum of 10nm for both CH(A-X) and OH(A-X) transitions. The field of view of the photomultiplier was wide enough to observe the entire radical jet and the main flame.

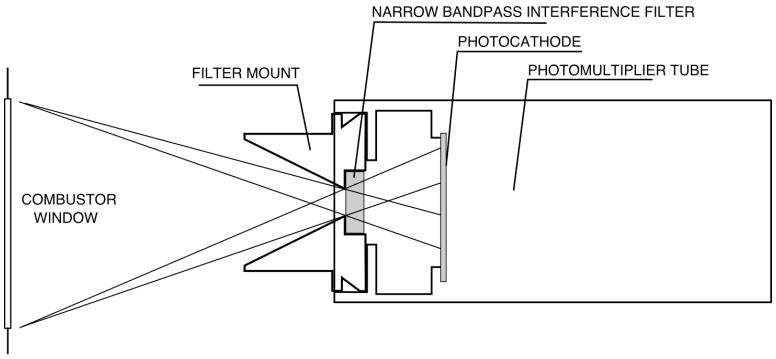

Figure 6: Optical detector set up

For cases with different measurement conditions, such as distance between the radiation source and the PMT or for different cathode voltages, the the resulting data can be related to each other using the relationship,

$$\frac{V_2}{V_1} = \left(\frac{d_1}{d_2}\right)^2 \exp\big(k(V_{c1} - V_{c2})\big). \tag{11}$$

where V and V_c are the PMT output and cathode voltage bias, respectively, and d is a distance from the source to the PMT window. A calibration constant k is obtained by measuring a variation of PMT output voltage against the cathode voltage.

2.5 *Measurement of the flammability limits of the main flow stabilized by a radical jet*

The flammability limits using a conventional bluff body flame holder are readily determined by experiment, and are typically represented by the blow off velocity as a function of the equivalence ratio for a given size flame holder, inlet temperature, and pressure. Although combustion tends to become unstable when operating close to the limits, this regime is usually very narrow. Therefore, these limits are often referred to as "sudden blow off." This is quite different when the flame is stabilized by a RJG. In that case, the limits can not be clearly determined by simple observation because the main flame disappears very gradually as the flow conditions approach the limit. In some cases, combustion becomes unstable over a very wide range of main and radical jet operating conditions because instant flame blow off is followed by a re-ignition of the flow. Therefore, an objective way of sensing the flame and determining blow off had to be developed. The following sections introduce a simple device for detecting the flame, and suggest a method to determine the flammability limits using the device.

2.5.1 Flame detector

One simple way to detect a flame in a combustor, is to demonstrate the existence of ions. It is well known that ions exist in a flame front [29, 38, 120]. These ions are generated by a process called *chemi-ionization*, where charged particles are produced from neutral species during a chemical reaction, such as the reaction [20, 38],

$$\mathrm{CH} + \mathrm{O} \rightarrow \mathrm{CHO}^{*} \rightarrow \mathrm{CHO}^{+} + e^{-}. \qquad \text{(R7)}$$

It is widely accepted that the dominant mechanism of ion generation in a flame is not thermally based because the maximum ion concentration occurs upstream of the region

of maximum temperature, and its magnitude is several order of magnitude above that predicted by thermal equilibrium calculation [20, 25, 38, 67]. Therefore, a flame can be distinguished from hot product and unburned gases by its different ion concentration. It is thus possible for the ion detector to sense a main flame independently of the radical jet, unless it contacts the latter directly.

Well known ion detecting tools are the Langmuir probe [65] and the flame ionization detector (FID) [83]. The former is a device used to measure the current variation versus an applied electric field at the flame, and has been widely used to determine the ion and electron temperatures in plasmas. The latter was developed to measure a degree of ionization in a flame. Although complicated theoretical analyses are required for their original applications, they are not necessary for this study because the probe is only used to determine the presence of ions and, therefore, the existence of a flame in the main combustor.

A schematics of the detector is shown in FIg. 7. The probe consists of two electrodes that are mounted parallel to each other with a 4 mm separation. One is connected in series with a resistor, R_1. The other and R_1 are connected to a DC power supply that provides a constant voltage, V_o. In the unburned gas stream, no current passes through the resistor since the entire circuit is broken by the air gap between two electrodes. If the flame contacts both electrodes, current flows because of the ions and electrons in the flame. The current increases with ion concentration in the flame for a given applied voltage. Its value is readily obtained from the measured potential difference, V_1 across R_1 using Ohm's Law. If we replace the flame in the gap by the resistance R_g, the voltage V_1 and R_g are related as,

$$V_1 = \frac{R_1}{R_g + R_1} V_o. \tag{12}$$

The gap resistance, R_g, consists of the flame resistance and the contact resistance caused by flame quenching near the electrode. The flame resistance depends on the electrical conductivity of a flame, σ, in mhos/m, the flame contact area on the electrode, A, and the gap distance, d_g, in m. If we neglect the contact resistance, the flame resistance can be written as,

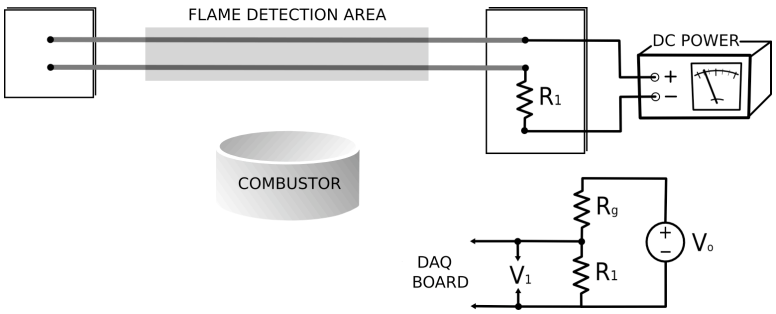

Figure 7: The schematic of a flame detector

$$R_g = \frac{d_g}{\sigma A}. \tag{13}$$

From Eqn. (12) and (13), it is clear that V_1 is proportional to the conductivity and the contact area,

$$V_1 \sim \sigma A. \tag{14}$$

The electrical conductivity of a flame[1] σ is proportional to the ion concentration, which is linearly dependent on the hydrocarbon concentration [13, 25]. The contact area A increases with the bulk size of the flame connecting the electrodes, and may be influenced by the degree of turbulence of the flow. The main role of the device used in this study, is to detect flames to determine the flammability limits, thus, more detail than that described above may not be necessary. However, it should be noted that V_1 increases with the bulk size of the flame, and it may thus be used to represent flame strength. In the rest of this study, V_1 is used as the parameter to determine the flammability limit of a main flame stabilized by the radical jet generator.

2.5.2 Determining the existence of a flame in the main combustor

Main flames stabilized by the RJG show fluctuations near their flammability limit, as mentioned in the introduction to this section. Therefore, fluctuations in the output of the detector must be considered. The frequencies of these fluctuations, which originate from the

[1] Electrical conductivity of inner cone in flame is 7.2×10^{-6} mhos/cm [42].

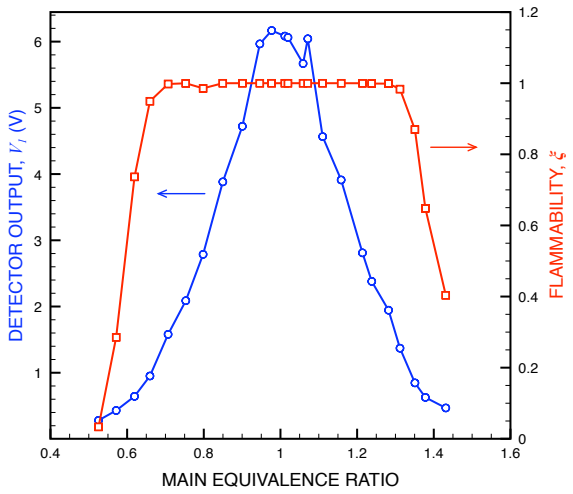

Figure 8: Time average of detector outputs and calculated flammabilities of a main flame determined by Eqn. (16). Main flow velocity is 85 m/s. The fuel-air ratio and the flow rate of the radical jet are given by the stoichiometry and 1.52 liters/sec, respectively.

pulsating radical jet, are typically very low (of the order of 10 Hz for lean and of the order of 100 Hz for rich operation in the RJG).

The detector described here can monitor the instant that the flame blows off of a relatively stable flame, as well as that of a periodically fluctuating flame. Figure 8 shows the typical flame strengths represented by a voltage output of the flame detector. Output values were time averaged. It is, therefore, difficult to distinguish whether the values drop because of the flame fluctuations or because the main flame becomes weaker as one moves away from stoichiometric conditions. In order to solve this problem, an expression for the "flammability" that can distinguish between these two cases is suggested:

$$\xi = \frac{1}{t}\int_0^t H\big(V(\tau) - V_{cr}\big)\mathrm{d}\tau \tag{15}$$

or for discrete voltage samples,

$$\xi = \frac{1}{N}\sum_{i=0}^{N} H\left(V_i - V_{cr}\right) \tag{16}$$

where H is the Heaviside step function, V_1 is the output voltage from the flame detector, and V_{cr} is a critical voltage that distinguishes the presence from the absence of a flame. In practice the signal is positive and somewhat larger than the noise from the HF sparks.

According to Eqn. (16), flammability may be determined by the fraction of time that the detector senses the flame in the main combustor during a given time period. An example is plotted in Fig. 8, in which the detector output voltages are converted to the defined flammability ξ. The reduction in probe output signal due to reduced flame intensity can now be differentiated from the drop in mean signal due to fluctuations in the flame, because ξ remains close to 1 until the onset of the latter.

2.6 Data acquisition system

A computerized data acquisition system monitors and records all output values from the different measurement devices, such as the photomultiplier, the flame detector, and the pressure transducer. Measured data are collected via a National Instruments PCI-6014 board. Labview v7.1 is used for data processing. For all cases scan rate are given at 5kHz, which is high enough to detect any fluctuations of the radical jets and the resulting main flame fluctuation. Measurement devices and the combustors are electrically well grounded, but interference from the strong spark discharge occasionally occurs. In these cases, the noise is removed during post processing of the data.

CHAPTER III

GENERATION OF RADICAL JET BY HIGH FRQUENCY SPARK DISCHARGE

Spark ignition of a combustible gas has been widely studied experimentally and theoretically. Important parameters, such as minimum ignition energy, are well understood for both a quiescent and a flowing gas. However, most early studies dealt with a single discharge as an ignition source. For flame stabilization as well as some ignition applications, a continuous, or very high frequency electrical discharge is required. This chapter describes the characteristics of the high frequency spark discharge in a flowing gas, and how a radical jet can be produced by the HF sparks in a combustible flow.

3.1 Characteristics of high frequency spark discharges in a flowing gas

Swett (1956) observed that discharge voltage and current varies when the length of discharge channel increases by a flow in a DC spark discharging for a long time [108]. Similar voltage and current variations were also observed in the present HF sparks. Because the breakdown voltage strongly depends on the temperature and composition of the gas between electrodes and because those conditions are continuously changing due to a flow, high frequency sparks discharging in a flow field show quite different behavior from those in a quiescent gas. Based on the spark frequency used in this study, the time interval between discharges is less than 100 microsecond. Therefore, each discharge can affect the next one by changing the gas conditions in the discharge path, such as, increasing ionization and temperature. On the other hand, the gas in the path is convected downstream by the flow. While the former reduces the voltage required for breakdown, the latter increases

it. The process that causes this breakdown voltage change is briefly summarized below.

When breakdown occurs, the gas molecules between the electrodes are ionized, which creates a thin plasma channel. Shortly after breakdown, current passing through the channel increases, which increases the temperature of the channel by ohmic heating. The high temperature zone remains in the gap after the source voltage drops to zero. Due to the high electrical conductivity of this region, the next spark prefers to follow the path of the previous discharge, and the breakdown voltage along that path is much lower than that in air under normal conditions. On the other hand, this high temperature "preionized" region moves downstream with the flow, which results in the spark channel being curved (A slightly curved spark channel can be observed, even under quiescent conditions due to buoyancy). As the region moves further downstream, the spark channel length and the corresponding electrical resistance of the channel increase, which leads to a higher required spark power for breakdown. Eventually the resistance along the preconditioned channel becomes greater than that in pure gas along the shortest path between the electrodes. The spark then returns to the shortest path and the process repeats itself, see Fig. 9. This behavior will be referred to simply as spark convection.

Figure 9 shows the variation of the breakdown voltages of the HF sparks for various flow velocities. Three different shapes of sparks were observed over a wide range of flow velocities. A stationary spark channel appears at relatively low flow velocities ($U < 2$ m/s), including under quiescent condition. At higher flow velocities, a stationary spark channel cannot exist. For a velocity range of $2 < U < 10$ m/s, a sawtooth shaped voltage variation with time is observed due to repeated spark convection downstream (see Fig. 9 d-f). For much higher velocity flows ($U > 10$ m/s), the plasma region created by the previous discharge does not seem to affect the following discharge since any ionization that has been created is washed too far downstream by the flow. In this velocity range, only short length sparks within the gap are observed, and the measured breakdown voltage is matched according to the estimates calculated using Eqn. (8). The color of the spark channel is also

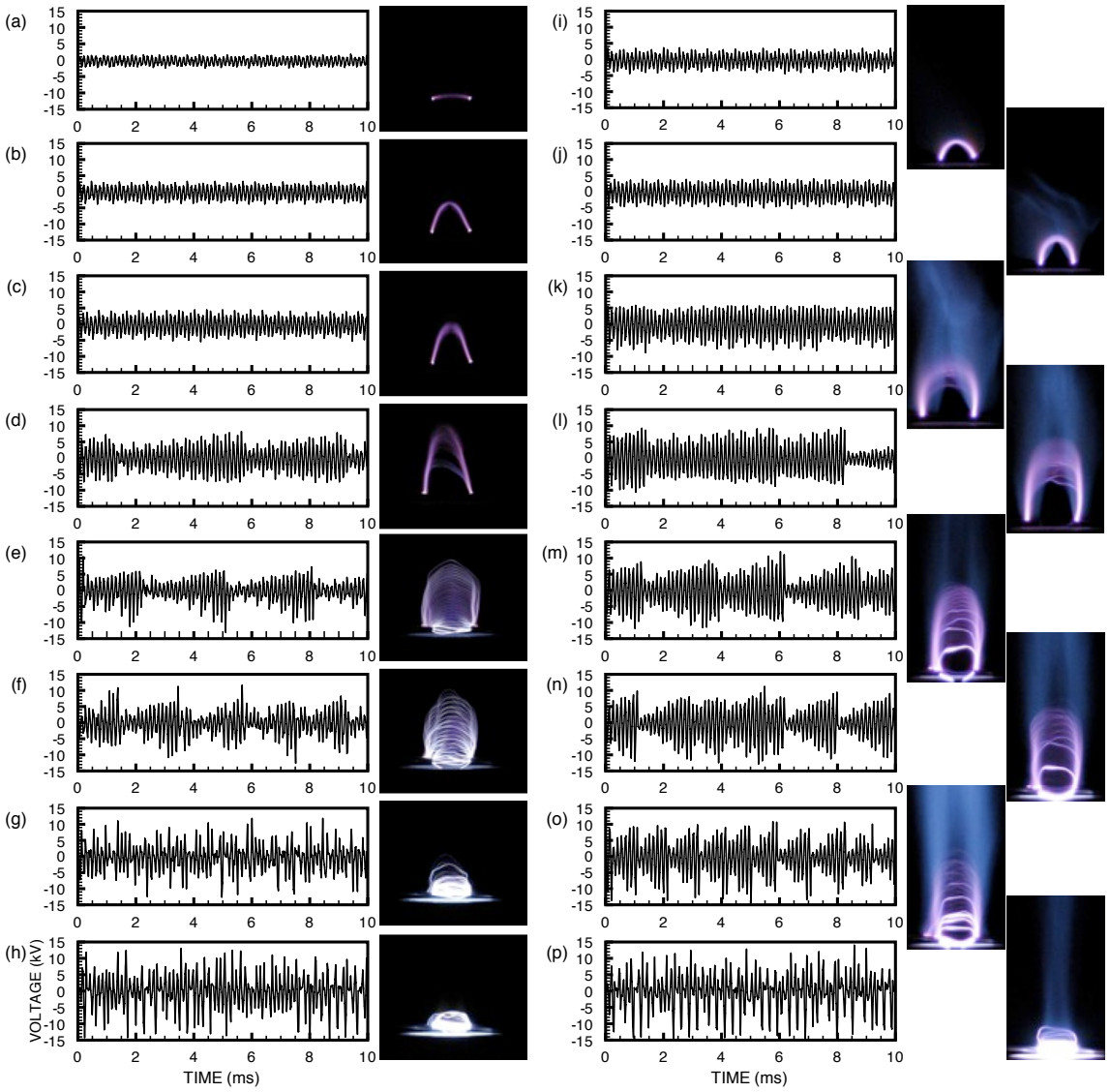

Figure 9: Spark voltage variation and corresponding shapes of high frequency spark discharges between two pin electrodes in an air flow [left] and in CH_4-Air flow [right]; flow velocities: (a)-0, (b),(i)-0.87, (c),(j)-1.31, (d),(k)-2.65, (e),(l)-4.57, (f),(m)-9.48, (g),(n)-10.06, (h),(o)-16.21, (p)-27.8 m/s

different for the different cases. Bright white sparks are observed in the fast flow whereas thick pink and brown colored spark channels are seen in the low velocity case. The sparks in the rapid flow are also very noisy.

3.2 Role of high frequency spark discharges in a combustible flow

3.2.1 Flame stabilization and radical production

Among the three different flow conditions, the second one is suitable to generate a radical jet. If the flow velocity is very low, the spark discharge is not required to stabilize a flame; the flame can anchor at the step inside the RJG. At very high flow rates, a flame can be observed, but its strength is so weak that the resulting radical jet does not generally hold flame in the main combustor.

To understand the process that generates a radical jet inside the RJG more high speed images were taken in the quartz tube RJG (see Fig. 4-a) using a high speed camera(Kodak Ektapro with image intensifier). To determine the mechanism by which the HF spark discharges stabilize the flame in the RJG the inlet was replaced by a duct carrying an atmospheric premixed methane and air mixture. The HF spark discharge was then turned on and a series of images were recorded with a high speed camera at a rate of 2000 frames per second. Because of the weak light intensity of a flame and the limited intensity gain and resolution provided by the camera, the frame speed was not sufficient to freeze the individual discharges. However, it was fast enough to show the instant flame shape and its variation with time.

As in the pure air flow, the discharge channels convect downstream until a short discharge is recreated. In Fig. 10, the short discharge is shown in red in contrast to the otherwise gray scale images. This may be due to the limited dynamic range of the image processing device. Interestingly, the discharge never occurred in a totally straight path between the two electrodes. This may have been because a flame was anchored at the end of electrodes.

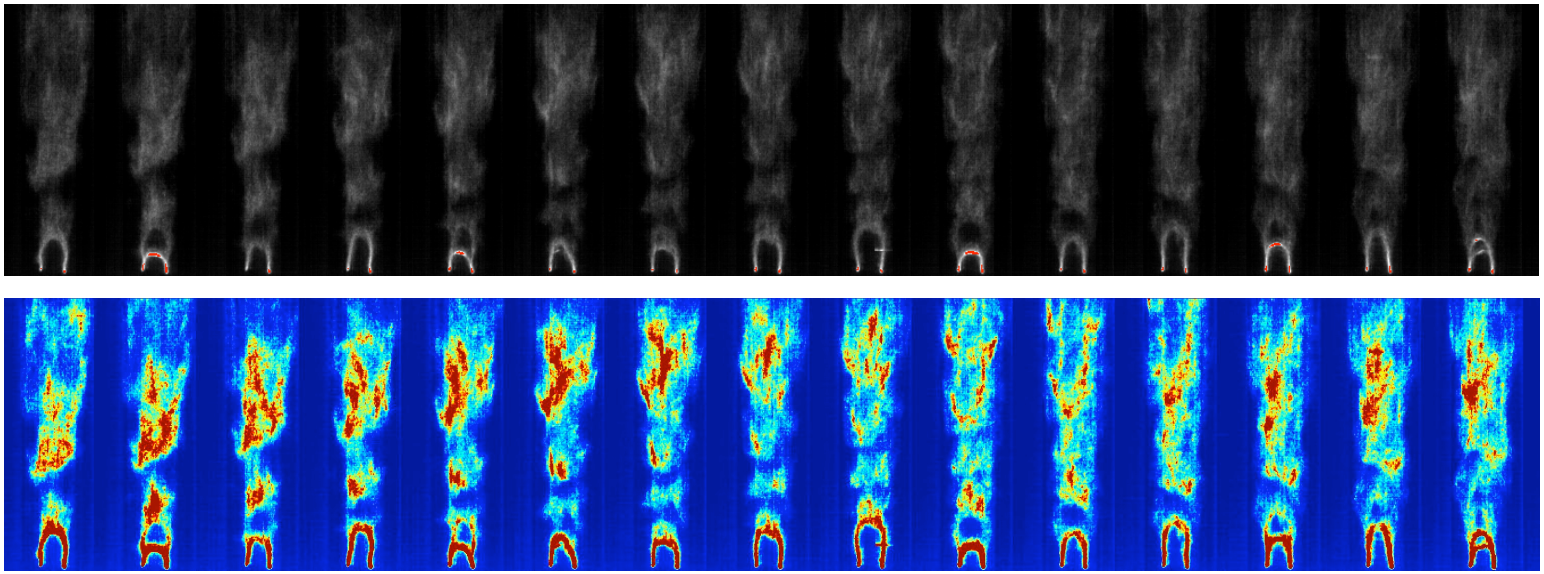

Figure 10: High speed images of unburned gas pocket generated in the quartz tube RJG. A time interval between images is 0.5ms.

Because of the very short spark intervals and the high electrode temperature, the flame did not extinguish between sparks.

The images in Fig. 10 show a periodic sequence of dark regions. When the discharge channel lengthened by the flow suddenly breaks and reforms along the shorter path it generates a new flame kernel, and a small amount of unburned mixture is trapped between the surrounding flame zones. The unburned gas mixture then moves downstream with the overall flow velocity and gradually disappears as the surrounding flame propagates through the mixture. As a result, the combustible mixture is fully burnt some distance downstream of the discharge. At the bottom of Fig. 10, false colors were added to the original gray scale images in order to highlight changes in light intensity. It is clearly seen that the majority of fuel burns downstream, where the unburned gas pockets have disappeared. Thus, this process provides a plentiful source of radicals at the location where the main flame is stabilized. The generation of the unburned gas pockets surrounded by the propagating flame is a unique feature of a flame stabilized by a HF spark discharge. This distinguishes it from a thermal jet, which can be generated by a flame anchored at a flame holder.

Ignition and flame stabilization performance by both kinds of jets were compared and the results are presented in Chapter 4. Before this comparison, the dependence of the flammability limits in the radical jet generator on the HF spark discharge will be discussed.

3.2.2 Flammability limits

The radical jet is generated by the partial combustion process, which is initiated by a high frequency spark discharge. In the last section, it was shown that an unburned combustible mixture was transported by the flow while being enclosed by a surrounding flame. The ignition and flame propagation in the RJG, including the depletion of the unburned gas pocket, depends on the flow velocity, the fuel-air ratio, and the spark power. Section 3.1 briefly described the dependence of the operational limits of the RJG on the inlet velocity

for a given discharge power. In this section, the results of the experimental investigation of the dependence of the operating limits of the RJG on flow velocity, fuel air ratio and discharge power are separated.

The lean flammability limit of premixed propane-air mixture in the RJG was measured over a range of relatively low flow velocities in the straight quartz tube RJG shown in Fig. 4-(a). The lean limits are presented in Fig. 11, and compared to the limits observed when the flame was stabilized on the step inside the RJG without the assistance of the spark discharge. Figure 12 shows results obtained when measurements were repeated using methane as a fuel. Here the measurements were extended to include the rich limit and carried out at higher flow velocities. According to the plot in Fig. 11, a lean premixed propane-air flame could be stabilized by the high frequency spark discharge at an equivalence ratio as low as 0.44 when the cold inlet flow velocity was about 0.75 m/s. The lean flammability limit gradually increased with increasing flow velocity. Similarly, the flammable range of equivalence ratios for premixed methane-air combustion became narrower as the flow velocity was increased, see Fig. 12. The reduction of the range of equivalence ratio over which

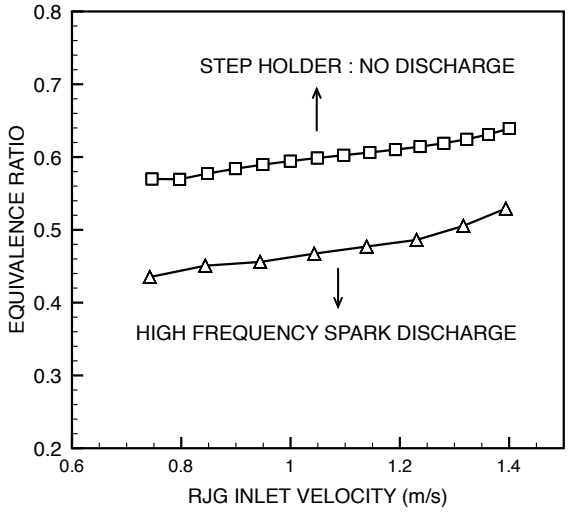

Figure 11: Lean flammability limit by a HF spark discharge in a quartz tube RJG for premixed propane and air flow

the flow is flammable with increasing inlet velocity may result from the limited discharge

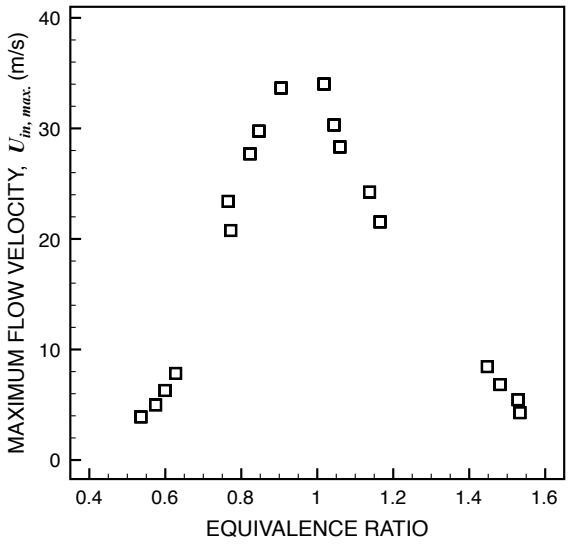

Figure 12: Fammability limit by a HF spark discharge in a quartz tube RJG for premixed methane and air flow

energy available. When the HF sparks ignite a combustible flow, the discharge energies of a series of sparks are added to the same flame kernel, until a new "short channel" is formed. The minimum discharge energy sufficient to ignite a flowing methane-air mixture in a RJG was estimated by measuring the minimum number of discharges necessary to form a single kernel. In this test, a pulse generator was used to control the number of HF discharges provided to the flow by varying the generator's pulse width. In each test the number of pulses was gradually decreased until the mixture failed to ignite. Because there is some inherent variability in the spark even for a given input power and pulse width, tests were repeated. The minimum pulse width was determined when the 80 ($\pm$10)% of ignition attempts failed. Successfully ignition was determined using a PMT mounted far downstream and fitted with an OH* emission bandpass filter. The minimum discharge energy for ignition was determined from the measured minimum pulse width (i.e., minimum number of sparks) using a previously obtained calibration curve.

The minimum discharge energies for ignition for two different inlet velocities are presented as a function of the equivalence ratio in Fig. 13. In the figure, although each series of data is represented by a single velocity, flow velocities varied slightly with inlet equivalence

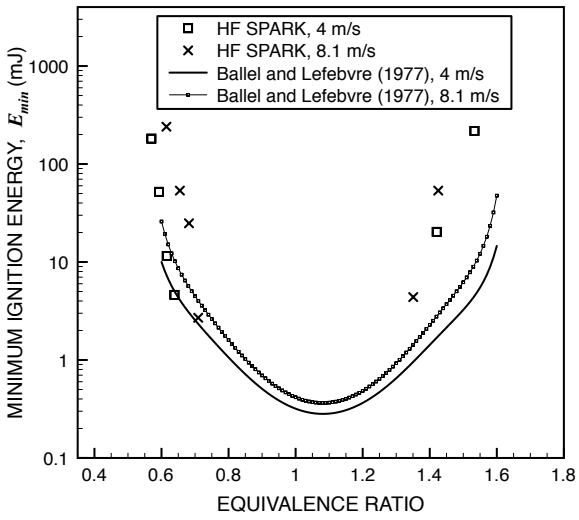

Figure 13: Minimum discharge energy to ignite a flame by high frequency sparks in a quartz tube RJG

ratios for each of the two cases because the equivalence ratio was changed by changing the fuel flow rate while keeping the air flow rate fixed. The deviations of inlet flow velocities over the range of equivalence ratios, based on that of the stoichoimetric mixture, were less than 6%. This is negligible compared to the difference in velocities between two cases, 4 and 8.1 m/s at stoichiometric conditions.

The results show that the required minimum ignition energy E_{min} sharply increased for very lean and rich mixtures. No data are reported near stoichiometric conditions because the number of spark for ignition in those cases was too small to produce by the system used in this study and, thus, repeatable data were not obtained. In those cases, the first strong discharge in a series was often sufficient to ignite flame. E_{min} also increased with increasing flow velocity. This effect in mainly due to changes in turbulence intensity [8, 9, 70, 79, 114]. In an ignition process of turbulent flow, turbulence increases both the burning velocity and the rate of heat loss to the surrounding gas. E_{min} tends to increase because of the former while it tends to decrease because of the latter. Results by Ballel and Lefebvre [9] suggest that the net effect is an increase of E_{min} with turbulent intensity. The same authors suggest

that the minimum ignition energy E_{min} in a flowing gas is given by the equation,

$$E_{min} = c_p \rho \Delta T \left[\frac{10\alpha}{(S_L - 0.16u')} \right]^3 \tag{17}$$

where α is thermal diffusivity and u' is a turbulence intensity. The minimum ignition energies in premixed methane/air flow at atmospheric pressure evaluated using Eqn. (17) are compared with experimentally obtained results in Fig. 13. The calculation of E_{min} using Eqn. (17) requires the laminar flame speed S_L and the turbulent intensity u' be known. For laminar flame speeds in methane-air, experimental data in Ref. [5] were used and the turbulent intensity was approximated by,

$$\frac{u'}{U} = 0.168 Re^{-0.119} \quad \text{for} \quad 3 \times 10^4 < Re < 7 \times 10^5 \tag{18}$$

where U is the mean center line axial velocity. This relation provides the radial turbulent velocity at the half radius of a pipe [1]. The calculated values are somewhat lower than the measured results. This difference may arise because the E_{min} data, which were used to derive Eqn. (17), were obtained by adjusting the voltage and current of a *single* discharge until the onset of ignition. In that case, the discharge duration was typically very short, and thus, the electrical discharge could be assumed to be an instantaneous energy source. However, for high frequency spark discharges used in this study, energy is deposited into the flame kernel over a relatively long period of time. Therefore, heat losses to the surrounding mixture may be larger than in the case of ignition by a single, strong spark. Furthermore, E_{min} in Eqn. (17), is inversely proportional to $(S_L - 0.16u')^3$, and thus, is very sensitive to small discrepancies in the value of S_L, or of u'. Indeed, the laminar flame speed data used in Eqn. (17) are slightly higher than those reported by other authors, especially under very lean and very rich conditions.

The minimum electrical power required to stabilize a flame in a flow of given velocity is of practical importance for the RJG. That value may be obtained from the method following. The successful ignition in the RJG occurs only when the total spark energy deposit is larger than the minimum ignition energy in the flow condition, and the total spark energy

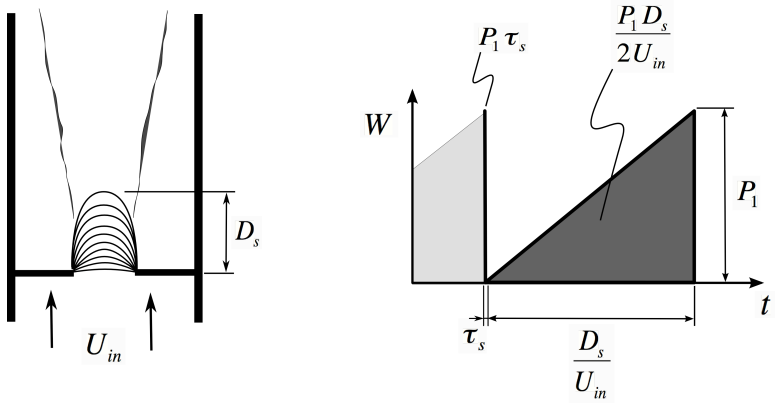

Figure 14: Simplified high frequency spark discharge energy versus time.

deposit into a single flame kernel is limited by the flow speed due to spark convection. The maximum velocity, $U_{\text{in,max}}$, at which the flow can be ignited by the HF sparks, is determined from the these relations, and the electrical power that provides the amount of energy enough to ignite a single flame kernel is also calculated. Based on this concept, a simple model was developed. Here the discharge was assumed to consist of a single, strong spark followed by a series of sparks with linearly increasing power (see Fig. 14). The electrical power of the first discharge P_1 was obtained by measuring the average power during a single discharge duration τ_s. The power of the following discharges cannot exceed that of the first one. If it is assumed that the maximum spark convection distance, D_s, is constant and is obtained from pictures in Fig. 9, and that the spark convection duration was limited to D_s/U_{in}, then the maximum total energy accumulated in the single flame kernel can be expressed by,

$$E_{s,max.} = P_1 \left(\frac{D_s}{2\,U_{in}} \right). \tag{19}$$

Furthermore, since $E_{s,max} \geq E_{min}$ must be satisfied for a successful ignition, the maximum velocity for ignition is given by,

$$U_{in} \leq \frac{P_1 D_s}{2E_{min}}. \tag{20}$$

The calculated maximum values of U_{in} were plotted in Fig. 15. Although the model is relatively simple, the result obtained were quite close to the experimental values.

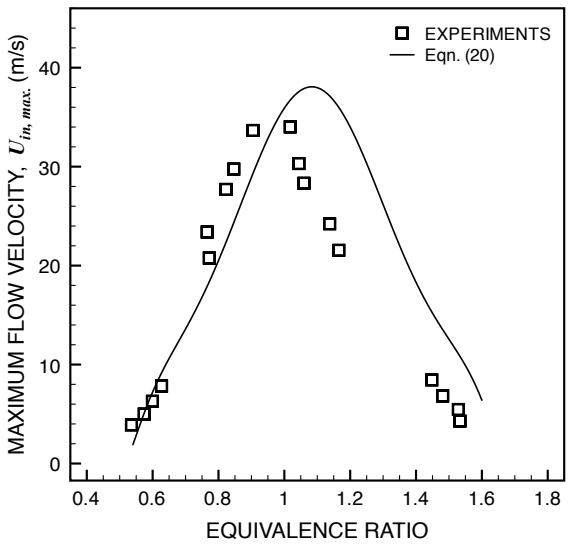

Figure 15: Flammability limit in the RJG estimated using a minimum energy model; experiment data are reproduced from Fig. 12

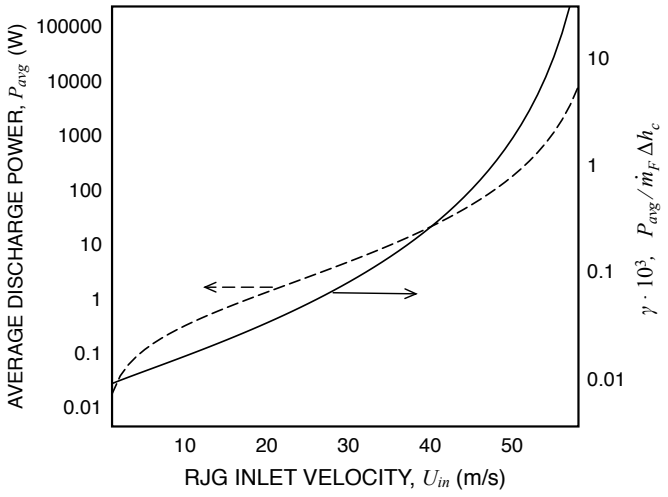

Figure 16: Increase of minimum average discharge power P_{avg} and the fraction γ of P_{avg} to the rate of combustion heat release as a function of the flow velocity for flame stabilization at the stoichiometric condition.

In conclusion, the high frequency spark discharge is able to stabilize combustion in a flow, at least as well as a backward facing step type flame holder. However, the spark energy required to ignite and stabilize a flame increases with increasing flow velocity. This resulted in an increasing ratio of required discharge power to the the rate of combustion heat release, γ, for a given RJG, see Fig. 16. The above restricts the direct use of HF sparks for flame stabilization to stabilize low velocity flow. The next chapter, therefore, focuses on techniques in which the radical jet produced by a HF sparks can be used to ignite and stabilize a flame in a high velocity combustor. Of particular interest is the role that radicals in the jet play in flame stabilization.

CHAPTER IV

RADICAL JET FOR FLAME STABILIZATION

The previous chapter showed that high frequency spark discharges can ignite and stabilize a flame in a RJG, using a relatively small amount of electrical energy compared to the heat release from the combustion process, in a low velocity flow. It also described how the periodic, unburned gas pockets created by the spark convection process produce a radical rich product downstream. This chapter describes flame ignition and stabilization by the product of a RJG injected into a main combustor carrying a combustible flow. The experiment consisted of a jet carrying both radicals and thermal energy produced by the combustion process and ejected from the RJG. To characterize these jets, the temperatures and levels of radicals were measured, and their variations with equivalence ratio in the RJG and main flow velocity were studied. Ignition and flame stabilization capability were measured for jets with different radical and thermal energy contents. This chapter also discusses the flammability limit of a main flame which is ignited and stabilized by a radical jets in a coaxial configuration. The length of radical jets were measured, and then used to calculate the characteristic residence time of the main flow in a mixing region for different radical jets and main flow conditions. The characteristic ignition delay time of the main flame was experimentally determined using the characteristic residence time at flame blow off. The blow off conditions, and, therefore, the maximum flame holding velocities, in the main combustor for various equivalence ratios were determined using a flame detector.

4.1 Characteristics of a radical jet

4.1.1 CH chemiluminescenct intensities

CH* chemiluminescence was used to measure the level of radicals because CH* radicals are formed only in a thin region of the flame front where most other radicals are also produced. To observe the interaction between the jet and the main flow the chemiluminescent levels were measured in this region. When the radical jet was injected normally into, and mixed with the main flow, its shape changed. In such a cross flow configuration, the main flow deflects the injected jet. The mixing between the jet and the main flow is influenced by four different characteristic features: a jet shear layer, a horseshoe vortex, wake vortices, and a counter-rotating vortex pair [81, 103]. The deflection of and mixing with the jet and the main flow at the junction of the RJG and the main combustor is a very complicated process. Characterizing chemiluminescent light emitted in the resulting flow is also difficult, because the mixing of the radicals with a cold, inert main flow promotes quenching of the excited species. If, the other hand, the radical jet is injected coaxially into the main combustor, mixing is dominated by the shear layer since the flow direction of both the radical jet and the main flow are parallel. This process is a lot better understood. For simplicity, the dependence of CH* chemiluminescent level on the RJG and the main flow conditions were measured using this configuration.

The combustor and associated diagnostic equipment were introduced in Ch 2. Because

Table 1: Cold flow conditions in a RJG and a main tube for the measurement of CH chemiluminescence

	low	high
RJG equivalence ratio, ϕ	0.61	1.33
RJG flow rate, *l*/s	1.19	1.28
RJG inlet velocity, m/s	11.6	12.4
Main air velocity, m/s	16.7	75.2

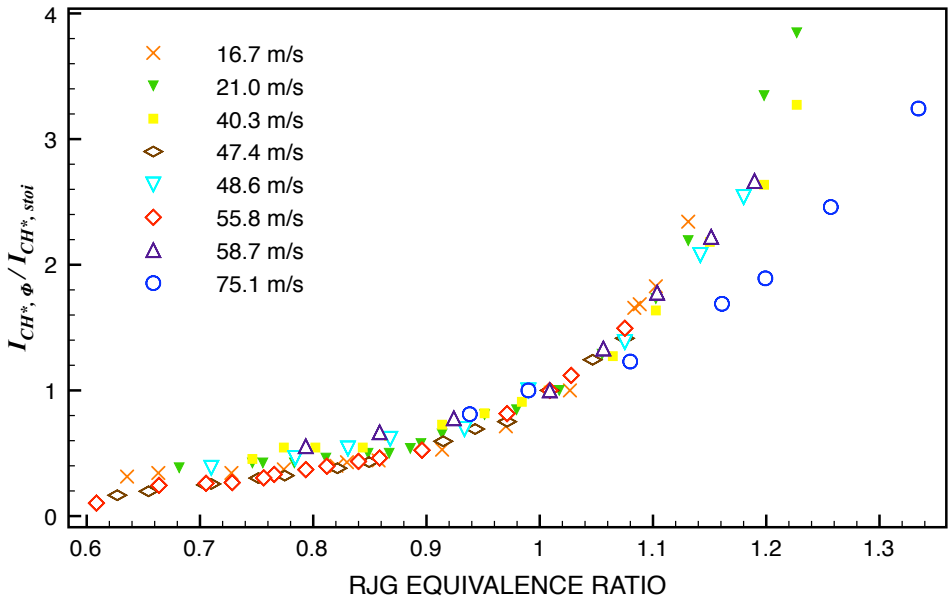

Figure 17: CH* radiation intensities as a function of equivalence ratio in the coaxial RJG for different main flow velocities

the level of PMT output varies linearly with the chemiluminescent radiation incident on the photocathode, and the radiation intensity is proportional to the number of CH* radicals, the total amount of CH* in the various radical jets relative to a reference condition can be evaluated without measuring the absolute intensity and converting it to a CH* number density, which is complex [68]. The flow conditions for the RJG and the main combustor used in these tests are given in Table 1. A premixed methane-air mixture was used to produce the radical jet. In this case, the air flow rate in the RJG was kept constant, and the fuel flow rate was varied to adjust the equivalence ratio. This changed the total flow rate in the RJG and the corresponding flow velocities slightly. Pure air was used for the main flow in order to clearly see the radical jet. This would have been difficult if a flame had been stabilized in the main tube. For each main flow velocity, the PMT outputs measured for the various RJG inlet equivalence ratios were normalized by the value that was obtained under stoichiometric conditions. The results, which represent the relative levels of CH*, were plotted in Fig. 17. Clearly, the values obtained for different main flow conditions collapse into a single curve. The PMT outputs monotonically increase with inlet equivalence ratio

of the RJG because the CH* concentration in a flame is proportional to the hydrocarbon concentration. Furthermore, for rich mixtures the length of the jet increases due to additional burning of excess fuel when it is mixed with main air downstream. For example, the latter effect can be seen in a series of pictures in Fig. 18, which shows the growth of flame length with the equivalence ratio for two different RJG inlet flow rates but constant main flow velocity. The flame lengths changed linearly except for very lean and rich conditions where the radical jet becomes unstable, which results in the flame lengths fluctuating. In this case, since the lengths recorded in low speed photography were time averaged values, they were not comparable to the lengths of the stable radical jet.

In Fig. 17, both the lean and rich regions beyond the points plotted represent the RJG equivalence ratios at which the radical jet becomes unstable. The frequencies of the flame fluctuation were about 7 and 110 Hz on the lean and rich sides, respectively. Since the main flow velocity did not significantly change during these tests, it cannot be responsible for the different frequencies. When the radical jet pulsated, the PMT output oscillated correspondingly. The lower values of the PMT signal were close to zero, which means that there was no part of the flame protruding from a RJG at that instant in the cycle. The peaks were slightly higher than the level corresponding to the stable flame just prior to the onset of pulsations. This suggests relatively intense combustion inside the RJG, which can produce a strong, pulsating jet. However, when the fuel-air ratio deviated further from stoichiometric, the peaks declined, and intervals between the pulsating flames became longer and irregular. Therefore, the measured mean values decreased.

The radiation measured by the PMT was strongly influenced by the size of the radical jet protruding beyond the nozzle. Assuming a conical jet, its sizes, both by volume and by surface area is only a function of the jet length. In coaxial flows, the length of the inner potential corn is inversely proportional to the ratio of the outer to the inner flow velocities, which here correspond to the main and radical jet velocities, respectively [96]. The potential core lengths were not measured in this study. However, the overall length of the jet is

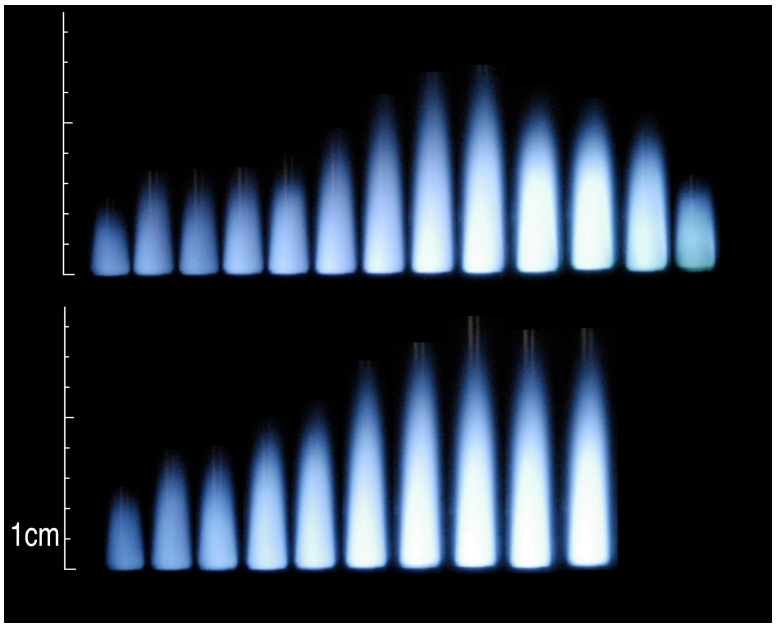

Figure 18: The radical jet length variation with RJG equivalence ratio in a coaxial RJG (right hand side is rich). In upper, RJG inlet flow rate was 1.21 l/s and the corresponding inlet velocity was 11.75 m/s at stoichiometry, and in lower, they are 1.73 l/s and 16.9 m/s, respectively. Main air flow velocity was maintained at 120.3 m/s.

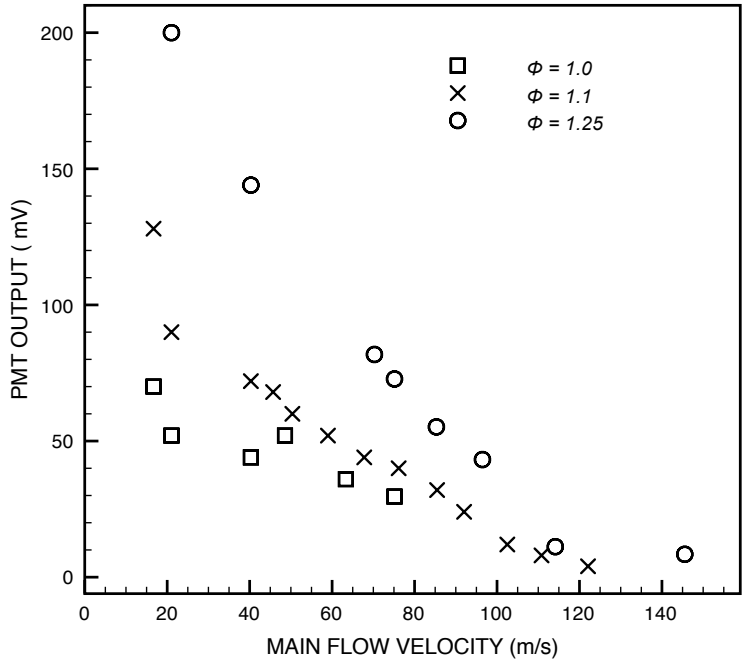

Figure 19: Variation of CH* chemiluminescence in a radical jet with increasing main flow velocity and fixed RJG flow rate.

observable because it is visible. The length of the jet and the corresponding radiation of CH* from the radical jet decreased with increasing main flow velocity, see, Fig. 19. This is probably caused because by the high velocity main flow sweeping away the edge of the radical jet, or because mixing with the higher flow rate of cold main air, under conditions of high strain in the mixing zone, promoting quenching of the reaction in the radical jet. Dependence of the radical jet length on the flow conditions will be discussed in the next section.

4.1.2 The length of radical jet

When the combustible main flow mixes with the radical jet, the residence time of the main flow in the mixing region strongly depends on the length of the radical jet. Thus, the blow off velocity is also affected by the length of the latter. In section 4.1.1, it was briefly mentioned that the jet length decreases with a main flow velocity, and increases with a equivalence ratio in the RJG.

The length of radical jet or, for that matter, those of a premixed turbulent flame injected into a coaxial flow or a cross flow with much larger flow rate have not been widely studied experimentally or theoretically because such conditions are not common in practical applications. Most studies carried out so far were usually related to the length of turbulent diffusion flames which are frequently used in industrial combustors [97, 116]. For a co-flowing jet, related theoretical studies have been carried out in cold flows [53, 96]. Furthermore, many of the dimensional analyses developed can be applied only far down stream, when the distance from the nozzle is many times the nozzle diameter. However, because the radical jet does not extend far into the main flow, see Fig. 18, the near field structure of the jet and its interaction with the outer flow is of importance.

Cold flow studies have shown that the velocity and the composition of the inner flow changes through entrainment of surrounding fluid into a free jet. Furthermore, the rate of

entrainment increases with axial distance [97]. Because the entrainment is attributed to the large vortex structure developed in the mixing layer [71], mixing between the inner and outer jet is proportional to the local turbulent intensities in a mixing layer [96]. This dependency on turbulence makes it difficult to estimate the inner jet length. The variations of the radial distribution of the axial jet velocity and of the mass fraction with axial distance have been studied [30, 122]. One useful characteristic length scale obtained from these studies is the length of an inner potential cone, L_i, in coaxial flow configurations. The main parameter that affects the length of inner core is the momentum flux ratio between two flow streams, $M = \rho_o U_o^2 / \rho_i U_i^2$. When inner and outer flow have the same density, the velocity ratio, r_u is used. In that case, the length of the inner cone related to the velocity ratio as [96],

$$\frac{L_i}{D_i} \sim \frac{C}{r_u} \tag{21}$$

where D_i is the diameter of the inner jet and C is a experimentally determined constant, whose value depends slightly on the configuration of inner and outer flows. For flow with different densities, r_u is replaced by $\sqrt{M}$ [53, 96]. Eqn. (21) states that the inner core length decreases with the outer flow velocity. This type of cold flow study may provide some insight into the functional dependencies of the flow properties on the length of the radical jet. However, since the combustion process inside a radical jet should be considered when estimating the proper jet length, in the present study the radical jet lengths were obtained experimentally.

The length of the radical jet can be measured by many different methods. In this study they were determined optically by taking pictures of the coaxial radical jet operating under the various RJG and main flow conditions. Because the length of radical jet fluctuated for very lean and rich conditions at frequencies up to 110Hz, sufficiently long exposure times (1 sec) were used. Thus, the obtained images correspond to the maximum length of radical jet for given operating conditions. During post image processing, color pictures of radical jets were converted to gray scale images. The edges of the jet were then examined to obtain

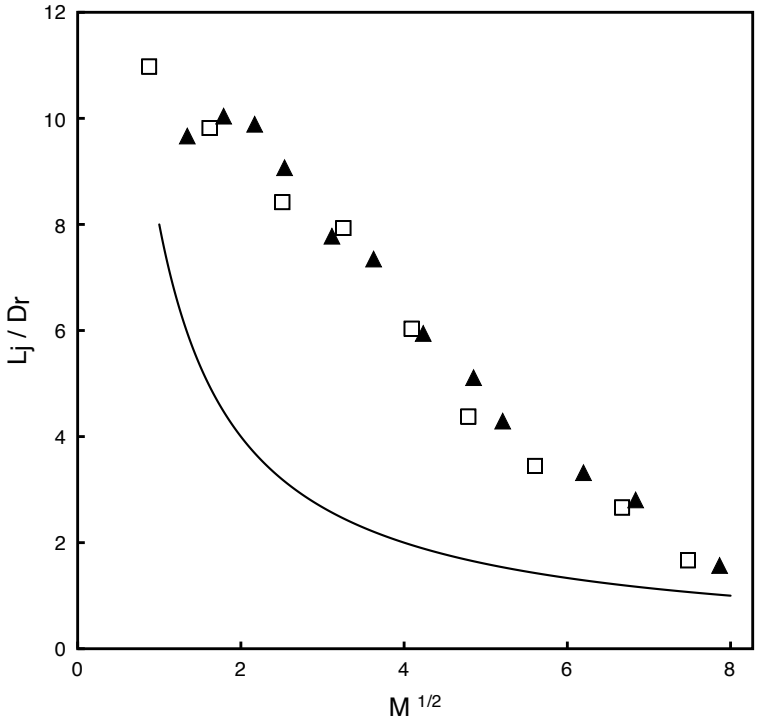

Figure 20: Variation of the length of the near stoichiometric radical jets with the main flow velocity; □, RJG ϕ = 0.96; ▲, ϕ = 1.04; −, $L_j/D_r = 8/M^{1/2}$, Rehab *et al.* (1997)

the jet length. The ratio of the main air velocity surrounding the radical jet to the RJG cold flow velocity ranged $2.8 < U_m/U_{RJG,cold} < 16.8$.

The effect of the main flow velocity

Similarly the length of potential core of a premixed flame in the coaxial configuration, the length of the radical jet is influenced by the main flow velocity, and thus, the ratio of the momentum flux between main and radical jet streams.

Figure 20 shows that the length of the near stoichiometric, radical, inner jet in a coaxial flow decreases with momentum flux ratio when the outer flow is a cold air stream. The jet length, L_j was normalized by the diameter of the RJG nozzle, D_r. Unlike the length of potential core, the jet length varied linearly while the former was inversely proportional to $\sqrt{M}$ according to Eqn. (21). Also, the radical jet is much longer than the inner core, because the chemical reaction in the radical jet can be sustained as long as the local mixture

is flammable downstream of the potential cone, even though an outer cold main flow impinges on the axis of the radical jet.

The effect of equivalence ratio

The measurement of the length of radical jet was repeated for various equivalence ratios in a RJG. Figure 21(a) shows that the jet length increases with increasing equivalence ratio at the RJG inlet. In Fig. 21(a) the jet lengths are normalized by their value at stoichiometric. The results shows that the rates increase with equivalence ratio are nearly independent of velocity ratios. This suggests that the effect of the equivalence ratio of the RJG inlet on the jet length is independent on the main flow velocity, or the velocity ratio.

Variations in equivalence ratio can change the properties of the jet, such as, the fuel mass fraction, the mass burning rate, and the burnt gas temperature. Without considering the interaction with the outer flow, the length of radical jet may be approximately determined by the distance from the ignition point of the radical jet, at which fuel start to be burnt. From a mass conservation, the differential change of the mass of fuel can be represented by

$$\dot{m}\frac{\mathrm{d}Y_F}{\mathrm{d}x} = \overline{\omega}_F A, \tag{22}$$

where Y_F is the mass fraction of fuel, $\overline{\omega}_F$ is average fuel mass burning rate and A is nozzle cross section area. For turbulent combustion, $\overline{\omega}_F$ is independent of the molecular level reaction rate and can be expressed by the well known *eddy-breakup-model* [107, 129], i.e.,

$$\overline{\omega}_F = -\rho C_F \frac{\varepsilon}{q}\sqrt{\overline{Y_F^{'2}}}, \tag{23}$$

where C_F is a constant, $Y_F^{'}$ is fuel mass fraction fluctuation, ε is turbulent dissipation rate, and q is a turbulent intensity. $\overline{Y_F^{'2}}$ is simply modeled by $\overline{Y}_F\left(1-\overline{Y}_F\right)$ [121]. Applying the model and integrating Eqn. (23) results in

$$L_{j,o} \sim U_{avg}\left\{\sin^{-1}(2\overline{Y}_{F,i}-1) - \sin^{-1}(2\overline{Y}_{F,L}-1)\right\}. \tag{24}$$

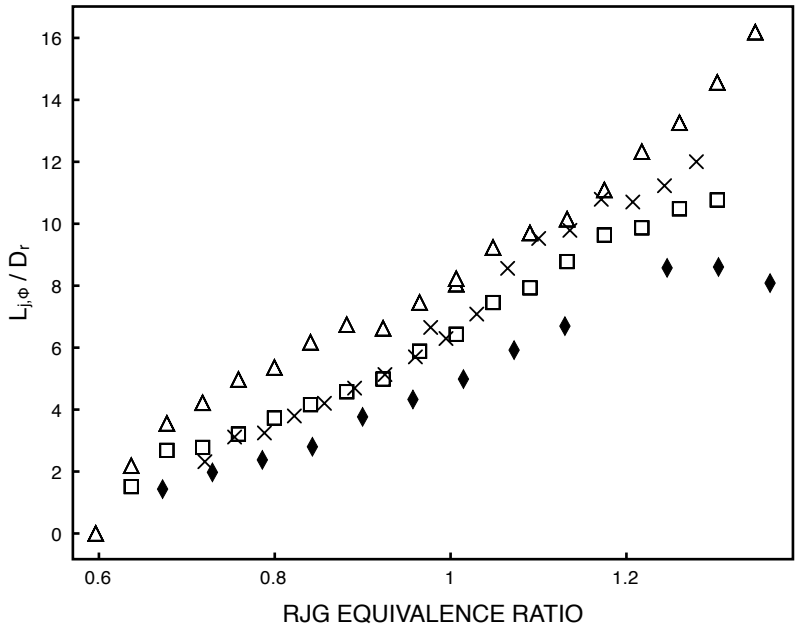

(a)

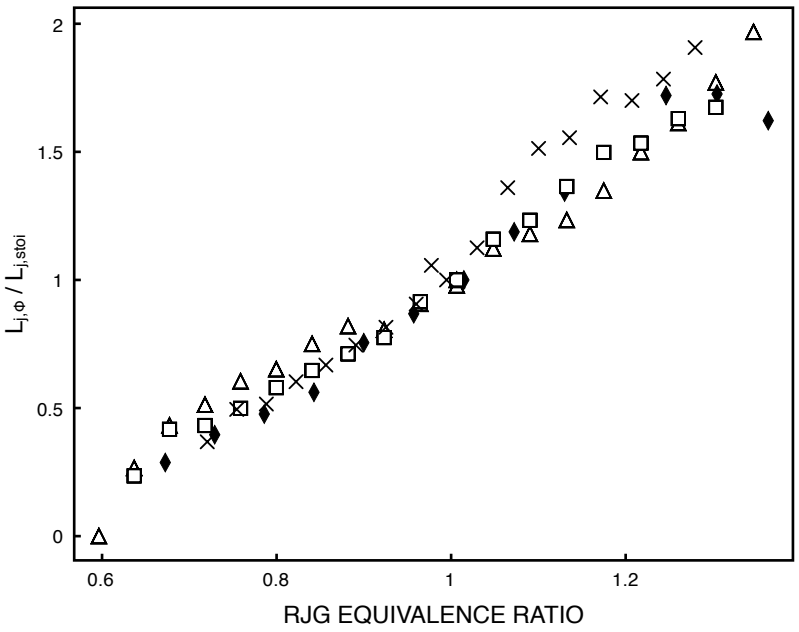

(b)

Figure 21: Variation of the length of the radical jets for various radical jet inlet equivalence ratio; (a) lengths normalized by the RJG diameter, (b) lengths normalized by the value at stoichiometric condition; △, U_{mc} = 67.7 m/s, U_{rc} = 13.8 m/s; ×, U_{mc} = 109 m/s, U_{rc} = 16.8 m/s; □, U_{mc} = 109 m/s, U_{rc} = 13.8 m/s; ♦, U_{mc} = 109 m/s, U_{rc} = 9.7 m/s.

Here, velocity changes in the x direction are not considered to make integration simpler, Thus, $U_{avg}(\approx U_{in}(1+T_{RJG}/T_{in})/2)$ is used. Parameters related to the turbulent flow are assumed to be constant because their variations with equivalence ratio are negligible when the flow rates of RJG and main flow are not changed. Equation (24) shows the simple functional dependence of the radical jet length on the inlet equivalence ratio when the effect of the outer flow is neglected.

In actual radical jets, the rate of fuel consumption may be affected by the chemical kinetics for cases with relatively low turbulent intensities. In those cases, the reaction rate peaks near stoichiometric because of the maximum flame temperature. This, in turn, causes shorter jet length. On the other hand, the high flame temperatures of such a mixture increases exit momentum flux of the radical jet, which increases L_j. This effect is taken into account by changes in U_{avg} in Eqn. (24). If one of these effects were to exceed the other, L_j would have a local minimum or maximum at stoichiometric. However, the measurement results show a linear increase with increasing equivalence ratio. Therefore, these two effects appear to each other.

4.1.3 Temperature of a radical jet

In addition to the quantities of active radicals, the jet temperature is also a very important parameter in the flame stabilization process. Experiments have shown that the strength of the radical jet, which results in different chemiluminescent light intensity, or jet length, etc., could be changed by varying many input conditions, such as spark power, equivalence ratio and flow rate in a RJG, as well as by RJG geometry. The temperature of the radical jet varied to some extent by changing any of those conditions. Since a radical jet contains significant quantities of unburned mixture, as described in the last chapter, the gas temperature is much lower than the equivalent adiabatic flame temperature. It should be noted that the low temperature obtained here was mostly not caused by heat loss to the surrounding. Except

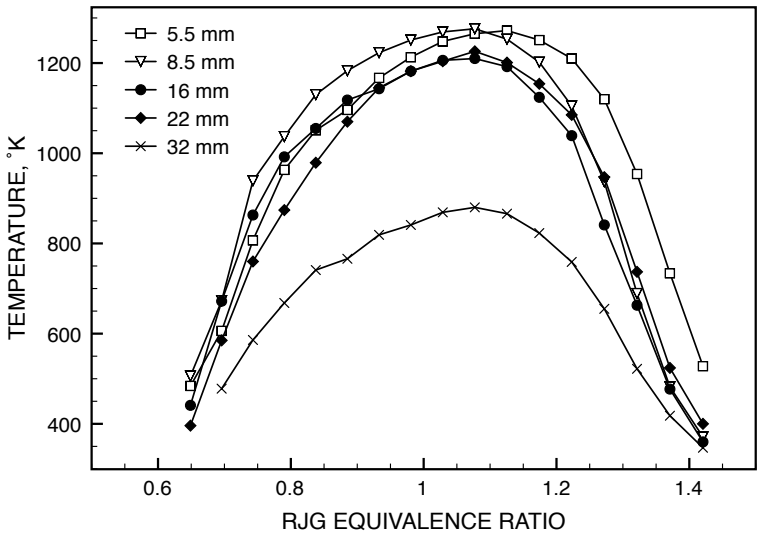

Figure 22: Variation of centerline temperature of radical jet with axial distance from the RJG nozzle exit; RJG inlet flow rate at stoichiometry, 1.21 l/s, and applied main air velocity, 48.5 m/s.

for low inlet flow rates and near stoichiometric, the RJG wall remained quite cool.

In these experiments, the flow temperature was measured using a shielded K-type thermocouples, which was located at the center of the jet. The position where the temperature is measured, is adjustable. Because the upper temperature measurement limit of K-type thermocouples is around 1300 °C, temperature data beyond this limit may not be reliable. In addition, an electrical measurement device like a thermocouple and its read-out may be influenced by the strong electric field associated with high frequency electrical discharges although it is shielded. Therefore, it should be noted that the temperature data presented here may subject to a larger error than usual for thermocouples, although positive and negative electric field noise was averaged. Although the absolute temperatures reported was not be totally reliable, the tendencies shown in the results are physically reasonable. Figure 22 shows the temperature variations with changing equivalence ratio of the inlet mixture at different jet axis locations downstream. The centerline temperatures on the lean and rich

sides are relatively low because of the lower flame temperature of those mixture. Interestingly, the exit temperatures do not drop significantly up to 22 mm downstream of the nozzle; i.e., up to about twice the nozzle diameter. This may be because of continued burning of fuel in the unburnt pockets throughout the jet.

Figure 23 shows the variation of radical jet exit temperature with inlet mixture equivalence ratio for three different inlet flow rates. The tube length of the RJG used in these measurement was slightly longer than that used to measure the temperatures reported in Fig. 22. The increase of residence time due to extended RJG length allows that the larger amount of fuel burned inside the RJG. Thus the temperatures reported here are relatively higher. In all three cases, the peak temperatures are not significantly different although case (c) has a 70% higher inlet velocity than case (a). However, in general, the maximum jet temperature decreases with increasing flow rate in the RJG, see Fig. 24.

Above results shows that the jet temperature depends on the inlet velocity, mixture equivalence ratio, and geometry of RJG. Because the exit temperature depends on the amount of burnt gas in the exhaust of the RJG, it increases with increasing the residence time of the flow in the RJG by lowering inlet velocity, or increasing RJG length. The exit temperature calculated using an one dimensional flame propagation in the RJG showed a similar trend with those obtained from experiment. A schematics and the derivation of the model are described in Appendix B.

4.2 Flame stabilization by radical jets

4.2.1 Overveiw

One of the goals in this study was to determine the ability and limitations of a radical jet to stabilize a flame in an afterburner. The method by which the radical jet is generated and limitations were discussed in the previous chapter. Both the results of measurements and of a simplified model showed that a radical jet can be generated when the electrical

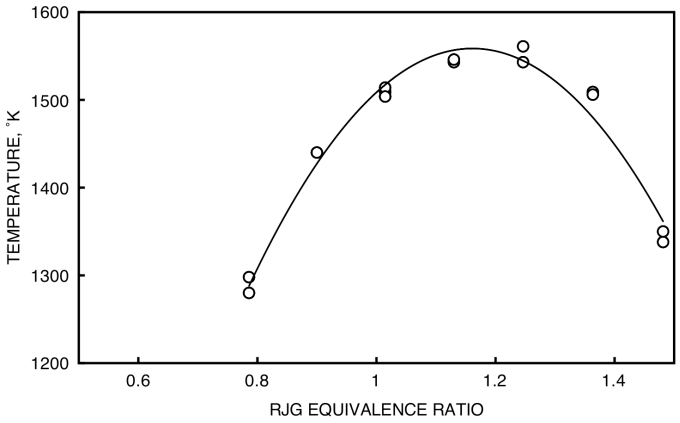

(a) $U_{in} = 10m/s$

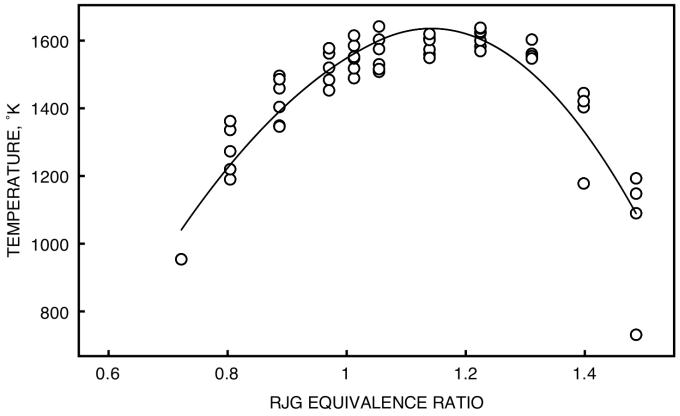

(b) $U_{in} = 13m/s$

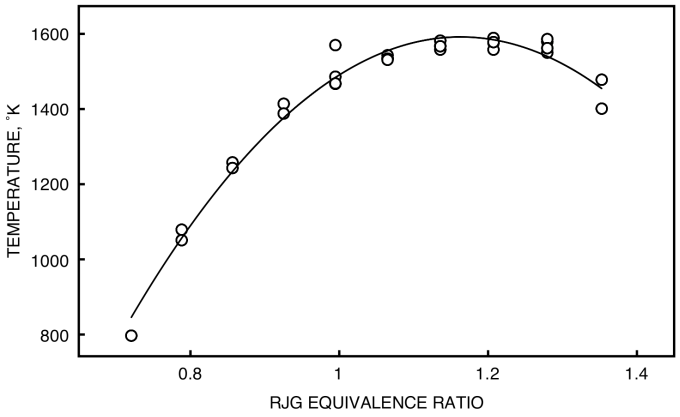

(c) $U_{in} = 17m/s$

Figure 23: Variation of exit temperature of radical jets with inlet equivalence ratio

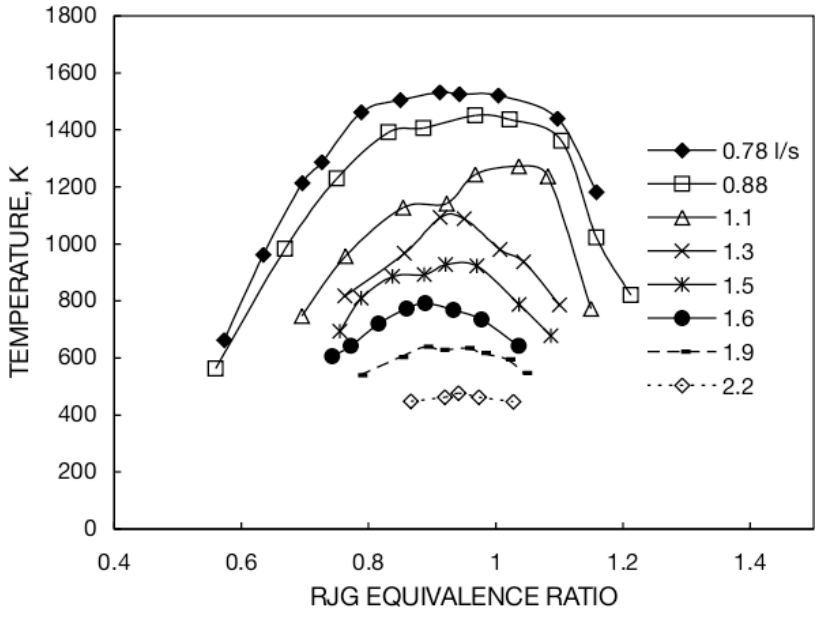

(a)

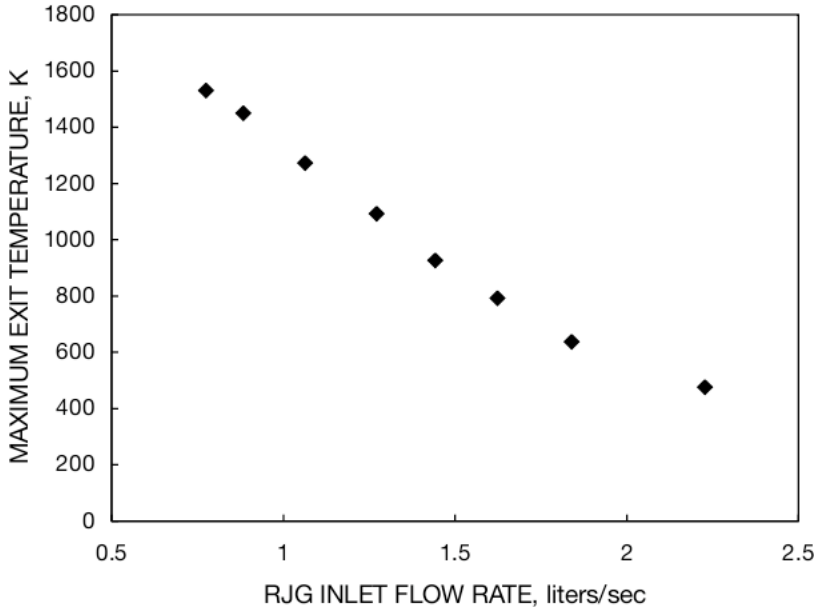

(b)

Figure 24: Variation of exit temperature of radical jets with inlet flow rate; (a) all Data, (b) maximum value for each flow rate

energy added to the flow is higher than its minimum ignition energy. However, this ignition model cannot explain the ability of the radical jet to stabilize a flame further downstream in a main burner. Indeed that is more closely related to the post-ignition processes, such as flame propagation in the downstream part of the jet, which multiply the level of radicals. The following sections describe the experimental results related to the capability of flame stabilization by the radical jet.

For a combustible gas mixture with homogeneous equivalence ratio and uniform flow conditions, ignition is followed by the flame propagation because the former is typically more difficult to achieve than the latter. For flame stabilization by a radical jet both the RJG and the main combustor operates with a combustible flow. The flow inside a RJG is then ignited. The flame propagates in the RJG, but it may or may not propagate into the main combustor. The flow conditions in the mixing region between the radical jet and the main flow can be complex, and the temperature and the equivalence ratio of the jet also vary because of mixing with the main flow. Therefore, the combustion process in the radical jet may or may not continue in the main flame. In the latter case, the flame stabilization by the radical jet, which is shown in Fig. 25, is not achieved although the radical jet on its own appears to operate normally. In fact, when the RJG was operated near its flammability limit, the resulting radical jet seemed to be weaker (i.e., operating at lower temperature) than when it was operated closed to stoichiometric conditions. Such a weak radical jet was not able to stabilize a main flame. Therefore, flame stabilization by a radical jet appears to be an ignition problem rather than a case of flame propagation. It was, therefore, necessary to study within which limitations the radical jet can ignite and stabilize a flame in the main combustor, independently of the ignition limit within the RJG. The former limitations were measured for given main flow equivalence ratio and flow rates because these main flow properties are factors in determining the flammability limit. In addition, the dependence of flame stabilization by the radical jet on spark input power was measured.

For these test, a quartz tube RJG was installed normal to the main combustor, see Fig.

5. Premixed methane-air mixtures at atmospheric pressure with different equivalence ratios and flow rates were supplied to the RJG. The HF spark discharge was used to initiate a radical jet, which penetrated perpendicularly into the main flow. The RJG inlet equivalence ratio was adjusted and recorded until the main flame was no longer ignited and stabilized by the radical jet. This test was repeated over a wide range of RJG inlet conditions. The entire set of tests was then repeated out using a 50% higher spark power.

4.2.2 Results

Figure 26 shows the limits of RJG inlet conditions within which the radical jet was able to successfully ignite and stabilize the given main flame. In other words, only points under the measured curves represent flow rate-equivalence ratio pairs in the RJG for which combustion is stabilized in the main flow. These results were compared with the limits of operation of the RJG itself reported in Fig. 12. Clearly those in Fig. 26 were comparatively narrower; i.e., radical jet resulting from RJG operated near the limits cannot ignite a flame in the main combustor. This suggested that certain jet conditions are required to ignite a flame in a given main flow, and that weak radical jets do not satisfy these requirements.

According to Eqn. (3), flammability limits are determined by balancing the characteristic ignition time and the characteristic residence time. Because the main flow velocity was kept constant in these tests, the limits in Fig. 26 were determined only by the characteristic ignition time, τ_c and the maximum jet length, L_j, which are dependent of the inlet flow rate, equivalence ratio and the applied spark power in the RJG. Fig. 26 shows that an increase in spark power broadens the operating velocity and fuel-air ratio of RJG, which can ignite and stabilize a flame in the main combustor. It also increases the maximum RJG inlet velocity. As the applied spark power is increased by increasing the current, the spark channel thickens while its temperature is unchanged. This leads to faster growth of the flame kernel, which allows a larger amount of gas to be burnt and more heat and radicals to be generated

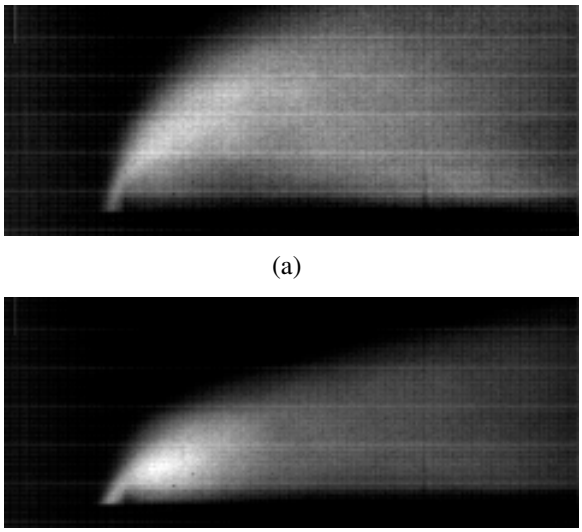

(a)

(b)

Figure 25: Flame stabilization by a radical jet in a cross flow; main mixture flows from left to right and a radical jet is injected from bottom; (a) main flow velocity, 8m/s; (b) main flow velocity, 10m/s; RJG inlet volume flow rate, 1.0 liters/s; radical jet is near stoichiometric, but equivalence ratio of the cross flow are not specified.

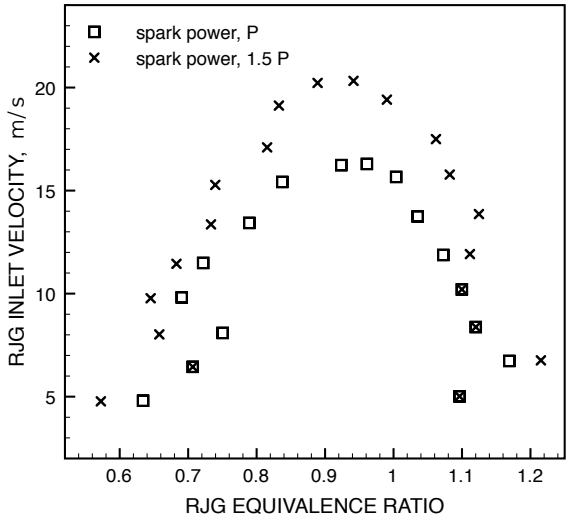

Figure 26: Limits of flame stabilization by the RJG with two different plasma powers in a premixed CH_4-Air main flow; flowrate and equivalence ratio 3.1 liters/s and 1.28 respectively. Points represented by $\times$ corresponding to 50 % higher electrical power than square points.

per unit time [99]. It was observed that the length of the jet injected into the main flow is proportional to the spark power. Furthermore, the stronger radical jet produced by the higher spark power may reduce the characteristic ignition delay time in the mixing region within the main flow. Because flame stabilization in the main combustor depends on the radical jet properties, which are affected by the spark power and the RJG inlet conditions, accurate measurement of these properties is necessary in order to understand the mechanism by which a radical jet ignites and stabilizes the main flame. The level of radicals and temperature distribution in the radical jet were measured, and their effect on the flame holding process in the main flow is discussed in the following sections.

4.3 Comparison of flame stabilization by both a radical jet and a thermal jet

4.3.1 Overview

The previous sections demonstrated the feasibility of flame stabilization by a radical jet. CH chemiluminescent intensity and temperature distribution were measured.

In this section, the effects of radicals and heat in a jet produced by the RJG on the flame stabilization performance in a main combustor were compared experimentally. Total separation of the effect of radicals from that of heat is impossible. However, difference in the amount of radicals and temperature can be produced by using two different types of jets, a radical jet and a thermal jet. When the combustion is completed inside the combustor tube, the exhaust gas contains fewer active radicals compared to a reacting jet, such as the radical jet. A method of generation for the thermal jet is described below.

To complete the combustion process inside a small RJG tube, a well stabilized flame is required. For this purpose a small step was incorporated as a flame holder in a “elbow type” RJG, see Fig. 4(b). (The small blunt structure that holds the electrodes, could also have been used as a flame holder but a flame could only be stabilized if the flow rate was relatively low and the fuel-air ratio was near stoichiometric.) In practice, the flame was

initially ignited and maintained by the spark discharge until the RJG warmed up. Once a stable flame was anchored behind the step, the discharge turned off. The resulting jet generated by the RJG operating with a stable flame was comprised of almost completely burnt products. On the other hand, a radical jet could be produced by increasing the flow rate, or using a lean or rich mixture.

A circular pipe with a much larger diameter than that of a RJG, and set below and perpendicular to the RJG was used to represent the main burner, see Fig. 27. The main burner tube was not extended downstream, beyond the RJG, in order to avoid recirculation in the main flow behind the jet ejected from the RJG. Because a recirculation zone can stabilize a flame by itself, and because the ability to hold a flame depends on the size of recirculation zone, it would have been difficult to study the difference between the thermal and the radical effect exclusively in the presence of such a zone. This recirculation problem also could have been reduced by using a coaxial configuration. However, in that case, the ”step stabilization” inside RJG required to generate a thermal jet could not be achieved, because the RJG wall would have been cooled too much by the outer, main flow.

An air flow rate in the RJG was chosen for which it was possible to create a radical jet when the inlet mixture was lean or rich, and a thermal jet when it was near stoichiometric. Temperature profiles along the axis and the level of radicals in the RJG jet were measured for the range of equivalence ratios used. The effects of different jet types on the ignition and stabilization process were compared by measuring the ability of the jet to ignite and stabilize a flame in a main burner and the strengths of the resulting flame. For this measurement, the flame detector introduced in chapter 2.5.1 was used. It was set far downstream of main flow such that the radial jet or thermal jet could not contact detector probes and thus produce a false positive. For each main flow of given velocity and equivalence ratio, the output from the detector was proportional to the amount of fuel burnt in a flame stabilized by a given augmentation jet configuration. The value of this flame detector output represents the “strength” of the main flame.

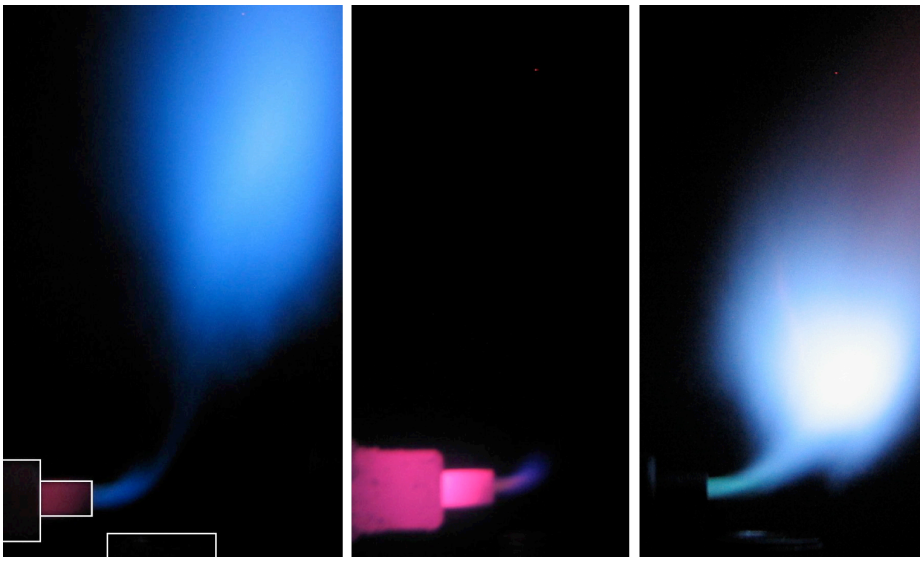

Figure 27: Test of flame stabilization by a "elbow type" RJG; from left, lean radical jet, attached thermal jet, and rich radical jet

4.3.2 Results

Figure 28 shows the radiation intensities from the OH(A-X) and CH(A-X) transitions for a wide range of RJG inlet equivalence ratios, and two main air flow velocities; i.e., 33.3 m/s and 16.3 m/s. In both cases, intensities were rather weak for RJG inlet equivalence ratios between 0.9 to 1.2. When comparing these results to those in Fig. 17, the difference is clear. The jets in this regime can thus be treated as thermal.

Temperature variations with equivalence ratio for both thermal and radical jet regimes are shown in Fig. 29. The exit temperatures for different equivalence ratios are similar to those obtained for the coaxial RJG in Fig. 22, which does not have a thermal jet regime. However, comparison of Fig. 22 and 29 shows that for the thermal jet, the temperature along the jet axis decreases faster than for a radical jet. This occurs because in the thermal jet the combustion process is essentially completed inside the RJG, while for the radical jet radical recombination causes heat to be generated in the flow ejected beyond the RJG nozzle. A rapid drop of the jet temperature along the jet axis can be interpreted as a decrease in the length of the jet that can act as a flame holder, and thus in the characteristic residence

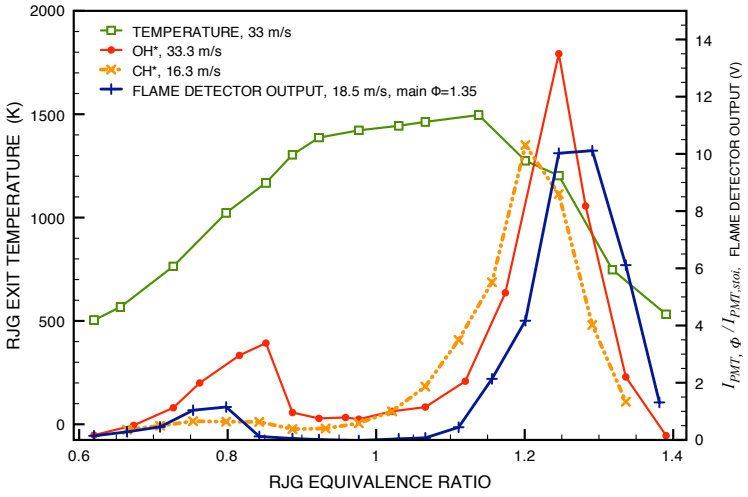

Figure 28: Variations of temperature measured in the exit of an elbow type RJG and OH* chemiluminescence normalized by the value at stoichiometric; for measurement of OH*, main flow is only air and main flow velocity is 33.3 m/s; for measurement of CH*, main flow is only air and main velocity is 16.3 m/s; for flame detection, main flow is combustible and main velocity is 18.5 m/s

time available to ignite a main flame.

Figure 28 also shows that the flame detector outputs were higher in a radical jet regime than in a thermal jet regime ($0.9 < \phi < 1.1$), where the values were negligible. Clearly the radical concentration follows a similar trend. Since a zero value in the flame detector output implies the absence of a flame in the main tube, it can be seen that a stoichiometric thermal jet, which has the highest temperature but negligible amounts of radicals, cannot ignite a flame, while much leaner and richer jets with relatively lower temperatures and lots of radicals, can, see Fig. 27. These results suggested that radicals generated by the plasma and multiplied by a cascade effect in the flame zone of the RJG dominate the ignition process of the main flow.

When using a conventional bluff body flame holders, the flame is stabilized by a near stationary pool of hot gases igniting an incoming combustible mixture. Therefore, flame holding by a thermal jet in this study is very similar to that by a bluff body. In fact, some researchers used a heated inert gas flow parallel to the main flow to study the mechanism by which a bluff body flame holder stabilizes a flame in an afterburner [80, 129].

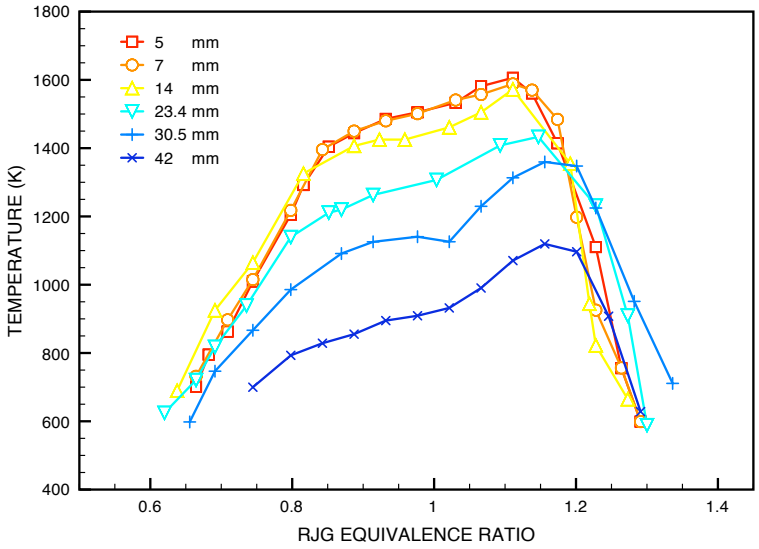

Figure 29: Variations of temperature with an equivalence ratio for various distance from the nozzle of an elbow type RJG

4.4 Limits of flame stabilization by a radical jet generator in a main combustor

4.4.1 Overview

Previous sections dealt with the ability of radical jets to stabilize combustion. It was also demonstrated that this process depends on the properties of the radical jet, such as the spark discharge power and flow rate and equivalence ratio. This section discusses the flammability limits in terms of equivalence ratio and velocity of the main flow when combustion there is stabilized by radical jet with given equivalence ratio and flow rate. In order to compare the ignition and flame stabilization limits by the radical jet with those of a conventional bluff body, similar flame detection technique must be used. This study uses a criterion described in Eqn. (3); i.e., the flame is considered extinguished when Dakohler number reaches a critical value of one.

The characteristic ignition delay time, τ_c is determined by the criterion using the contact duration between the fluid element in the main combustible flow and the source of ignition, the recirculation wake behind the bluff body when the flame blows off. For a given bluff body flame holder, τ_c depend primarily on the characteristics of the reactant mixture because the temperature and the composition of the hot gas in the recirculation zone, which is used as the ignition source, are determined by the reactant itself. However, when a flame is stabilized by a radical jet, the temperature and species composition of the radical jet are independent of the main flow. Therefore, τ_c of the main flow can be changed by varying the properties of the radical jet. This implies that τ_c in this case is a function of the properties of the radical jet as well as of the main reactant mixture. Therefore, τ_c calculated using Eqn. (3) can be used to compare the flame holding performance of a bluff bodies with that of a radical jet.

In order to estimate τ_c for a flame stabilization by a radical jet, the length of radical jet and the main flow velocity at which the main flame is blown off must be determined accurately. Blow off conditions are not very obvious when a flame is stabilized by a radical jet. Therefore, a flame detector is used to quantify the instantaneous strength of the main flame, which is then represented by the predefined "flammability," ξ in Eqn. (16). Since ξ drops below one when the main flame is unstable[1], the main flow velocity under this condition may be a limit of practical operating range for the combustor. However, using a main velocity, at which the pulsation just begins, may result in overestimating τ_c because the former is determined by the fluctuations of the radical jet, i.e., by a purely fluid dynamic effects, and it may be independent of the level of radicals. Therefore, present study uses the conditions, at which ξ becomes close to zero, as a flammability limit of the main flame.

[1]Rehab *et al.* reported that, in a coaxial jet configuration, inner flow oscillations appears when the momentum flux ratio between the outer flow and the inner flow increases above a certain value. In this case, the frequency of the oscillation is lower and the amplitude is higher than those of Kelvin-Helmholtz mode [50, 96, 115, 123]. For a case including combustion Kim *et al.* showed that the very low frequency combustion instability of a spark driven, confined jet flame is caused by the interference between the periodic formation of flame kernel and the rest of combustion process [59]

4.4.2 Characteristic ignition delay time

These tests were carried out using two coaxial flows. The inner is a radical jet with limited range of inlet conditions, while the outer is a main flow for which the characteristic chemical times of combustion evaluated. The characteristic chemical time, which is also referred to as the characteristic ignition delay time, is obtained by dividing the length of radical jet by the main flow velocity. The measurement of the radical jet length was already described in Sec. 4.1.2. Because the length of radical jet was measured when the main flow was air only, it may differ from the length which is measured when the main mixture is combustible. However, such problems were neglected because no noticeable changes in radical jet length due to variations in equivalence ratio of the main flow were observed near blow off conditions. The velocity of the main flow bypassing the radical jet, U_{mc}, was calculated by $Q_m/(A_m - A_{RJG})$ where Q_m is a volume flow rate of a main flow, and A_m and A_{RJG} are the cross section area of the main tube and RJG, respectively. This method was also used to estimate τ_c in many bluff body flame holder studies, except here the length of the recirculation wake was replaced with that of a radical jet [138].

Figure 30 (left) shows the maximum main flow velocity for which ignition occurs as a function of equivalence ratio of the main flow. Three radical jets with equivalence ratios, 0.88, 1.0, and 1.22, were used to stabilize the main flame. The limiting main flow equivalence ratios are also shown in the figure. The flammability limits significantly vary with ξ, which ranged from 0.99 to 0.1. According to a definition of ξ, 0.99 is at the threshold of an unstable flame, and 0.1 is almost of the limit where the radical jet can barely stabilize the main flame. For all cases, the dependence of the flame holding velocity on the main mixture equivalence ratio are very large. Usually the peak velocities appeared when the main flow was stoichiometric. Comparing Fig. 30-(a), (b), and (c) left hand side, the maximum flame holding velocities increase with increasing the equivalence ratio of RJG. However,

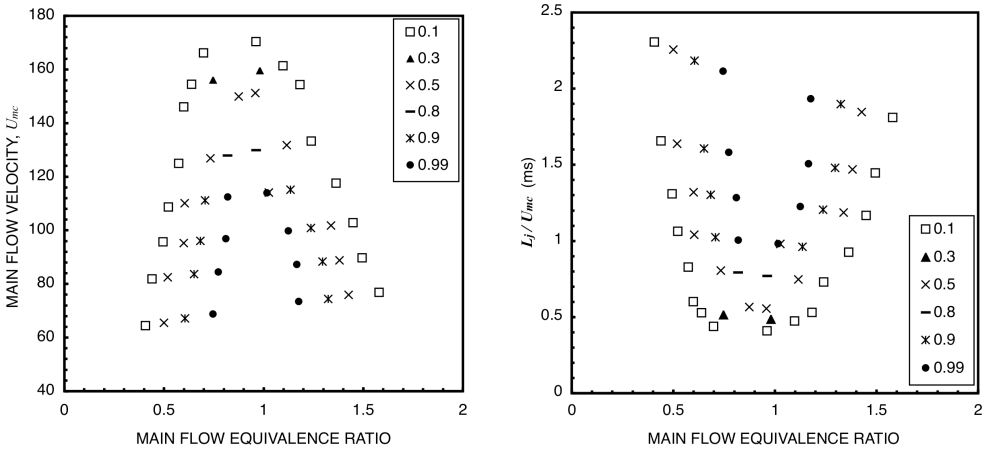

(a)

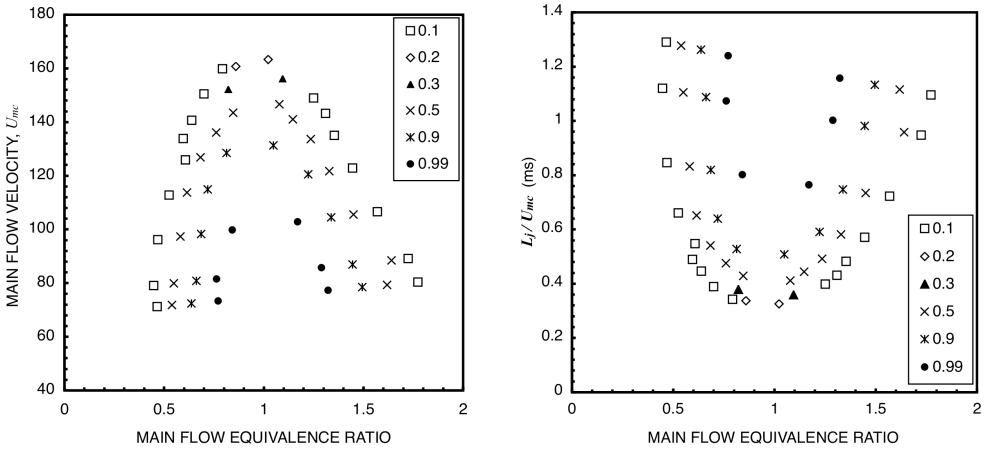

(b)

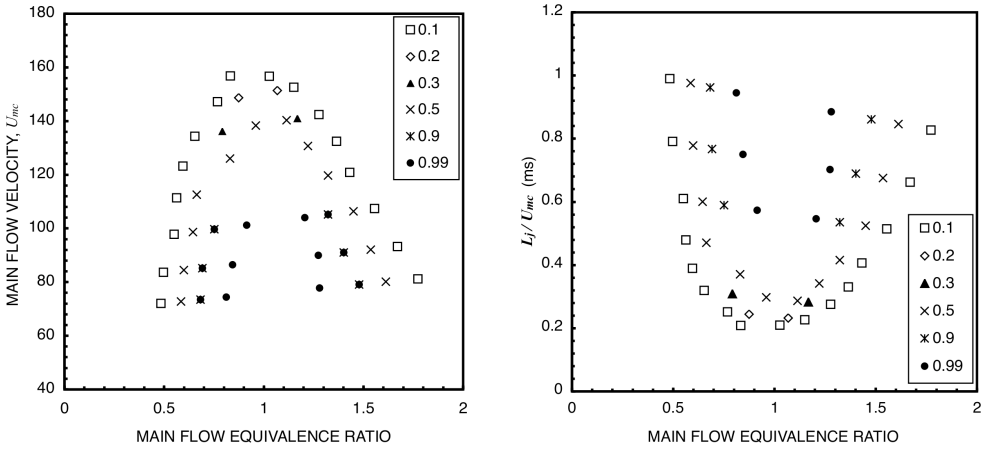

(c)

Figure 30: Flame stabilization velocities in a main combustor with various equivalence ratios for different radical jet equivalence ratios; (a) RJG ϕ = 1.22, (b)RJG ϕ = 1, (c) RJG ϕ = 0.88; Legend represents the flame strength expressed by the pre-defined flammability, ξ.

this variation is small. Using these main flow velocities, the characteristic residence times were calculated using L_j/U_{mc} and plotted on the right hand side in the figure. Because the flammability limits were defined as the conditions at which ξ is equal to 0.1, the residence time under those conditions is equal to the characteristic ignition delay time. These results show that the characteristic ignition time increases by factor of 2 when the equivalence ratio of the radical jet is increased from 0.88 to 1.22. This is expected because the length of radical jet increases with equivalence ratio of the radical jet significantly while U_{mc} does so only very slightly. Although the detailed reasons are not yet understood, the experimental results suggest that a rich radical jet can stabilize a flame in the higher velocity flow, because the longer τ_c is compensated by the longer jet length. Since a small amount of unburned mixture is included in the radical jet, local equivalence ratio in the mixing layer between radical jet and main flow, where the main flame is ignited and attached, may differ from that of the initial main flow. Figure 30 shows that the main mixture equivalence ratio corresponding to the peak flame holding velocity shifts slightly toward lean side when the equivalence ratio of the radical jet increases. This is more clearly seen when ξ is taken as 0.99. As the amount of unburned gas increases, this effect can become important. However, under typical radical jet conditions, this effect is not significant compared to other changes caused by varying the radical jet equivalence ratio, such as, the level of radicals, the temperature, and the jet length.

4.4.3 Ignition distance

Another method to characterize the ignition performance of a radical jet and compare it to that of the conventional bluff body flame holder is to measure the axial distance from the radical jet nozzle exit to the point of ignition of the main flame. Similar studies have been carried out for the ignition of a laminar flame by a hot, inert gas stream parallel to the laminar flow [24, 80]. In the case of a radical jet with flow direction parallel to the main

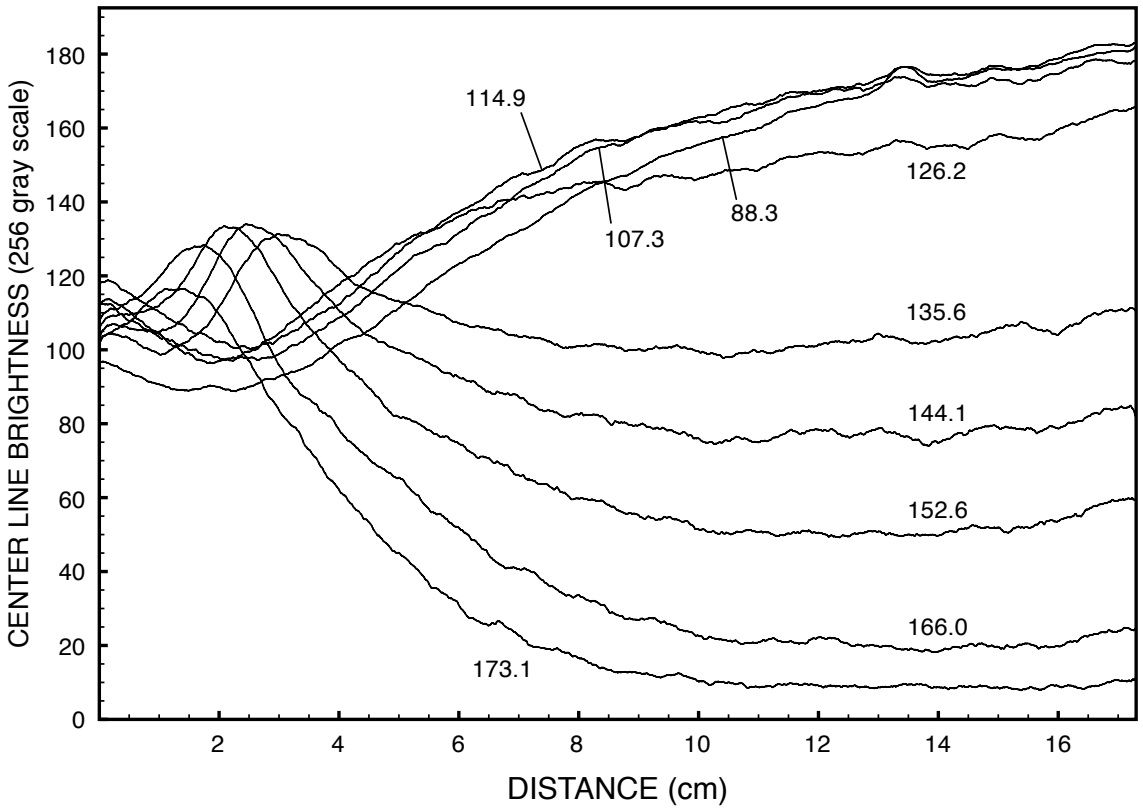

Figure 31: Variations of chemiluminescent intensities along the center line of the radical jet / main flame for different main flow velocities (marked in m/s); radical jet flow rate is 1.4 l/s; equivalence ratio of the radical jet and main mixture are stoichiometric.

flow, the chemiluminescent intensity from the reaction zone of the radical jet drops along the axis because the amount of reactant continuously decreases. If the intensity downstream increases or, at least, shows sudden slowing in its rate of decrease, then another source must produce radicals at that location. That new source must be beginning of the main flame. The ignition distance can be, therefore, measured by tracking the axial variation of the radiation intensity along the radical jet and the main flame.

Figure 31 shows that the typical change in intensity along the jet / main flame centerline. This figure was generated from a digital image of the radical jet / a main flame combination. The light intensity of the flame zone is represented by 256 gray scales.

Figure 31 shows two different trends for the change of chemiluminescence intensity along the axis at different main flow velocities. When the main flow velocity is relatively

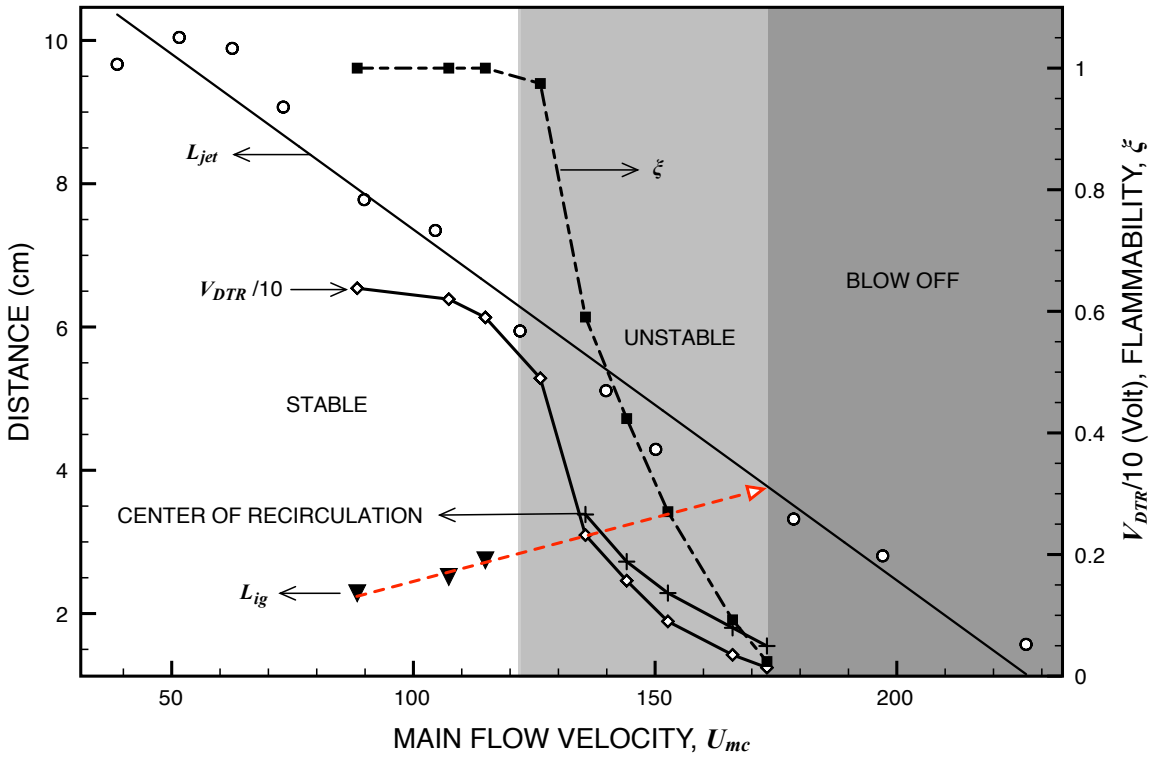

Figure 32: Ignition distances of main flames and the distance of the center of the recirculation zone from the radical jet nozzle for various main flow velocities; the length of radical jet in an air flow with same velocity; the corresponding main flame strength and flame detector voltages.

low ($U_{mc} < 127$ m/s), the intensity first decreases and then increases again shortly thereafter. These local minimum intensities indicate the location where the main flame is stabilized. The distance from the nozzle exit to that point is referred to as the ignition distance, L_{ig}. The ignition distance becomes longer as the main flow velocity is increased. Intensities of the main flames are usually stronger than those of the radical jet but are independent of main flow velocities over the range. When the main flow velocities are higher ($U_{mc} > 135$ m/s), the variations of the intensities exhibit a local maximum close to the nozzle exit, that is higher than the level of radiation from the radical jet in the lower velocity regime.The distance from the nozzle exit to the locations where this local maximum intensity appears decrease with increasing main flow velocity. This locally bright region is easily distinguished in the images, even without post processing. This is a recirculation region, which is caused

by the high momentum flux ratio between the outer and inner jet. The combustion intensity in this recirculation region is very intense. However, the appearance of this recirculation region is accompanied by the fluctuation of the main flame. Thus, the mean intensities generated by the main flames are relatively weak compared to those measured when the main flow velocities are low. Furthermore, the intensity decreases with increasing main flow velocity. Figure. 32 clearly shows that the value of ξ starts to drop as soon as the recirculation zone appears. In this fluctuating regime, it is difficult to obtain the ignition distance. Thus L_{ig} can be obtained only when the main flame is stable. Ignition distance were extrapolated to higher main flow velocities beyond the stable condition. This extended curve and the line representing the radical jet length intersect at the main flow velocity at which blow off is first observed. Using the ignition distances and the main flow velocity, a characteristic ignition delay can be calculated. The values thus determined agree well with those obtained from Fig. 30(b).

Table 2: Characteristic ignition delay time of methane-air mixture measured by different methods and those reported in literatures

Source	Fuel	ϕ_{RJG}	ϕ_{main}	τ_c [ms]
RJG : Fig. 30	Methane	1	1	0.33
RJG : Fig. 32 (ignition distance)	Methane	1	1	0.24
Cylinder in 3×3" tunnel, [93]	Propane		1	0.35
Cylinder in 1×3" tunnel, [93]	Propane		1	0.28
Bluff body [139]	Paint thinner		1	0.29

4.4.4 Comparison with a bluff body flame holder

The flame stabilization performance of flame holders is typically represented using the flammability limit curves . For flame stabilization by radical jets with various equivalence ratios, two main velocity limits (ξ=0.99 and 0.1) are plotted again in Fig. 33, where they are

compared to those obtained for bluff body flame stabilization. Because flammability limit data for methane-air flame stabilized by bluff bodies are not available in the literature, blow off velocities were measured using a circular disk flame holder with about 30% blockage. For other types of flame holders and fuels, data in references [4, 37, 132, 133] were used. Since, in those references, the limit velocities are represented by the average velocities upstream of the flame holder instead of by velocities next to the flame holder, all velocity limits taken from Fig. 30 were adjusted the corresponding inlet velocities.

Figure 33 shows that the radical jet can stabilize a flame at a much higher flow velocity, even if the value of ξ =0.99 is used to determine the limits, compared to the maximum flame holding velocities obtained when other types of flame holders, such as a cylindrical rod, a V-gutter, or a reverse flow jet, are used. According to Eqn. (3) this result means that the radical jet can reduce the characteristic chemical time significantly, or that the radical jet has a much longer effective length than other ignition sources.

For flame stabilized on a radical jet, τ_c ranged from 0.21 to 0.41 ms depending on the radical jet equivalence ratio, as shown in Fig. 30. Unfortunately, these values cannot be directly compared to those for bluff body flame holders because there are no data available for methane-air flames. One possible alternative would be to compare with data obtained using other fuels. Zukoski reported that the average value of τ_c for a paint thinner is 0.29 [139]. Potter and Wong measured τ_c for stoichiometric propane-air flames at pressures lower than atmospheric pressure in ducts with two different cross section areas. They extrapolated the results to τ_c at atmospheric pressure and reported that the values were 0.28 and 0.35 ms for smaller and larger ducts respectively[2] [93]. They also suggested that τ_c is probably related to the laminar flame speed since the laminar flame speeds are similar for many hydrocarbon fuels [93]. Based on this assumption, it can be expected that τ_c for a stoichiometric methane-air flame stabilized by a bluff body should have a similar value

[2]Potter and Wong assumed that these variation of τ_c for a given fuel with the tunnel size was caused by different heat losses from the recirculation zone to the flame holder, which changes the temperature in the recirculation zone [93]

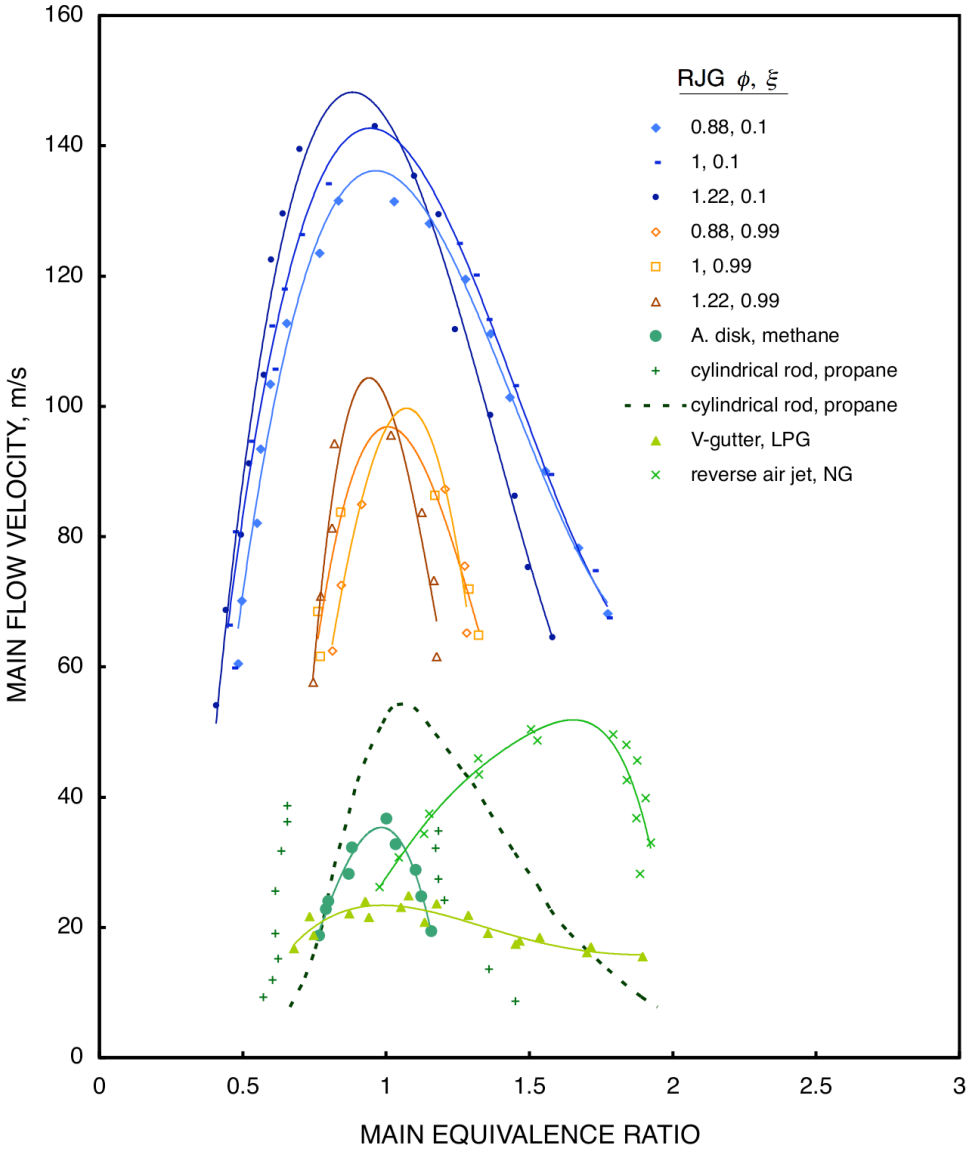

Figure 33: Maximum flame holding velocity in a main combustor for radical jet with various conditions and for various flame holders and fuel types; A. disk, methane, 30% blockage, measured by author; B. cylindrical rod, 40% blockage, propane [132]; C. cylindrical rod, propane, 10% blockage [37]; D. V gutter, LPG [133] ; E. reverse air jet, natural gas [4]

to that of a propane-air mixture because the laminar flame speeds for those two fuels are similar; for instance, 45.6 and 43.4 cm/s at stoichiometric conditions, respectively [41]. It thus seems reasonable to assume that the value of τ_c for a stoichiometric methane-air flame is about the same as that for a stoichiometric propane-air flame. At the same time the value of τ_c obtained for flames stabilized by stoichiometric radical jets is close to that for bluff body flame holders. Since the temperature of the stoichiometric radical jet is typically much lower than that in the recirculation zone of a bluff body, which is typically within 5 to 10% of the adiabatic flame temperature [138], this result strongly suggests that there must be a radical effect on τ_c, which compensates for the lower temperature in radical jet and thus maintains τ_c at the same order of magnitude as for traditional recirculation zones.

On the other hand, the observed increase of the flammability limits can be attributed to the difference between the length of radical jet and that of the recirculation zone. In order to compare lengths, data in the literature are examined. Potter and Wong [93] demonstrated the length of recirculation zone varies with the flow velocity for various size flame holders and ducts. Among these results the cases with half inches diameter flame holders were selected for comparison in this study, because the radical jet exit diameter is 0.45 inch. Figure 34 shows that the recirculation zone length increased with the flow velocity when the velocity is low, and remains unchanged when the velocity is relatively high. These flat regions are observed for all sizes of flame holders [93]. For a RJG, it was already shown in Fig. 20 that the length of radical jet decreases with increasing main flow velocity. Thus, over a certain range of main flow velocities, the length of radical jet must be shorter than the recirculation zone length. However, this does not usually happened when the RJG is operated at an appropriate flow rate, and is, therefore, able to stabilize the main flame. Because of the differences in U_{max}, Figs. 32 and 34 show that the length of the recirculation zone at blow off is notably shorter than the length of the radical jets for a given main flow velocity.

In summary, flame stabilization limits by radical jet and by conventional bluff body

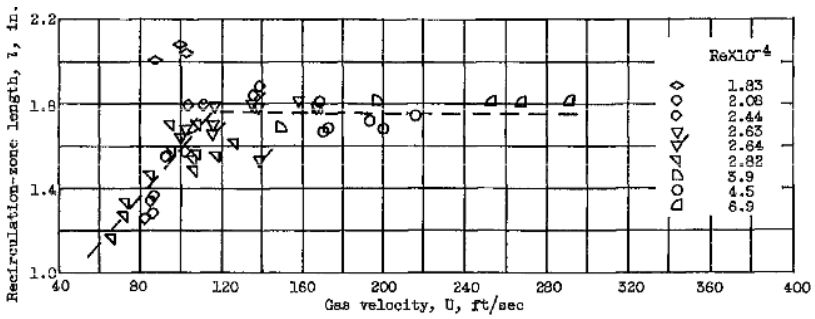

(a) 1/2 inch flame holder in 1 by 3 inch duct.

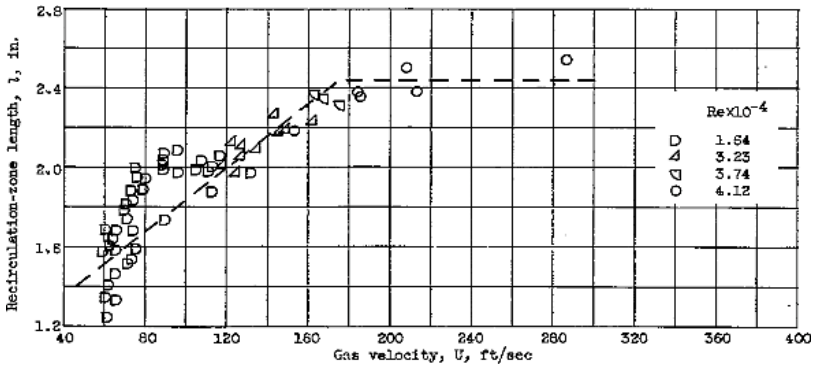

(b) 1/2 inch flame holder in 3 by 3 inch duct.

Figure 34: Recirculation zone length as function of gas velocity for propane-air flame stabilized by different cylindrical flame holders; graph reproduced from Potter and Wong [93].

flame holders were compared using experimental results and data from the literature. The results showed a significant improvement in maximum flame holding velocity when the radical jets were used. The results suggested that further this improvement was achieved because of the longer ignition source provided by the radical jet. Experimental result also showed that the characteristic chemical time is affected by different radical jets. Rough comparison with those obtained from the conventional method of flame stabilization did not reveal big differences. However, the effect of radicals on τ_c is still important to explain the excellent flame holding performance of the RJG as well as effects of the length of the radical jet. In the next chapter, the results of CHEMKIN based numerical studies will be reported, which will shed further light on the mechanism by which the radical jet stabilizes combustion.

CHAPTER V

NUMERICAL SIMULATION

The experimental results in Chapter 4 were analyzed using the computational chemical kinetics code, CHEMKIN [58]. Throughout this chapter a radical jet was characterized by a high temperature flow which includes a certain amount of active species. Using different cases with two extreme levels of radicals, the difference of ignition delay was investigated when such gases are mixed with cold unburned methane-air mixture. The calculation of ignition delays for both types of gas condition is carried out using a series of reactor models, PREMIX and plug flow reactor (PFR) supported by CHEMKIN (see Fig. 37). PREMIX is a fortran program for modeling steady laminar one-dimensional premixed flame [57]. Resulting change of ignition delay of fresh CH_4-air mixture by different gaseous conditions are further refined to apply the case of a radical jet. For the purpose species composition of radical jet was characterized by the mean values of entire jet volume. The limit velocity at which the main flame can be stabilized by a radical jet is estimated.

5.1 Overview

5.1.1 Reaction mechanisms

GRI-Mech 3.0 is widely used reaction mechanism for natural gas combustion. This mechanism contains 325 elementary reactions for 53 species and is optimized for an extensive range of combustion conditions, which includes all conditions covered by this study. More details of this mechanism are available in the release note and descriptions on the web [101]. Because electronically excited species are not included in this set of reaction mechanism, reactions related to the electronically excited species, which give rise to chemiluminescence, are added. Table 5.1.1 shows the reactions involving excited species, CH* and

OH* [68]. Reactions No. 1-5 describe chemi-excitation processes that produce the electronically excited CH* and OH* in methane and air flames. Reactions No. 6 to 19 represent collisional quenching processes, which de-excite electronically excited species and return them to their ground states without light emission. Reaction rate coefficients for these reactions are chosen as recommendation in Ref. [68]. The author compared CH* and OH* emission with values computed using different rate of coefficients with those measured experimentally. The thermochemical and transport parameters of ground state species were also used for the excited species, except for the enthalpies. These were calculated by adding excitation energies to the ground state enthalpies. The excitation energies per mole were estimated from the radiation energy, $N_{AV}h\nu$, where ν was calculated using the average wavelengths of the A-X transitions, 309 nm for OH and 431nm for CH.

5.1.2 CH* mole concentration in a premixed laminar flame

Due to the lack of simple computer models for a turbulent combustion, as takes place in a radical jet, the turbulent combustion is often replaced by a wrinkled laminar flame. Similarly in this work, the combustion properties calculated assuming a laminar flame are used to characterize combustion in the radical jets. The variations of species concentrations in premixed laminar flames were calculated using PREMIX for inlet equivalence ratios ranging from 0.7 to 1.3 in 0.1 interval. For simplicity, the reaction was assumed to be adiabatic.

Figure 35 shows the change in mole fractions of several active species and local temperature along the axis normal to the flame. The concentrations of active species increase rapidly in the flame front and decrease to their equilibrium concentration in the product region. The mole fractions of the electronically excited species are much lower than those of the ground state species. However, their distributions along the axis are quite similar.

Table 3: OH* and CH* excitation and quenching reactions[a]

No.	Reaction	A	b	E	Source
Excitation					
1	O+H+M → OH*+M	3.63×10^{13}	0	0	[56, 102, 32]
2	CH+O_2 → CO+OH*	3.72×10^{10}	0	167.2	[21]
3	C_2H+O → CO+CH*	2.50×10^{12}	0	0	[44]
4	C+H+M → CH*+M	3.63×10^{13}	0	0	[102]
5	C_2H+O_2 → CO_2+CH*	3.20×10^{11}	0	805	[44]
Quenching					
6	OH*+N_2 → OH+N_2	1.08×10^{11}	0.5	-1238	[102, 111]
7	OH*+O_2 → OH+O_2	2.10×10^{12}	0.5	-482	[102, 111]
8	OH*+H_2O → OH+H_2O	5.92×10^{12}	0.5	-861	[102, 111]
9	OH*+H_2 → OH+H_2	2.95×10^{12}	0.5	-444	[102, 111]
10	OH*+CO_2 → OH+CO_2	2.75×10^{12}	0.5	-968	[102, 111]
11	OH*+CO → OH+CO	3.23×10^{12}	0.5	-787	[102, 111]
12	OH*+CH_4 → OH+CH_4	3.36×10^{12}	0.5	-635	[102, 111]
13	CH*+N_2 → CH+N_2	3.03×10^{2}	3.4	-381	[102, 111]
14	CH*+O_2 → CH+O_2	2.48×10^{6}	2.14	-1720	[102, 111]
15	CH*+H_2O → CH+H_2O	5.30×10^{13}	0	0	[102, 111]
16	CH*+H_2 → CH+H_2	1.47×10^{14}	0	1361	[102, 111]
17	CH*+CO_2 → CH+CO_2	0.241	4.3	-1694	[102, 111]
18	CH*+CO → CH+CO	2.44×10^{12}	0.5	0	[102, 111]
19	CH*+CH_4 → CH+CH_4	1.73×10^{13}	0	167	[102, 111]
Relaxation					
20	OH* → OH	1.45×10^{6}	0	0	[102, 35]
21	CH* → CH	1.86×10^{6}	0	0	[102, 12]

[a] Reaction rate coefficient $k = AT^b \exp(-E/RT)$. R is the universal gas constant, T is the temperature in K. Units are mol cm cal s.

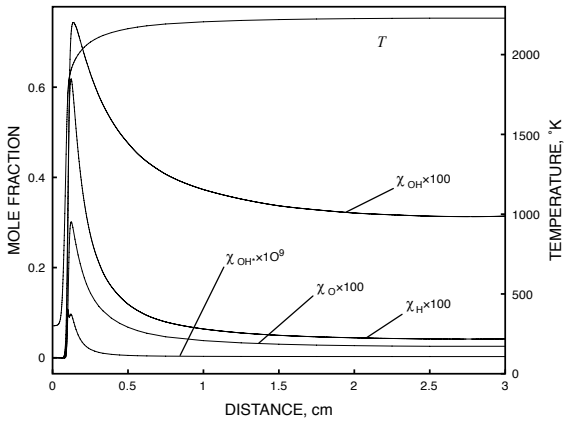

(a)

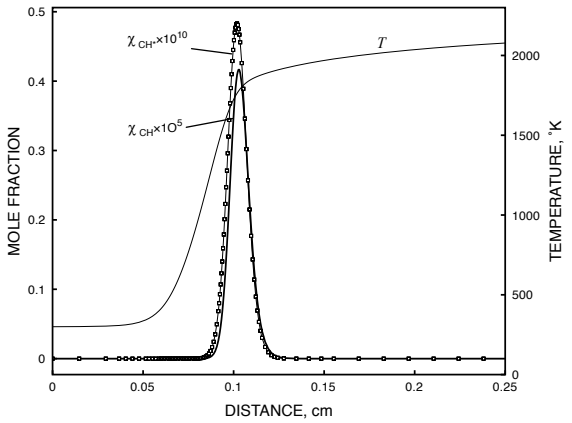

(b)

Figure 35: Species mole fraction and temperature profiles for stoichiometric CH_4-air premixed flame; (a) T, χ_{H}, χ_{OH}, and χ_{OH^*}; (b) T, χ_{CH}, and χ_{CH^*}

The variations of mole concentrations for OH^* and CH^* with equivalence ratio were plotted in Fig. 36. Here mole fractions, χ_i obtained from CHEMKIN were converted to molar concentrations $[\mathrm{X_i}]$ by

$$[\mathrm{X_i}] = \chi_i \frac{\rho}{MW_{\mathrm{mix}}} \tag{25}$$

$$= \chi_i \frac{P}{R_u T}, \tag{26}$$

where ρ and MW_{mix} are density and molecular weight of the mixture at a given distance along the axis, respectively. P is the local pressure, T is the local temperature of the mixture, and R_u is the universal gas constant.

For CH^*, the molar concentration was integrated along the entire axis and normalized

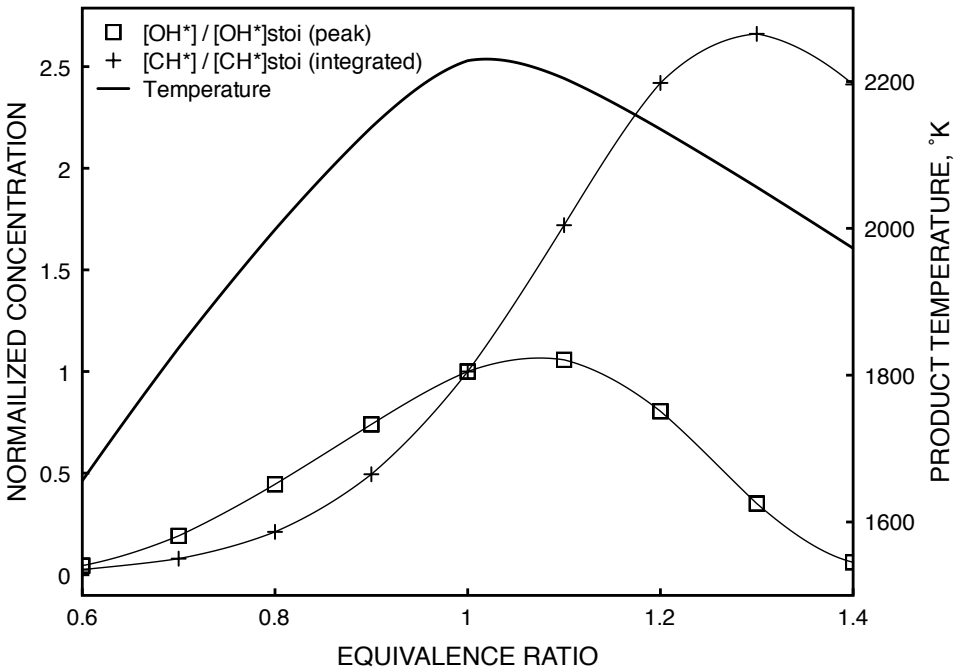

Figure 36: Variation of temperature and normalized molar concentrations of excited OH and CH radicals with equivalence ratio, calculated using PREMIX

by dividing by its stoichiometric value. Since CH appears only in a very thin flame zone, its integration is almost identical to the value estimated by integrating in the flame zone only. On the other hand, the relative peak values were used for OH^* mole concentrations because its integrated value depends strongly on the length of the axis included in the calculation (see Fig. 35(a)).

Figure 36 shows that the CH^* mole concentration increases with the equivalence ratio. This tendency was also observed experimentally (see Fig. 17). Due to the extensive presence of OH^* in the combustion products, OH^* mole concentration obtained by this method could not be compared to the chemiluminescent intensities obtained experimentally.

5.1.3 Ignition delay in a plug flow reactor

Experimental results in Fig. 28 suggested that a radical laden jet stabilizes a flame at least as well as, if not better than a purely thermal jet. This ability of radicals to stabilize a flame is

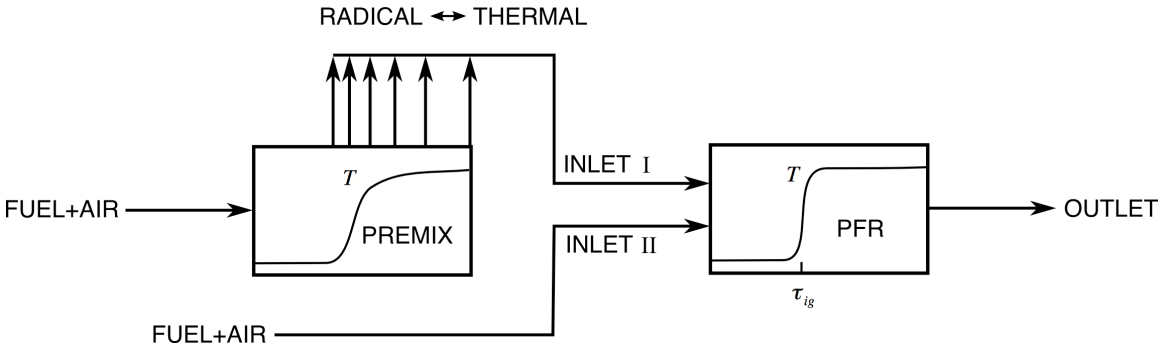

Figure 37: Schematics of premixed flame to plug flow reactor model

analyzed by calculating the ignition delay of a cold combustible mixture, when it is mixed with gas stream containing large quantities of active radicals. This ignition delay is then related to the flame stabilization limit according to the a criteria expressed in Eqn. (3); i.e.,

$$Da = \tau_c/\tau_f = 1, \tag{27}$$

where Da, the Damkohler number, is defined by the ratio of the characteristic ignition time, τ_c to the characteristic flow time, τ_f. In order to differentiate between the effect of the radicals and that of thermal energy on the ignition delay, first of all, two different gas conditions were modeled. One included a jet full of radicals while the other consisted of a completely burnt combustion product. One simple way to model a radical jet is to represent it as a premixed flame containing significant amount of active radicals. The species compositions and temperature vary along the axis normal to the flame as shown in Fig. 35. The two different types of jets can, therefore, be modeled by taking advantage of the species compositions at different locations along the axis. For example, the species compositions and gas temperature in the flame front, where there is an abundance of active radicals, while the gas temperature is still lower than the adiabatic flame temperature, was used to represent the radical jet. On the other hand, far downstream of the flame, where the combustion process was completed, was used for the thermal jet.

In the model one of these mixtures (INLET I) is then mixed with a cold stoichiometric methane-air mixture (INLET II) in a PFR, see Fig. 37. There the ignition delay time of the

cold mixture (INLET II) was calculated. This simple model assumes the following mechanism for flame ignition and stabilization by a radical jet: RJG produces a turbulent reacting jet containing many active radicals. The radicals are then rapidly, partially quenched when they mix with the cold combustible flow. The mixture then re-ignites after an ignition delay.

The abscissa in Fig. 38(a) represents the position on the axis across the premixed flame that corresponds to the local species compositions and temperature of the gas introduced through INLET I. The temperature shows the relative position of the flame. The ordinate represents the ignition delay in the PFR. Fig. 38(a) shows that the minimum ignition delay occurs when the species composition and temperature corresponding to the flame front is introduced as INLET I. Referring back to Fig. 35, it is apparent that the radical concentration at the flame front is much higher, while the temperature is lower than in the product.

Similar calculations were repeated for various equivalence ratios at INLET I. The minimum and the maximum ignition delays for these cases are plotted in Fig. 38(b). For all equivalence ratios ignition delays are significantly lower when the input to INLET I corresponds to conditions near the flame, compared to those using the fully burnt products. Since the products of rich mixtures contain more radicals than those of lean mixtures, the ignition delay decreases with equivalence ratio.

For the calculation leading to the above results, the ratio of the volumetric flow rate of INLET I to those of INLET II were 10. Because this is an arbitrarily chosen value, absolute values of ignition delay in Fig. 38 cannot be compared to experimental results. The mixing ratio will be discussed later when the maximum flame stabilization velocity by the radical jet is discussed.

This section briefly demonstrated the reduction of ignition delay by active species compared to heat. The following section develops this model further to allow it to predict the differences in ignition delays observed for the actual radical jets used in this study.

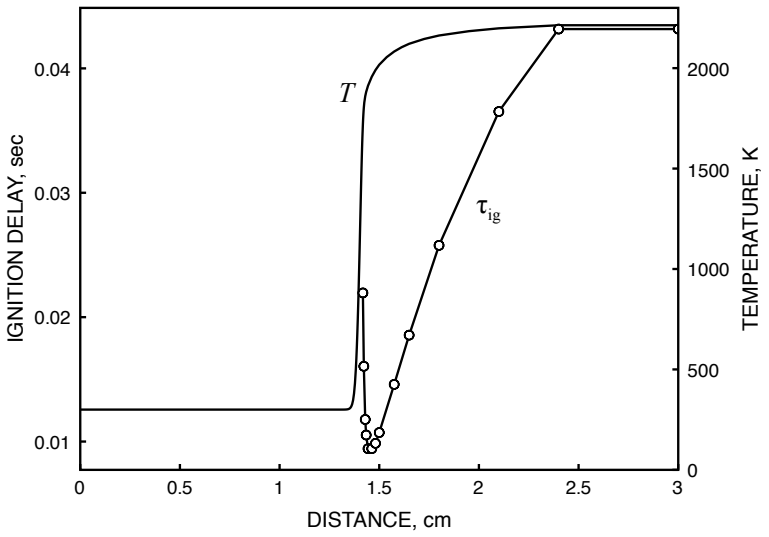

(a)

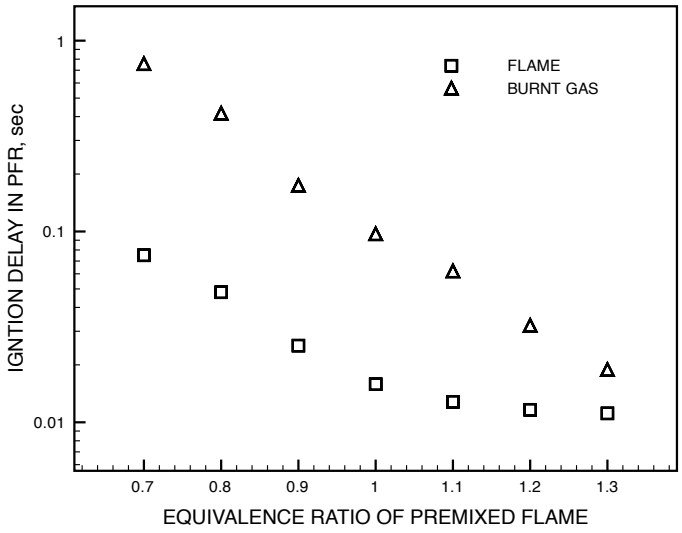

(b)

Figure 38: (a) Temperature distribution of a premixed flame of stoichiometric methane-air mixture and resulting ignition delays in a PFR (b) Difference of ignition delays between cold methane-air mixture mixed with partially and fully burnt gas, which composition is picked up at different location of premixed flame

5.2 Estimation of mean molar concentration in a radical jet

Computation of ignition delays using CHEMKIN in a previous section showed that the small amount of active radicals contained in a hot gas jet reduces the ignition delay of a cold combustible mixture significantly. Thus, the different performance on the flame stabilization by the radical jet and by the thermal jet, shown in Fig. 28, can probably be explained by the effect of active radicals contained in the radical jet. However, to confirm this explanation we must quantify the level of active radicals in the radical jet. This section introduces a method to characterize the species mole concentrations in a radical jet. These values will then be used to estimate the ignition delay in the main flow quantitatively. Furthermore, these results were then used to predict the maximum flame stabilization velocity in a main flow.

5.2.1 CH chemiluminescent intensity in a premixed laminar flame

In section 4.1, relative CH chemiluminescent levels from radical jets with various equivalence ratios were measured. The first step in characterizing the species compositions in a radical jet is to convert these relative CH chemiluminescent levels into absolute values[1]. A PMT output for CH* emission at stoichiometric in a Bunsen burner flame was obtained, and at the same time, a digital camera took a picture of the shape of the flame to calculate a flame surface area. CH* mole concentration in a flame at stoichiometric condition was then computed using CHEMKIN with extended mechanism for the excited species. The relationship between the level of PMT output and CH* concentration in a flame was estimated from these results. To avoid errors due to the geometry of the optics, all measurement of the chemiluminescent levels was carried out in the same set up.

The PMT output level is proportional to the rate of decay of the CH* to its ground state.

[1] Leo *et al.* reported a method to measure the CH* concentration in a flame using optical devices, and also reported that the CH* concentration estimated using CHEMKIN was well agreed with those obtained from experiments [68].

The rates of destruction computed with CHEMKIN show that the order of magnitude of the spontaneous decay rate of CH* to CH with emission of a photon is much smaller than those of decay rates due to other reactions such as excitations or collisional quenching. Thus the change of the mole concentration by the photon emitting reaction is negligible. Table 5.1.1 shows that the reaction rate coefficient of the reaction No. 21 is independent of the temperature of system. This implies that the rate of decay is proportional to the mole concentration only. Therefore, it can be assumed that the concentration of CH* is proportional to the level of the PMT output. The PMT output voltage per mole of CH*, κ, is given by,

$$\kappa = \frac{I_{CH^*,L}}{A_L} \left(\int_{\delta} [\mathrm{CH}^*]_c \, \mathrm{d}x \right)^{-1}, \tag{28}$$

where A_L is the flame surface area, δ is the flame thickness, $I_{CH^*,L}$ is the PMT output for the laminar Bunsen burner flame, and $[\mathrm{CH}^*]_c$ is the CH* molar concentration along the normal axis to the flame, which was calculated using CHEMKIN. For stoichiometric condition the resulting value of κ was 1.17873×10^{16}[Volt/mol] for a PMT cathode voltage of -550 V and a distance from the flame to the PMT of 27.94 cm. Here the absolute value of the PMT output is used to calculate κ.

5.2.2 Laminar flame model for radical jet

Using κ, the PMT outputs for the radical jets with the arbitrary inlet conditions can then be related to the total number of moles of CH* contained in a radical jet by,

$$I_{\mathrm{CH}^*,\phi} = \kappa \int_{jet} [\mathrm{CH}^*]_\phi \, \mathrm{d}V. \tag{29}$$

where $[\mathrm{CH}^*]_\phi$ is a local mole concentration of CH* in the radical jet. The next step is to estimate the number of mole or mole fractions of the other species contained in the radical jet. Because direct measurement of these values is impossible, they were calculated based on some experimental data in combination with a CHEMKIN simulation.

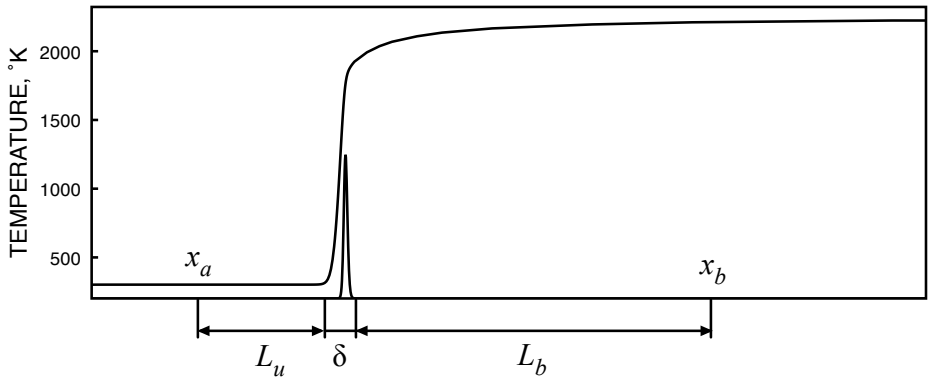

Figure 39: Schematic for estimating species mean molar concentrations in a radical jet using the laminar premixed flame result calculated by the PREMIX code; here the flame thickness is determined by CH^* distribution; L_u and L_b, are the relative width of unburned and burnt gas region, respectively, based on δ.

It was assumed that the turbulent flame in the radical jet can be represented by a laminar flame. Because the mixing region between a radical jet and a main flow is a highly turbulent, it is further assumed that the species mole fraction of the radical jet for the calculation of the ignition delay can be represented by their mean values over the entire jet volume. Using these simplifications, the mean molar concentration of CH* in a radical jet is given by,

$$\overline{[\mathrm{CH}^*]_\phi} = \frac{I_{\mathrm{CH}^*,\phi}}{\kappa V_{jet}}. \tag{30}$$

where V_{jet} is a volume of a radical jet.

A radical jet is a mixture of unburned, partially burnt, and fully burnt gas. Because it is represented here by laminar flamelets at different locations in the radical jet, species mole concentrations should correspond to the values at corresponding locations in the premixed, laminar flame. Since species mole concentrations across the premixed laminar flame are already known, if the axial positions, x_a and x_b are determined in the flame such that,

$$\overline{[\mathrm{CH}^*]_\phi} = \frac{1}{x_b - x_a}\int_\delta [\mathrm{CH}^*]_{c,\phi}\ \mathrm{d}x, \tag{31}$$

mole concentrations for other species at that location can be approximately estimated (see Fig. 39).

Since the distance from x_a to x_b is equal to the sum of the thicknesses of the unburned

mixture, L_u, the burnt mixture, L_b, and the flame, δ, Eqn. (31) is rewritten as

$$\overline{[\mathrm{CH}^*]_\phi} = \frac{1}{L_u + L_b + \delta} \int_\delta [\mathrm{CH}^*]_{c,\phi} \, \mathrm{d}x. \tag{32}$$

From the 1-D energy equation, the ratio between the length of the burnt gas to the unburned gas mixture in the model, γ is given by,

$$\gamma = L_\mathrm{b}/L_\mathrm{u} \tag{33}$$

$$= \frac{T_\mathrm{mix} - T_m}{T_\mathrm{f} - T_\mathrm{mix}} \left(\frac{\rho_\mathrm{u}}{\rho_\mathrm{b}} \right), \tag{34}$$

where T_mix is the mixture temperature obtained experimentally. From Eqn. (32) and (34), L_u is written as,

$$L_\mathrm{u} = \frac{1}{1+\gamma} \left(\frac{1}{\overline{[\mathrm{CH}^*]_\phi}} \int_\delta [\mathrm{CH}^*]_{c,\phi} \, \mathrm{d}x - \delta \right), \tag{35}$$

or by using Eqn. (30) as,

$$L_\mathrm{u} = \frac{1}{1+\gamma} \left(\frac{\kappa V_{jet}}{I_{\mathrm{CH}^*}} \int_\delta [\mathrm{CH}^*]_{c,\phi} \, \mathrm{d}x - \delta \right). \tag{36}$$

In Eqn. (36), V_{jet} and I_{CH^*} are measured experimentally and the integral of $[\mathrm{CH}^*]_{\mathrm{c},\phi}$ is calculated from the CHEMKIN result. The volume of a radical jet can be approximated as $L_j A_{jet}$ from a simple measurement by assuming that the shape of radical jet is cylindrical where A_{jet} is the cross section area of the RJG. Using these data, L_u and L_b can be calculated.

The first term inside parentheses in Eqn. (36) is obtained from Eqn. (29), which can also be written as

$$I_{\mathrm{CH}^*,\phi} = \kappa A_{s,jet} \int_\delta [\mathrm{CH}^*]_{c,\phi} \, \mathrm{d}x \tag{37}$$

from the laminar flame concept where $A_{s,jet}$ is a total flame surface area in the radical jet. Then, the flame surface area per unit volume in a radical jet, ψ, is determined by

$$\psi = \frac{A_{s,jet}}{V_{jet}} \tag{38}$$

$$= \frac{I_{\mathrm{CH}^*,\phi}}{\kappa V_{jet}} \left(\int_\delta [\mathrm{CH}^*]_{c,\phi} \, \mathrm{d}x \right)^{-1} \tag{39}$$

Therefore, Eqn. (36) can be expressed simply as

$$L_{\mathrm{u}} = \frac{1}{1+\gamma}\left(\frac{1}{\psi} - \delta\right). \tag{40}$$

With values of γ and ψ obtained from Eqn, (34) and (39), respectively, L_u and L_b are determined. Using these thicknesses, mean molar concentrations for species contained in a radical jet are estimated by equations similar to Eqn. (32),

$$\overline{[\mathrm{X_i}]_\phi} = \frac{1}{L_u + L_b + \delta}\int_{x_a}^{x_b} [\mathrm{X_i}]_{c,\phi}\ \mathrm{d}x. \tag{41}$$

Results from Eqn. (41) give the mean mole concentrations for all other species in the radical jet. Resulting mole concentrations or mole fractions replace the input conditions for the INLET I in a PREMIX-PFR model. This inlet condition characterizes a radical jet which is distinguished from the corresponding thermal jet.

5.2.3 CH* concentration in a stretched flame

The flame inside a radical jet is modeled as a laminar flame and the species mole fractions are calculated based on those in a laminar flame. Since a flame is stretched during a turbulent combustion, species composition calculated using PREMIX for an unstretched laminar flame, do not properly represent those of the flame in a radical jet. Therefore, $[\mathrm{X_i}]_{c,\phi}$ was calculated using CHEMKIN Opposed-flow Flame Model [78]. In this model, flame stretch rate is determined by the flow velocity and a distance from nozzle to a stagnation point.

For infinitesimal fraction of the flame surface, A, flame stretch is expressed in terms of local flow field and flame geometry as,

$$\frac{1}{A}\frac{\mathrm{d}A}{\mathrm{d}t} = a_T + S_d \nabla \cdot n, \tag{42}$$

where a_T is a tangential strain rate, $\nabla \cdot n$ is a flame curvature, and n is a unit vector normal to the flame surface [10, 17, 23]. The displacement speed of the flame surface, S_d is the sum of the flame speed and the flow velocity in that direction. For a flat flame in counter

flow injected from circular pipes, where there is no curvature, the flame stretch rate of cold material surface in front of the flame is expressed in cylindrical coordinates as

$$\frac{1}{A}\frac{\mathrm{d}A}{\mathrm{d}t} = \frac{\partial v_r}{\partial r} + \frac{v_r}{r} + \frac{\partial v_\theta}{r\partial\theta}. \tag{43}$$

The continuity equation results in that the stretch rate being equal to $-\partial v_x/\partial x$ where x

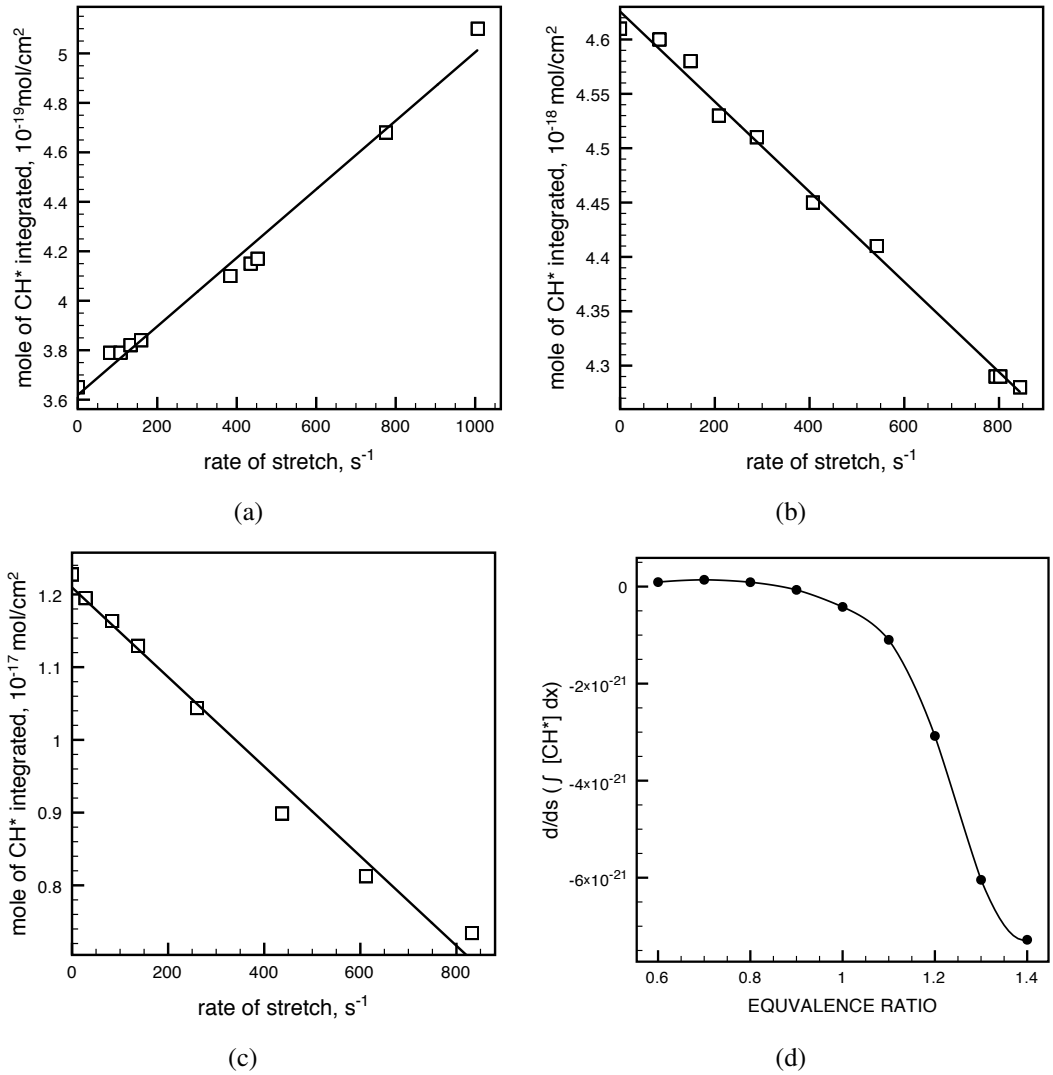

Figure 40: Variation of CH* mole concentration integrated along the axis with the rate of strain; (a) ϕ=0.7, (b) ϕ=1.0, (c) ϕ=1.3, (d) rate of change of CH* with equivalence ratio, s is a rate of stretch

is in the direction perpendicular to the flame surface. In a simulation with CHEMKIN, the normal strain rate, $-\partial v_x/\partial x$ shows a local maximum just in front of the flame where the

flow velocity is not yet affected by the temperature increase. These values were used for the stretch rate of the flame. The CH* mole concentration was integrated along the axis in a opposed flow flat flame for a given equivalence ratio for conditions with different normal strain rates. When the strain rate is very high, flame was extinguished in a symmetric counter flow with cold fuel-air mixture. In this cases, asymmetric conditions with a product flow for one side was used. Because of the presence of product in any region with turbulent combustion, the use of results based on the asymmetric condition is more appropriate [17]. Figure 40 shows how the number of moles of CH* per unit flame area varies with the stretch rate and how this dependence varies when the equivalence ratio is changed. In a lean mixture, the number of mols of CH* increases with the stretch rate, but it decrease with the stretch rate in stoichiometric and rich mixtures. For all cases, these variations are linear.

To characterize the turbulent combustion in a radical jet the r.m.s flame stretch is determined by assuming homogeneous, isotropic turbulence for simplicity. In turbulent combustion with high turbulent velocities, flame propagation and curvature effect to flame stretch become less important than the flame stretch caused by the stretch of the flow field in front of the flame. As a result the mean Lagrangian stretch rate is proportional to the Eulerian mean strain rate, u'/λ for isotropic turbulence [10, 17]. Yeung *et al.* reported the result of direct numerical simulation for the distribution of the stretch rate about the mean in constant density, homogeneous, isotropic turbulence. On the basis of this results, Bradley *et al.* reported that r.m.s stretch rate, σ_s, of a premixed flame is determined by,

$$\sigma_s = 1.32\, u'/\lambda \tag{44}$$

for a material surface, and

$$\sigma_s = u'/\lambda. \tag{45}$$

for a randomly orientated surface where λ is the Taylor microscale [17, 134]. Eqn. (44) is appropriate when the laminar flame speed is not much larger than the Kolmogorov velocity

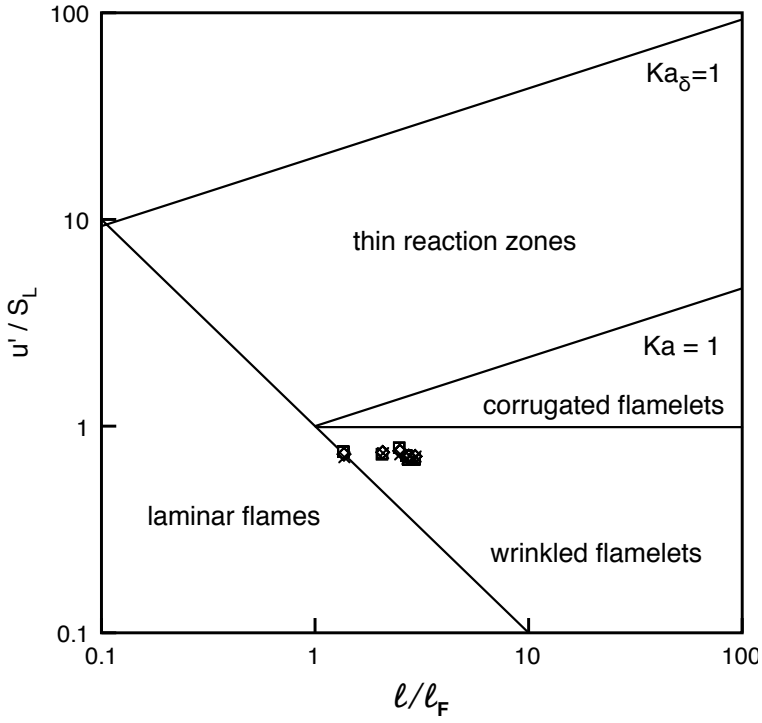

Figure 41: Borghi diagram, turbulent regime

scale, so the flame surface is close to the initially coincident material surface. This limit condition is expressed by $Ka \geqslant 1$ where Ka is a Karlovitz number. On the other hand, Eqn. (45) is used if the laminar flame speed is much larger than to the Kolmogorov velocity scale since, in that case, the flame surface element is randomly oriented and similar to the Eulerian stretch rate [17, 134]. The flow conditions of a radical jets are examined using proper length and velocity scales obtained from the empirical correlations reported in Refs. [1] and [17]. For a given RJG geometry and inlet flow conditions, turbulent intensity, u' and the integral length scale, ℓ are calculated using Eqn. (18) and

$$R_\ell = 13.45 \times 10^{-3} Re^{0.902} \quad \text{for} \quad 70 < R_\ell < 3000, \tag{46}$$

where R_ℓ is the turbulent Reynolds number$(= u'\ell/\nu)$, respectively. For isotropic turbulence, λ is obtained from integral length scale by,

$$\frac{\lambda}{\ell} = \left(\frac{A}{R_\ell}\right)^{1/2} \tag{47}$$

with the value of A equal to 40.4 [17]. The resulting values of the turbulent intensities and

the integral length scale yields the regime of the turbulent combustion in the radical jet approximately.

Figure 41 shows the regimes of turbulent combustion based on the the length and velocity scales related to the flow and chemical reaction. Turbulent combustion created by the conditions, which were typically used for the radical jet in this study falls into the flamelet regime. This implies that the r.m.s stretch rate for turbulent combustion in a radical jet can be determined by Eqn. (44).

The number of moles of CH* per unit flame area in a laminar flame with stretch corresponding to the inlet conditions used in the experiments was calculated using the method described above. These values and the measurement results for CH chemiluminescent levels as well as the volume of the radical jets were used in Eqn. (39) and (40) to yield the flame surface area per unit volume and the unburned gas thickness in the model, respectively.

5.2.4 Results

Figure 42 shows γ for different radical jet equivalence ratios. Since the fraction of burnt gas in a mixture increases with the flame speed for a given geometry of the RJG, γ, the volume ratio of burnt to unburned gas increases when the equivalence ratio of the mixture becomes closed to stoichiometric. Values of γ plotted in Fig. 42 correspond to the temperature data measured in the coaxial flow RJG with an inlet velocity of about 13.7 m/s. Since the temperature of the radical jet is influenced by the type and size of the RJG, by the operating flow velocity, and, especially for a coaxial RJG, by the main flow velocity, γ depends also on these parameters. For example, the jet temperature data obtained from the test using an elbow type RJG are slightly higher than those obtained from co-flow RJG, because lower inlet flow velocities were used and there was no heat loss to the outer flow (see Fig. 29). In that case, the values of γ are slightly larger than those shown in Fig. 42.

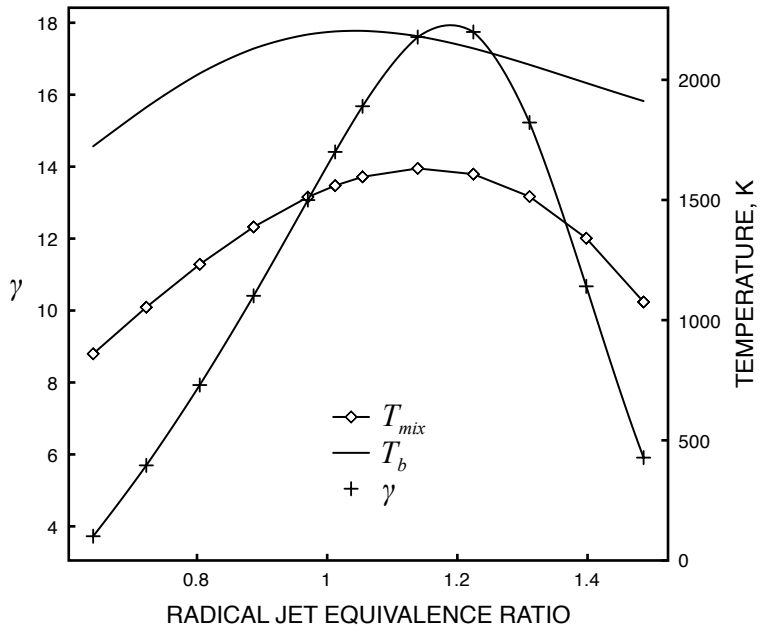

Figure 42: Ratio of L_b to L_u in a mean mole concentration model; T_b, burnt gas temperatures are obtained from CHEMKIN; T_{mix}, radical jet temperatures are curve fitted with average values measured at the centerline of RJG exit.

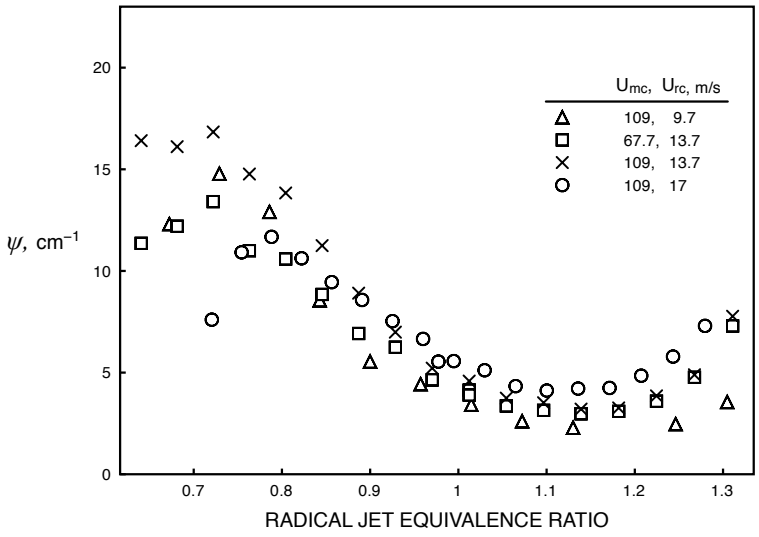

Figure 43: Fame surface area in a unit volume of radical jet with various equivalence ratios and velocities

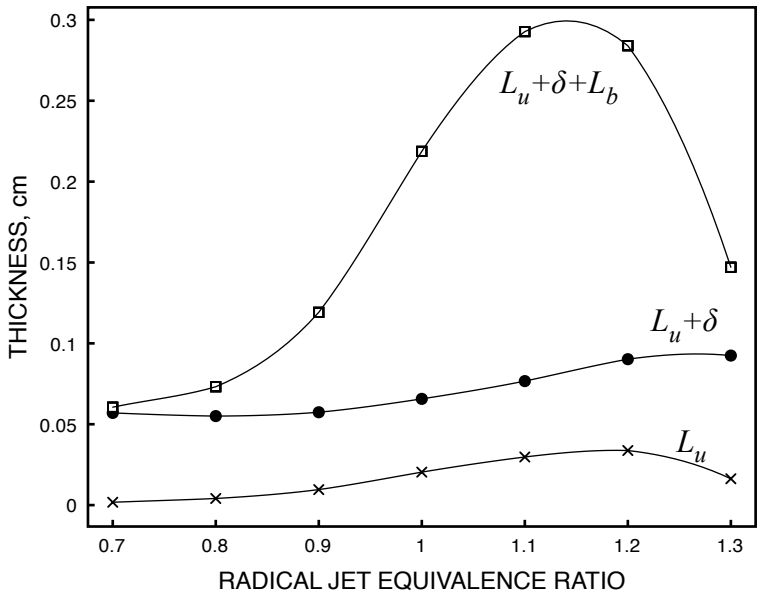

Figure 44: Calculated thickness of L_u, L_b, and δ in a mean mole concentration model

Figure 43 shows the flame surface area per unit volume of radical jet, ψ as calculated using Eqn. (39). The figure shows that lean and rich radical jets contain larger flame surface areas per volume of jet than the stoichiometric jet. The flame surface area can be increased by increased wrinkling of the flame. However, for a given flow velocities, which means a given turbulent intensity, the wrinkling of the flame does not vary significantly with change in equivalence ratios [48]. Therefore, a decrease in flame surface area may be caused by smaller amounts of unburned gas remaining in the mixture and the resulting higher flame temperature in the stoichiometric or slightly rich radical jet (see Fig. 42).

When CH* chemiluminescent levels were measured for radical jets with fuel rich mixtures in a high velocity outer air flow, the chemiluminescence from the rich flame was mixed with that from the partially premixed or diffusion flame. Since the latter is leaner than the initial pre-mixture the light intensity was reduced. Thus the value of the PMT output divided by the number of moles of CH* calculated for premixed flame of given rich equivalence ratio can be under estimated, and, consequently, ψ can be under estimated. This may be the reason that Fig. 43 shows relatively low values of ψ under rich conditions compared to those under the lean conditions. In addition, there exists an uncertainty in the

measurement of the volume of the jet, which also affects the values of ψ. The effect of these uncertainty on the final results, i.e., on the ignition delay and maximum flame stabilization velocity, will be discussed later.

Species mole fractions in a given radical jet were estimated using Eqn. (41) and compared to those in the flame zone and products of a stoichiometric methane-air premixed flame. Figure 45(a) shows that the mole fractions of active species in the radical jet (gray) are higher than those in the products gas (white), although the radical jet contains some unburned fuel. Figure 45(b) shows that the mole fractions of radicals changes with the RJG inlet velocity. Since high inlet velocities in the radical jet increase the turbulent intensity causing the flame in the jet to become more wrinkled, the flame surface area per unit volume increases. This, in turn, reduces the total thickness of a laminar flame, $L_u + L_b + \delta$ in the model. Therefore, according to Eqn. (40), the relative ratio of unburned and product gas to reacting gas in the flame decreases. This results in high radical mole fraction in the radical jet with high inlet velocity, unless the temperature drop that can increase the amount of the unburned gas is not significant.

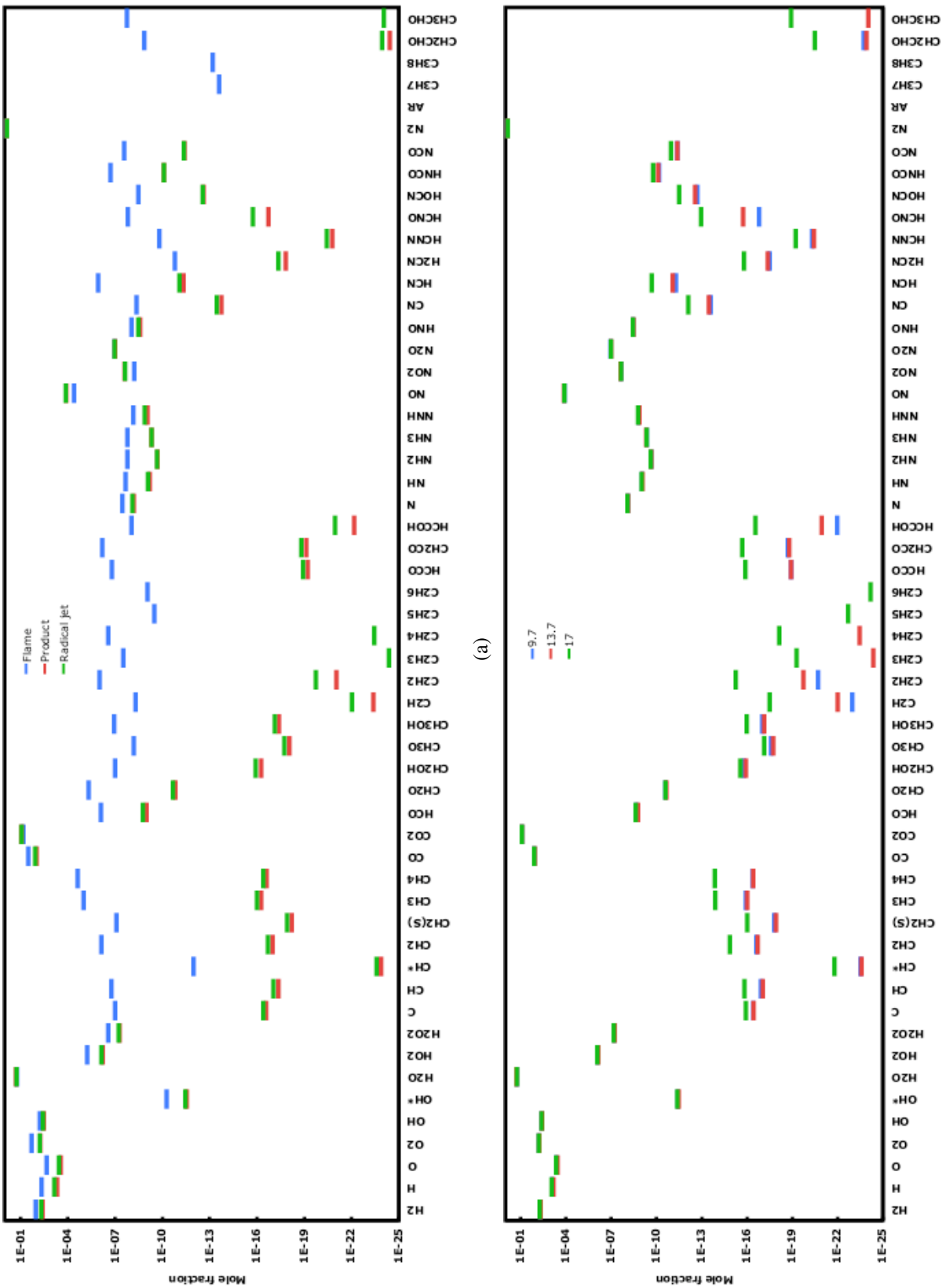

Figure 45: Mole fractions of radicals (a) in a flame zone, products, and radical jet, (b) in radical jets with different flow velocities

5.3 Reduction of ignition delay by active radicals

The previous section describes method by which the average molar concentration of species in a radical jet were determined. This section focuses on the effect of active radicals added into an otherwise thermal ignition regime, and the change of ignition delay caused by these radical jet. Based on these results, a relationship between the ignition delay for a given mixture condition and the to be expected maximum flame stabilization velocity will be developed in the next section.

5.3.1 Role of radicals on ignition delay

Ignition delay is determined by the rate of accumulation of active radicals during pre-ignition chemistry [66]. Figure 45 shows that H, O, and OH are major radicals in flame and product gases. Thus, these radicals may be expected to play an important role in the process of ignition by radical jets. During the initial stage of methane-air combustion, H radicals are produced by the reactions $CH_4 + M \rightarrow H + CH_3$, and $CH_3O + M \rightarrow H + CH_2O + M$. Third body collision and the reaction $N_2 + O_2 \rightarrow N_2O + O$ are main mechanisms to produce O. OH radicals are produced by the reaction $CH_3 + O_2 \rightarrow OH + CH_2O$. These reactions promote radical accumulation, while radicals are terminated, for example, by the reaction with CH_4 from which CH_3 is produced.

$$\{H,\ O,\ OH\} + CH_4 \rightarrow \{H_2,\ OH,\ H_2O\} + CH_3. \tag{48}$$

When a radical jet is injected into a high speed combustible flow, the two flows mix with each other in a highly turbulent mixing layer. Most active radicals contained in a flame in the hot product region of the radical jet are terminated by reactions, such as those in Eqn. (48), shortly after mixing. However, small amount of radicals remain. The molar concentrations of the remaining radicals are still much higher than those in the early stage of pre-ignition chemistry of a combustible mixture ignited by a purely thermal ignition

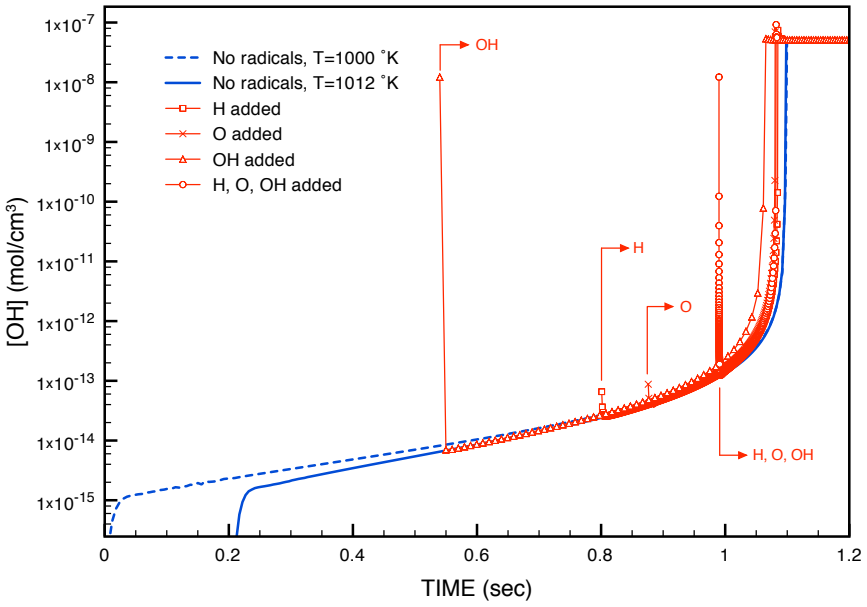

Figure 46: Variation of OH mole concentration with time for stoichiometric CH_4-air mixture with additional radicals

source. Therefore, the ignition delay time is reduced by the time it would have taken the ignition chemistry to generate the additional radicals supplied by the radical jet.

Figure 46 shows the variations of OH molar concentrations with time during an induction period calculated in a plug flow reactor for a stoichiometric CH_4-air mixture. The cases without radicals augmented with inlet temperature of 1000°K and 1012°K are represented by the dotted and solid lines, respectively. For the latter case, the time axis is shifted to match the steep increase in [OH] at ignition with the former. Other cases represented by various symbols show accumulations of [OH] when small amount of H, O, or OH radicals were added at the time indicated. When H radicals, which normally amount to 0.01% of the CH_4-air mixture, are augmented, the total mixture temperature increases from 1000°K to 1012°K. Augmentations of O and OH radicals cause similar temperature increase. For the cases with radicals augmentation, the time axes were shifted such that the OH mole concentrations after recombination or termination are equal to those of the pure mixture with initial temperature, 1012°K. Figure shows that the rate of radical accumulation is not changed significantly by the small augmentation of radicals. However, it changes the initial

concentrations of radicals instantaneously and can reduce ignition delay significantly.

5.3.2 Simple expression for ignition delay

Any prediction of the ignition and the flame stabilization by a radical jet requires an estimate of the ignition delay of the high speed combustible flow ignited by the jet. When the igniting gas properties are given, the ignition delays are readily evaluated by computational codes as was shown in Sec 5.1. However, the use of these codes depends on the assumption of idealized reactors, such as, a perfectly stirred reactor or a plug flow reactor. Extensive computations are required to model more precisely the ignition distance for radical jet ignition that can be compared with the characteristic chemical time data reported for the cases of many bluff body flame holders. This is because the full chemical mechanism for the combustion process mush be solved together with the flow model. This must be solved repeatedly for the ignition delay depending on the local mixture conditions. To avoid this problem, this study uses a relatively simple experimental correlation to determine the local ignition delay.

The ignition delay times have been measured from shock tube experiments by many researchers for homogeneous methane-oxygen-diluent gas mixtures for various temperatures, pressures, and mixing ratios. It has been found that the ignition delays of such mixtures are correlated in the following empirical form (see Ref. in Table 4),

$$\tau_{\mathrm{ig}} = A \exp\left(E/R_u T\right) [\mathrm{CH_4}]^{\alpha} [\mathrm{O_2}]^{\beta}, \tag{49}$$

where ignition delay, τ_{ig} is in sec, and $[\mathrm{CH_4}]$ and $[\mathrm{O_2}]$ are the molar concentrations $(\mathrm{mol}/\mathrm{cm}^3)$ of the reactants. A is an empirically determined constant and E is an apparent energy of the induction period, which is equivalent to a global activation energy [105]. Exponents, α and β represent the power dependencies of the ignition delay on the mole concentrations of $\mathrm{CH_4}$ and $\mathrm{O_2}$. The exponents of the mole concentration of diluting gases, such as Ar or $\mathrm{N_2}$,

Table 4: Coefficients for an empirical correlation representing τ_{ig} in a homogeneous methane-air mixture

A	α	β	E_a (kJ/mol)	Temperature ($^\circ$K)	Source
-	-	-	159−264	1200 − 1800	Skinner [100]
-	-	-	88−117	850 <	Terao [112]
-	-	-	138		Kistiakowsky [61]
-	−1.0	−1.0	86	900 − 1400	Asaba [7][a]
-	−1.0	−1.0	221	1300 − 2000	Asaba [7][b]
2.77×10^{-12}	0	1.0	83.7		Walker [125]
-	-	-	133.8	1800 − 2500	Higgin [52]
-	-	-	144	800 − 2500	Soloukhin [104]
-	-	-	207	1420 − 2010	Miyama [86]
-	-	-	234	2000 − 2600	Glass [40]
7.65×10^{-18}	0.4	−1.6	215	1150 − 1880	Seery [98]
3.62×10^{-14}	0.33	−1.03	194.5	1500 − 2150	Lifshitz [72]
$1.00 \times 10^{-13.1}$	0	−1	213.4		White [128, 119]
2.50×10^{-15}	0.32	−1.02	222	1200 − 2100	Tsuboi [119]
4.40×10^{-15}	0.33	−1.03	218.8	1640 − 2150	Grillo [45]

[a] For cases with $CH_4/O_2 \leqslant 50/50$.
[b] For cases with $CH_4/O_2 > 50/50$.

are typically equal to zero [72, 119]. Researchers have determined the values of these parameters by plotting log τ_{ig} against $1/T$ or log [X_i] and finding slopes, while other variables remained unchanged. Table 4 summarized some results suggested by these researchers.

Equation (49) is applicable only for the thermal ignitions. However, the effect of the presence of radicals may be accounted for by adjusting the apparent energy of ignition in the same equation. The apparent energy of ignition for use with the radical jet is obtained by adjusting its value until the ignition delay of a methane-air mixture ignited by an inert gas with the same temperature as that of a radical jet is equal to that of the same mixture ignited by the radical jet. In this case, the latter is calculated using CHEMKIN and the species compositions of the radical jet are modeled by the method described in the previous

section.

When thermal ignition delays are calculated using Eqn. (49), the temperature, and fuel and oxygen concentrations in the mixture of hot N_2 and cold reactants are determined by the mixing ratio of the volume flow rates and initial gas temperatures before mixing. Assuming constant pressure, adiabatic, and non-reacting conditions, the mixture temperature can be calculated using from the energy conservation,

$$\frac{Q_{re}}{Q_j}\frac{T_h}{T_c}\left(\sum_i \chi_{i,re}\, MW_i \int_{T_c}^{T} c_{p,i}\, \mathrm{d}T\right) = MW_j \int_{T}^{T_h} c_{p,j}\, \mathrm{d}T, \tag{50}$$

where $\chi_{i,re}$ is the mole fraction of the species i in the cold reactants, and Q_{re}/Q_j and T_h/T_c are the ratios of the initial volume flow rate, and temperature of the cold reactant to hot gas, respectively. The subscript j represents the hot gas species. Typically N_2 is used as the diluent. Mole concentrations of the fuel and the oxygen in the mixture were calculated using initial flow conditions and the temperature obtained from Eqn. (50). Species mole fractions in the mixture were determined from their definition as,

$$\chi_{i,mix} = \chi_{i,re}\frac{N_{re}}{N_{re}+N_j} \tag{51}$$

where N_{re} and N_j are the molar flow rates of the reactant and the hot gas before mixing, respectively. Mole fractions of the reactants in a final mixture are rewritten in terms of the initial volume flow rates and temperature as

$$\chi_{i,mix} = \chi_{i,re}\left(1+\frac{\dot{Q}_j}{\dot{Q}_{re}}\frac{T_c}{T_h}\right)^{-1}. \tag{52}$$

and thus, the mole concentrations are obtained from Eqn. (26) and (52),

$$[\mathrm{X_i}] = \chi_{i,re}\left(\frac{P}{R_u T}\right)\left(1+\frac{\dot{Q}_j}{\dot{Q}_{re}}\frac{T_c}{T_h}\right)^{-1}. \tag{53}$$

Figure 47 shows the ignition delays obtained when a 300°K methane-air mixture was ignited by N_2 gas at various temperatures (solid lines). The ratio of the volume flow rate of the hot gas to that of the cold reactant is assumed to be 10. Values of parameters in Eqn. (49) refer to those recommended by Grillo *et al.* [45]. Figure 47 also shows the ignition

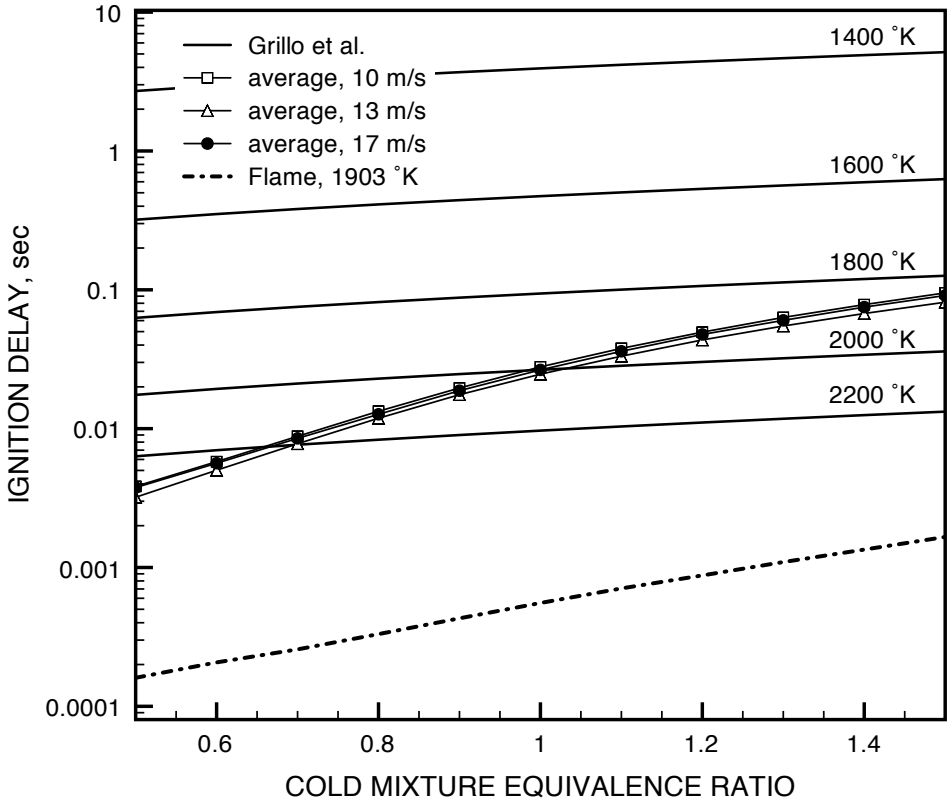

Figure 47: Thermal ignition delays calculated with empirical correlation and ignition delays by RJG calculated by CHEMKIN

delays calculated using CHEMKIN when the hot gas is replaced by a mixture with the compositions of the radical jet, as calculated in Sec. 5.2. For a stoichiometric reaction, the ignition delay by the radical jet, whose temperature is about 1500°K, is equivalent to that of an equivalent thermal (N_2 only) jet at 2000°K. In these cases, the gas temperatures after mixing are about 1110°K and 1340°K, respectively. This means that the effect of the radicals is equivalent to raising the temperature of the mixture by 230°K or decreasing the activation energy from 218.8 to 181.2 kJ. Similarly, when the radical mole fractions and the temperature in the flame front where H radical has a peak value is used to characterize the radical jet, ignition delay became much shorter. The equivalent energy of ignition in this case is about 170 kJ.

Interestingly, ignition delays for the radical jets show larger variations with reactant equivalence ratio than those by the pure N_2 gas. Because the variation of the final mixture

temperature between lean and rich cases is not significant, this result suggests that the reactions involving active species added by the radical jet are sensitive to the reactant equivalence ratio. As described in Sec. 5.3.1, ignition delays are strongly affected by the minimum concentrations of radicals such as, O, H, and OH available to the ignition process shortly after mixing. The reactions in Eqn. (48) are responsible for the initial decrease of those radicals. Among these reactions, the reaction between OH and CH_4 has been known to be fastest [41]. Time variations in the rate of production of CH_3 simulated using CHEMKIN also showed that the reaction between OH and CH_4 is a major source of CH_3. This reaction is followed by reaction:

$$OH + CH_3 \rightarrow CH_2(S) + H_2O, \tag{54}$$

where $CH_2(S)$ is a singlet state of the methylene radical. This represents a mechanism for reducing OH just ahead of the ignition process. Once the excessive OH are terminated, normal ignition process starts and, in this period, the total rate of production of OH increases due to reactions like,

$$H + O_2 \rightarrow O + OH. \tag{55}$$

Comparison between lean and rich cases showed no big differences in reactions responsible for determining the minimum concentrations of the active species except for their rate of reaction. Resulting monotonic variations of ignition delay also suggests that no different reaction mechanisms exist that governs the delay time for different equivalence ratio of the reactants. Therefore, high mole concentrations of CH_4 in rich mixture, and, thus high reaction rate of Eqn. (48) and (54) may be the primary reason for the lower minimum concentration of active species after mixing, which results in the observed longer ignition delays through. The relatively low reaction rate of Eqn. (55) also appears to contribute.

This large variation of the ignition delay with reactant equivalence ratio does not allow the use of a single value of the apparent activation energy, E to characterize ignition delay using Eqn. (48) for a given radical jet. Another obstacle to the development of a correlation between an adjusted value of E and the ignition delay is the dependency of the mole

concentrations on the mixing ratio between hot and cold reactants. However, the deviation of ΔE due to the change of the mixing ratio is relatively small. Thus, a given value of E, adjusted for a radical jet, may be used if the reactant equivalence ratio is given.

Another farther that has to be considered in determining the maximum flame holding velocity is the presence of a recirculation zone. Rehab *et al.* observed that, for concentric flows, the outer flow causes a reverse flow downstream of the potential core of inner jet. Furthermore, the potential core is truncated by the outer flow when the the velocity ratio, r_u, or momentum flux ratio, M, of the outer flow to the inner one increases beyond a critical value, which is about 8 [96]. Such a recirculation zone was readily observed in this experiment, for example, as brightness changes along the centerline of the radical jet images when the outer main flow velocity is very high, see Fig. 31 and 32. When such a recirculation zone is created, the properties of the radical jet downstream are changed. First of all, a temperature change is expected because of a certain amount of the main flow enters into a radical jet and may be burnt there. This can change the temperatures of radical jet downstream of the recirculation zone, from those shown in Fig. 22. In this case, the radial jet temperature depends also on the main flow equivalence ratio, and degree of entrainment of the recirculating gas. Another effect is the change in the average composition of the radical jet, which requires that the activation energy to be adjusted.

Because of these change of jet properties, maximum flame holding velocity cannot be estimated and cannot be compared to the experimental results without considering recirculation. The results in Fig. 47 and the experimental results in Fig. 30 can there be explained: In Fig. 30 the maximum flame holding velocities are observed when the main flow equivalence ratio is near stoichiometric. However, ignition delay study showed that the leaner mixture always has a shorter ignition delay, which means that such a mixture should be able to stabilize combustion at the higher velocity when the temperature of the ignition source is fixed. SInce the above mentioned entrainment changes the properties in the radical jet, the activation energy and radical jet temperature need to be adjusted to take into

account the effect of recirculating flow.

5.4 Approximation solution for flame stabilization limit

5.4.1 Ignition distance model

In the flame stabilization by a coaxial radical jet, the main flame is ignited and anchored in a mixing layer between the inner, high temperature jet and the annular, combustible main flow. If it is assumed that the radical jet, which may include a recirculation zone downstream, is a non-reacitive gas jet, this configuration is modeled by a compressible turbulent mixing layer theory with different stream velocities, different densities, multi species, and a chemical source term. Since the turbulent mixing layer is very thin compared to the RJG nozzle radius, the effect of curvature can be assumed to be negligible, and thus, the mixing layer can be treated as a plane mixing layer. Some references further demonstrated experimentally that a plane mixing layer approximates the axisymmetric case very well, certainly with precision sufficient for engineering applications [113].

In bluff body flame stabilization, similar problems have been solved using various methods to determine the ignition distance [80, 24, 129]. Those studies used the same configuration to solve the ignition location at which the first temperature peak appears. However, the results were very sensitive to the method used to solve the problem, as well as to initial conditions, as pointed out by Williams [129]. The main difficulties in solving this problem analytically arise from the presence of the chemical reaction term, which causes no similarity solution to be available. In this study the chemical source term is neglected because the heat production in a pre-ignition chemistry is negligible, i.e, it is assumed that the chemical reaction starts suddenly when ignition delay time has passed, and the ignition delay time varied with the local mixture conditions. Then, the ignition distance is determined by the location, at which the flow time of combustible mixture element equals the local ignition delay time. A radical jet is assumed by a non-reactive gas. Then the effect of radicals

is applied through modifying the apparent energy of ignition which was developed in the previous section. Using this method, ignition distances and maximum flame stabilization velocities in the main combustor can be estimated for various operating conditions.

Without the chemical source term, the mixing layer between the radical jet and the main flow is represented by much simpler forms of the compressible flow equations. These equations can be further simplified by transforming them into an incompressible form using proper coordinate transformations, such as the Howarth transformation [54] which assumed that $\rho\mu$ is constant [24, 54, 80]. According to that, the coordinate system is transformed using

$$y = \int_0^{y_o} \frac{\rho}{\rho_\infty} \mathrm{d}y_o \tag{56}$$

$$x = x_o. \tag{57}$$

Additionally, a constant pressure field is assumed in the momentum equation and the viscous dissipation is neglected in the energy equation. It should be noted that the longitudinal dimension is not affected by the above transformation. Because the axial ignition distance from the origin is only interesting quantity, and the scale of axial distance is not changed by the above transformation, an inverse transformation is not required [24]. Applying the transformation and the assumptions leads to a set of incompressible conservation equations for mass, momentum in the x direction, energy, and species. Then, the resulting velocity, temperature, and the reactant mass fractions are self-similar in the transformed coordinate system.

In a self-similar plane mixing layer, the cross-stream coordinate scale, η, is defined by

$$\eta = \frac{y}{\delta(x)} \tag{58}$$

where $\delta(x)$ is the mixing layer thickness determined in the transformed coordinate. Then, two characteristic velocities which are not functions of x, are defined to represent a scaled velocity, i.e., the average velocity,

$$U_c = \frac{1}{2}\left(U_h + U_l\right), \tag{59}$$

and the velocity difference,

$$U_s = U_h - U_l. \tag{60}$$

U_h and U_l represent a high and low stream velocities, respectively. In this study the main flow velocity is usually higher than that of radical jet. The main flow velocity, U_m, and the radical jet velocity, $U_{RJG,hot}$, correspond to U_h and U_l in Eqns. (59) and (60), respectively.

The scaled velocity which is independent of the axial distance is defined as

$$f(\eta) = \frac{U - U_c}{U_s}. \tag{61}$$

Provided that the Prandtl number and Schmidt number are constant and equal to one for simplicity, and since the energy and species equations have the same mathematical form as the momentum equation, other scaled variables can be similarly defined using the velocity profile as,

$$\frac{F - F_c}{F_s} = f, \tag{62}$$

$$\frac{O - O_c}{O_s} = f, \tag{63}$$

$$\frac{T - T_c}{T_s} = -f \tag{64}$$

where F and O are the fuel and air mass fraction, respectively. Then local variables are then expressed in terms of the scaled velocity, f,

$$U = U_s f + U_c, \tag{65}$$

$$F = F_s f + F_c = F_s(f + \frac{1}{2}), \tag{66}$$

$$O = O_s f + O_c = O_s(f + \frac{1}{2}), \tag{67}$$

$$T = T_c - T_s f, \tag{68}$$

$$\rho = \frac{pMW_{mix}}{R_u(T_c - T_s f)}. \tag{69}$$

For example, when the turbulent viscosity is uniform, the similarity solution has the form of an error function. These results agrees well with experimental data [91]. Because a similarity solution for plain mixing layer has been known, the resulting profiles can be used for f, or more simple profiles may be assumed to simplify further calculations.

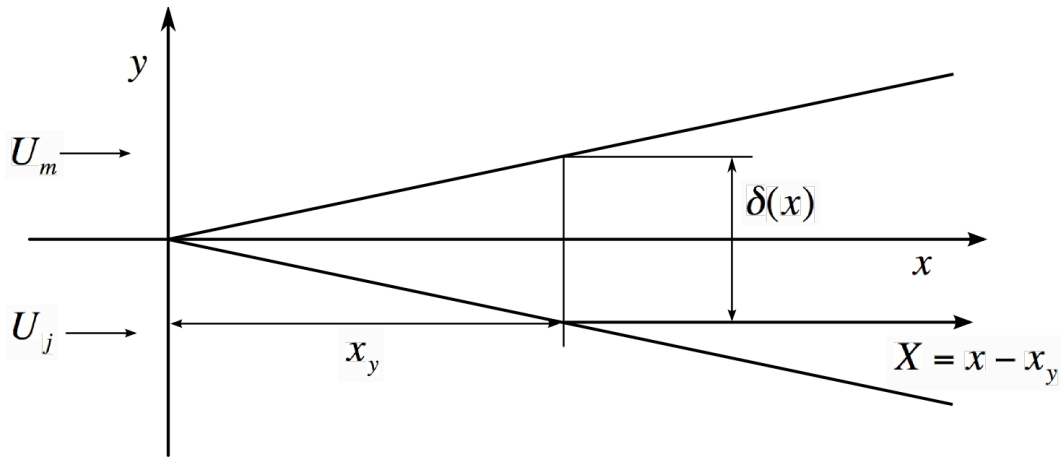

Figure 48: Transformed coordinate to describe a mixing layer between a hot gas jet (lower) and a cold main flow (upper)

Figure 48 shows the simplified mixing layer between the hot gas and cold main flow in a transformed coordinate system. Here, the virtual origin is assumed to be located at $x = 0$. Outside of the mixing layer, the ignition delay is infinite, because there is no combustible mixture on the hot gas side, and on a cold mixture side, the temperature is too low to ignite the flow. A finite ignition delay time is available only inside the mixing layer. Another longitudinal dimension, X is therefore defined to represent the distance measured from the edge of a mixing layer. Since the local temperature, and fuel and oxidizer concentrations vary with X, the ignition delay of the mixture traveling in a mixing layer between a non-reacting hot gas and a cold combustible mixture is expressed using Eqn. (49) as,

$$\tau_{ig} = A \exp\left(\frac{B}{T(X)}\right)\left(\frac{F(X)}{MW_{\mathrm{F}}}\right)^{\alpha}\left(\frac{O(X)}{MW_{\mathrm{Ox}}}\right)^{\beta}\rho(X)^{\alpha+\beta} \tag{70}$$

Because we are only interested in the axial distance, it is assumed that mean flow stream lines are parallel to x-axis throughout the mixing layer. The flow, therefore, experiences change in local velocity, temperature, and reactant concentrations along X.

Figure. 49 shows the cross stream variation of ignition delay in a mixing layer calculated using Eqn. (70). Approximate profiles are used for $f(\eta)$ to represent the mass fraction of reactants. Consequently, the temperature distribution is expressed by $-f$. The values of f show that the hot gas exists in a left side where $\eta < 0$, and the main combustible mixture

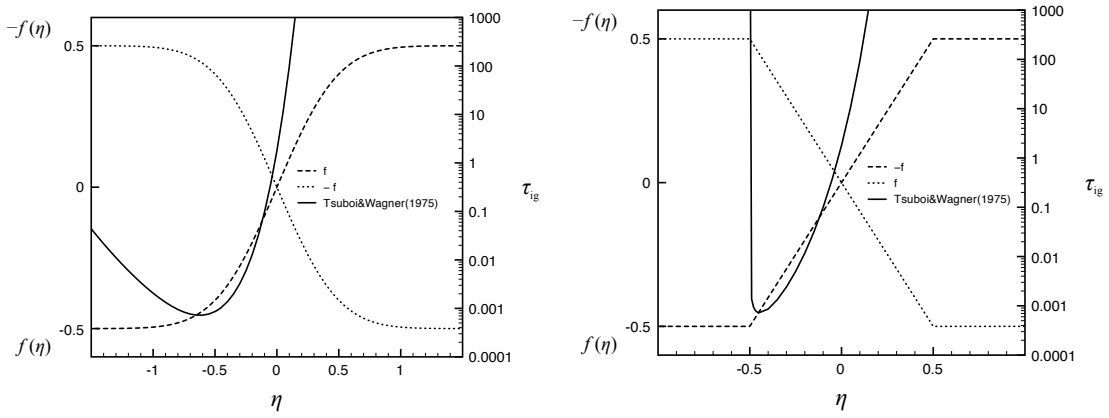

Figure 49: Variation of ignition delay in the cross stream direction in a mixing layer, calculated using Eqn. (49) with local temperature and reactant concentration; self similar temperature and mass fractions of reactant are distributed by (a) error function and (b) a straight line; negative η represent the hot gas side.

is in the other side. Since the ignition delay is strongly influenced by the mixture temperature, which decreases with decreasing η. However, the ignition delay increases again at the vicinity of a mixing layer edge in a radical jet side because of the very low reactant concentrations in that region.

The travel time to reach to an arbitrary location X from the mixing layer edge is expressed simply as

$$\tau_f = \int_0^X \frac{\mathrm{d}X}{U} \tag{71}$$

By definition of the ignition distance, ignition occurs at the location where

$$\tau_f = \tau_{ig}. \tag{72}$$

Because any point, at which $X \geqslant 0$, falls inside the mixing layer, the properties at the ignition point can also be represented by those at a certain value of η. Therefore, substituting Eqn. (66) to (69) into Eqn. (71) allows that the ignition delay at a certain point in mixing layer to be represented by the similarity variable. Then, Eqn. (72) can be written as

$$\int_0^X \frac{\mathrm{d}X}{U} = A \exp\left(\frac{B}{T_c - T_s f}\right) \left(\frac{F_s}{MW_{\mathrm{F}}}\right)^{\alpha} \left(\frac{O_s}{MW_{\mathrm{Ox}}}\right)^{\beta} \left(\frac{pMW_{mix}}{R_u} \frac{f + 1/2}{T_c - T_s f}\right)^{\alpha+\beta}. \tag{73}$$

In a plane self-similar mixing layer, the spreading rate, $\mathrm{d}\delta/\mathrm{d}x$ is independent of axial distance, and is determined using a non-dimensional parameter,

$$S = \frac{U_c}{U_s}\frac{\mathrm{d}\delta}{\mathrm{d}x} \tag{74}$$

The value of S measured experimentally ranges from 0.06 to 0.11[91]. Using this linear spreading rate of a mixing layer, the axial distance from the nozzle exit to the ignition point, x is simply related to X and η by

$$X = x - x_y = x - \frac{2x|y|}{\delta} = x(1-2|\eta|). \tag{75}$$

As seen in Fig. 49, τ_{ig} is much shorter in a hot gas side than in a main flow side. This means that typically $\eta < 0$.

In the following, Eqn. (73) is solved for a simple case, in which the velocity profile is linear in the mixing layer. A linear velocity profile was used because the flow time had to be started inside the edge of layer, where the ignition delay time is finite. It is, therefore, difficult to use an error function type of profile, in which the edge is not defined clearly. The same functions were used for profiles of temperature, and reactant mass fractions. By assuming linear profiles, f becomes equal to η and $\tau_f(X)$ becomes,

$$\int_0^X \frac{\mathrm{d}X}{U(X)} = \int_0^X \left[\frac{U_s}{2}\left(\frac{X}{X+x_y}-1\right)+Uc\right]^{-1}\mathrm{d}X \tag{76}$$

$$= xG(\eta). \tag{77}$$

where

$$G(\eta) = \left\{\left(\frac{1+2\eta}{U_c}\right) - \frac{U_s\eta}{U_c^2}\ln\left[\frac{U_c+U_s\eta}{\eta(U_s-2U_c)}\right]\right\}. \tag{78}$$

Here,

Substituting Eqn. (77) into Eqn. (73) gives

$$x = \frac{H(\eta)}{G(\eta)}, \tag{79}$$

where

$$H(\eta) = A_1 \exp\left(\frac{B}{T_c - T_s\eta}\right)\left(\frac{\eta+1/2}{T_c-T_s\eta}\right)^{\alpha+\beta}, \tag{80}$$

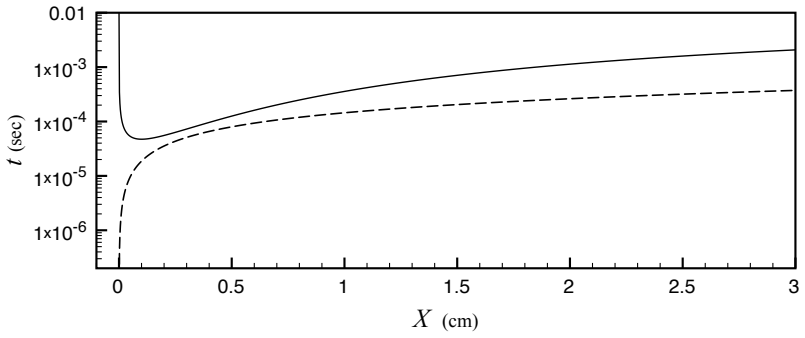

(a)

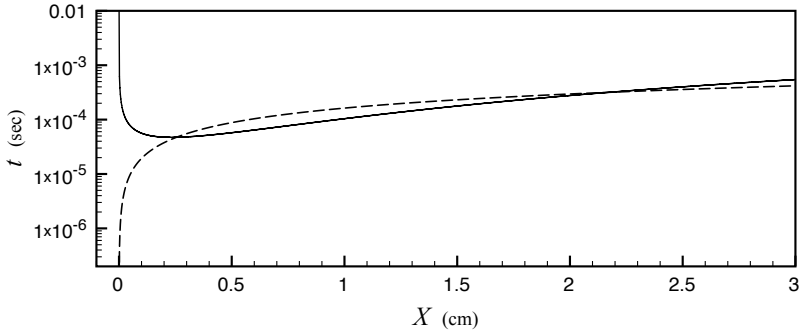

(b)

Figure 50: Example solution of Eqn. (70) and (71) for different ys; solid, τ_{ig}, dashed, τ_f; U_h=150 m/s, U_l=50 m/s, T_h=1800 K, T_l=300 K; (a) y=−0.03 cm, (b) y=−0.07 cm

and

$$A_1 = A\left(\frac{F_s}{MW_{\mathrm{F}}}\right)^{\alpha}\left(\frac{O_s}{MW_{\mathrm{Ox}}}\right)^{\beta}\left(\frac{pMW_{mix}}{R_u}\right)^{\alpha+\beta}. \tag{81}$$

Equation (79) represents the ignition distance for certain value of y, i.e., the location of ignition for fluid element moving parallel to the x-axis at a distance y from it. Because the relation between X and η is known, the variation of τ_{ig} and τ_f can be calculated using these equations, as long as the specific value of spreading rate, S is known.

Figure 50 shows the variations of τ_{ig} and τ_f along the X-axis for two different y locations. In a case (a), the increase of the ignition delay along X is faster than that of the flow time. Therefore, no ignition occurred. On the other hand, for a case (b), there exists a region over which the flow time is long enough for ignition to occur. Thus, the ignition distance clearly depends on the choice of transverse distance y in a mixing layer. The value of interest is only the minimum distance x where ignition can occur. This can be found by

differentiating Eqn. (79) with respect to y and solving the resulting equation for $\mathrm{d}x/\mathrm{d}y = 0$. Because the derivative is equal to $(1/\delta)(\mathrm{d}x/\mathrm{d}\eta)$, we can differentiate Eqn. (79) with η directly, provided that $\delta(x) > 0$. The resulting η then corresponds to the minimum value of x.

Differentiating Eqn. (79) with respect to η and setting $dx/d\eta$=0 results in

$$H'G - HG' = 0 \tag{82}$$

and

$$G^2 \neq 0. \tag{83}$$

where

$$G'(\eta) = \frac{2}{U_c} - \frac{U_s}{U_c^2}\left\{\ln\left(\frac{U_c + U_s\eta}{-2U_l\eta}\right) - \frac{U_c}{U_s\eta + U_c}\right\} \tag{84}$$

and

$$\begin{aligned} H'(\eta) = A_1 \exp\left(\frac{B}{T_c - T_s\eta}\right) \frac{(\eta + 1/2)^{\alpha+\beta}}{(T_c - T_s\eta)^{\alpha+\beta+2}} \\ \times \left\{BT_s + (\alpha+\beta)\left(T_c + \frac{T_s}{2}\right)\left(\frac{T_c - T_s\eta}{\eta + 1/2}\right)\right\}. \end{aligned} \tag{85}$$

Equation (83) is usually not solved explicitly for η even for a very simple profile for f. However, it can be solved by an iteratively. For given flow velocities, temperatures, and mixture equivalence ratio, the ignition distance is then calculated by substituting the resulting value of η into Eqn. (79).

The maximum flame stabilization velocity is also calculated using Eqn. (79) and (83). For this purpose, the length of the radical jet is required as an input. As described in Chapter 4.1.2, the length of radical jet depends on the type of RJG, on the main flow velocity, and on the flow rate and the equivalence ratio in the RJG. The following experimental relation may be used to approximate the radical jet length which is required to solve for the maximum flame stabilization velocity later,

$$L_{jet} = (C_1 U_{mc} + C_2) C_3 \left\{C_\phi(\phi - 1) + 1\right\} U_{rc}, \tag{86}$$

where

$$C_1 = -0.007$$

$$C_2 = 1.66$$

$$C_3 = 0.0055$$

$$C_\phi = 2.2.$$

L_{jet} is in meter, and U_{rc} is the cold RJG inlet flow velocity (m/s). Equation (86) can be used when the equivalence ratio ranges from 0.6 to 1.4 and the main flow velocity is less than 237 m/s. Constants, C_1, C_2, C_3, and C_ϕ were obtained from the experimental data in Fig. 20 and 21. To obtain these value, it was assumed that the jet length changes linearly with the RJG inlet velocity, equivalence ratio, and main flow velocity.

Replacing x in Eqn. (79) with L_{jet}, and solving for η and U_{mc} iteratively gives the maximum flame stabilization velocity. In the calculation, it must be remembered that the apparent energy of ignition and inner jet temperature need to be modified to take into account the effect of recirculation of the main flow. Simply, a fraction factor, m is used, and E and T_h are modified to yield

$$E = mE_m + (1-m)E_{RJG} \tag{87}$$

$$T_h = mT_m + (1-m)T_{RJG}, \tag{88}$$

where E_m and T_m are an equivalent energy of ignition for spontaneous ignition and the adiabatic flame temperature of a given the main mixture, respectively. E_{RJG} and T_{RJG} were obtained from Chapter 5.3.2 and the measured data, respectively.

5.4.2 Result

The flammability limit curves in a main combustor were calculated for various values of m, i.e., different amount of recirculating main flow. Two different RJG conditions were investigated. In one, experimentally measured exit temperatures, and the mean molar concentrations in a radical jet, which were obtained by the method in Chapter 5.2, were used. In the other, radical concentrations and temperatures at the location where the H radical is maximum in the premixed flame, which was modeled using CHEMKIN, were used to describe the inner jet. In both cases, the cold, inlet flow velocity in the RJG was taken to be 13.8 m/s and the mixture to be stoichiometric. The apparent energies of ignition to calculate the ignition delay time was estimated by the method described in Sec. 5.3.2.

The ignition delay strongly depends on the value of E/T according to Eqn. (49), and the value of E/T varies with the value of m. Therefore, the increasing or decreasing tendency of the ignition delay with increasing value of m is determined by the apparent energies of ignition and the temperatures used in the model for the radical jet and the main flow. Without plotting figures, it can be then predicted by checking the inequality between $(E/T)_{RJG}$ and $(E/T)_m$. This results in that the value of the former is larger than the latter when the radical jet was characterized using the average mole fractions of radicals and temperature, while the former is smaller than the latter when the mole fractions of the radicals and the temperature in a flame were used. This results in that the maximum flame holding velocity, U_{max}, decreases with decreasing m in Fig. 51(a), while Fig. 51(b) shows the opposite tendency.

For low values of m, which means that the main flame is stabilized mainly by the radical jet, the calculated maximum flame holding velocities depend strongly on the gas properties used to model the radial jet. For the case shown in Fig. 51(a), which used an averaged level of radicals and temperature to model the radical jet the maximum flame holding velocity is underpredicted. This may be because the average level of radicals and mean temperature are too low to characterize those in an actual radical jet. Alternatively, the experimental

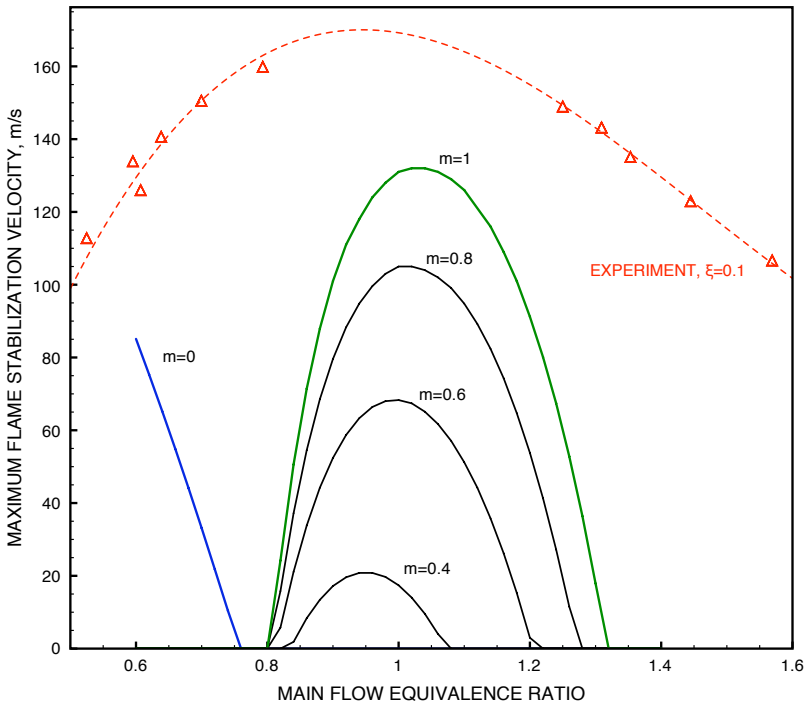

(a) *Average radical composition*, $T_{RJG} = 1547^{\circ}K$ *(measured)*

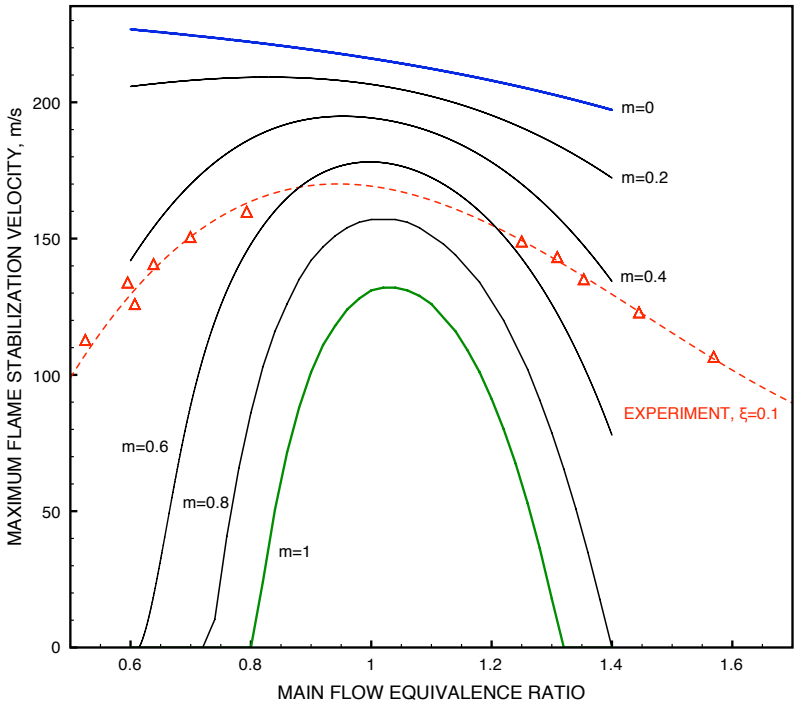

(b) *Maximum radical composition*, $T_{RJG} = 1903^{\circ}K$ *(CHEMKIN)*

Figure 51: Maximum flame stabilization velocity estimated by ignition distance method; RJG conditions used : $U_{RJG,cold}$=13.8 m/s, ϕ=1

values are underestimated because of measurement errors. The results of the case when the value of m is equal to one in case (a) will be discussed later, together with those obtained for case (b).

Based on the condition in the radical jet, the ignition process in case (b) can be interpreted as through a local flamelet that exists in the radical jet plays a dominant role in the ignition of the main flow instead of a radical jet modeled by its average properties. As shown in Fig. 45(a), because the molar concentrations of active species are much higher in the jet for case (b), the ignition delay time is much shorter than that calculated from the averaged properties. This high radical concentration results in very low value of the energy of ignition, E_{RJG}. Therefore, increasing the fraction of recirculating flow reduces the maximum flame stabilization velocity due to reduction of the effect of radicals on the ignition delay. Because the apparent energy of ignition and the radical jet temperature are all theoretical values, cases where m =0 or 1 represent the results of this model for two extreme conditions. In other words, the former corresponds to the maximum number of radicals and, therefore, the maximum flow velocity, at which the flame can be stabilized by the radical jet. The latter, on the other hand, corresponds to the U_{max}, at which the flame is stabilized by an inert gas mixture at the same temperature as the flame temperature of the main flow. Thus the conditions of the actual radical jet should exist in between these two extreme conditions.

The situation in the latter is also similar to that during bluff body flame stabilization. The only difference is that the length of radical jet was used in the model instead of the length of the recirculation zone. Although measurements of the recirculation zone length were not carried out in this study, experimental data reported in [93] showed that they are typically shorter than the length of radical jet when the dimensions of the bluff body is similar to the diameter of RJG. Therefore, all other conditions being the same, the bluff body flame holder cannot stabilize the main flame at as high a velocity as the radical jet.

The maximum flame stabilization velocity predicted using this model and plotted in

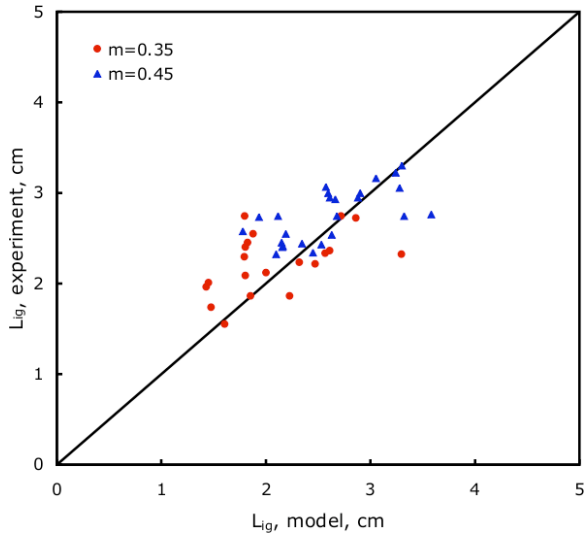

Figure 52: Comparison of ignition distance between model and experiments, m=0.35 for more stable condition, m=0.45 for stronger fluctuating condition.

Fig. 51 increases continuously as the equivalence ratio in the main mixture become leaner for m=0. This occurs because the theoretical ignition delay decreases with decreasing fuel-air ratio. However, the mechanism by which the flame may be quenched in a turbulent flow was not included in this model. This quenching mechanism can decrease the maximum flame stabilization velocities when the main flow mixture is either lean or rich. In addition, the flammability limit of the methane-air mixture ($0.5 < \phi < 1.7$ [41]) also restricts the main flow equivalence ratio that can be addressed by this model.

The ignition distances for various RJG and main flow conditions were calculated using this model, and the results were compared to those obtained from experiments. The species compositions and gas temperature in the flame front, such as those shown in Fig. 51(b), were used to determine E of the radical jet in this calculation. As shown in Fig. 51, the solutions of the model were significantly influenced by the value of m as well as the properties of the main flow and the radical jet. The comparison also showed a lack of correlation between the experimentally measured ignition distances and those calculated using a model, when a single value was used for m. Unfortunately, the degree of recirculation, m is difficult to be obtained experimentally. Therefore, the experimental data were

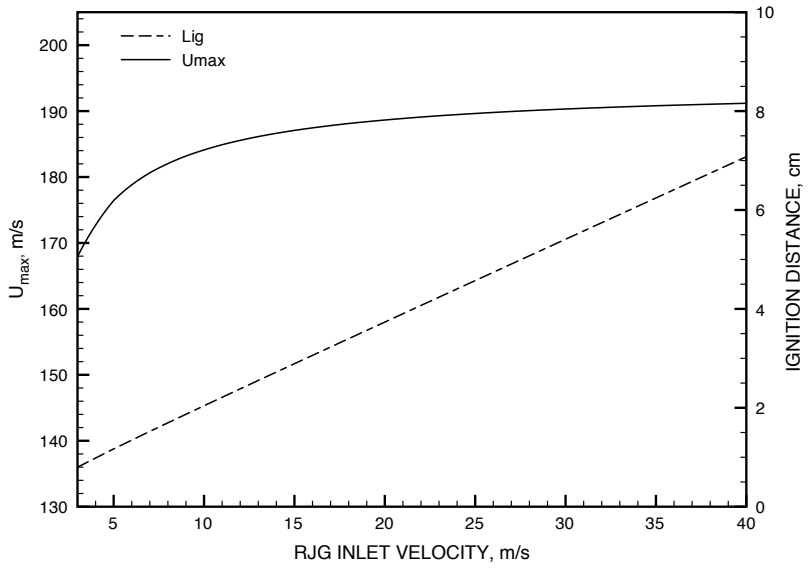

Figure 53: Variation of the maximum flame stabilization velocity and ignition distance with the RJG inlet velocity; *m* is assumed to be 0.5 and main flow is stoichiometric

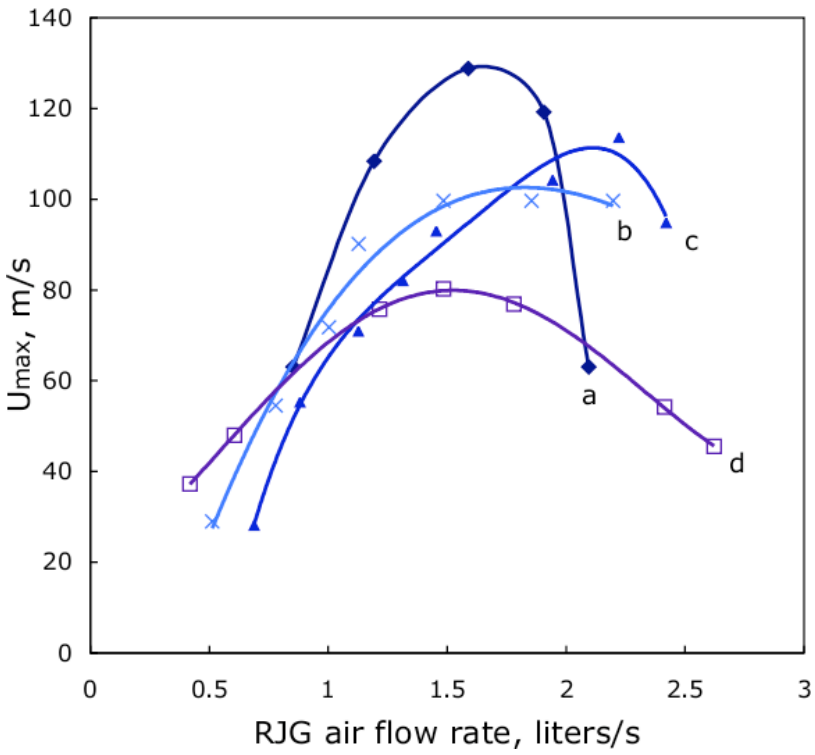

Figure 54: Variation of the maximum flame stabilization velocity measured in a cross flow combustor using various RJGs; the volume and the nozzle diameter in the RJGs: a, b, c - 13.6 cm^3, 1.27 cm, d - 6.3 cm^3, 0.64 cm; discharge frequency: a - 11kHz, b, c, d - 8kHz; relative spark power: a, b $<$ c, d

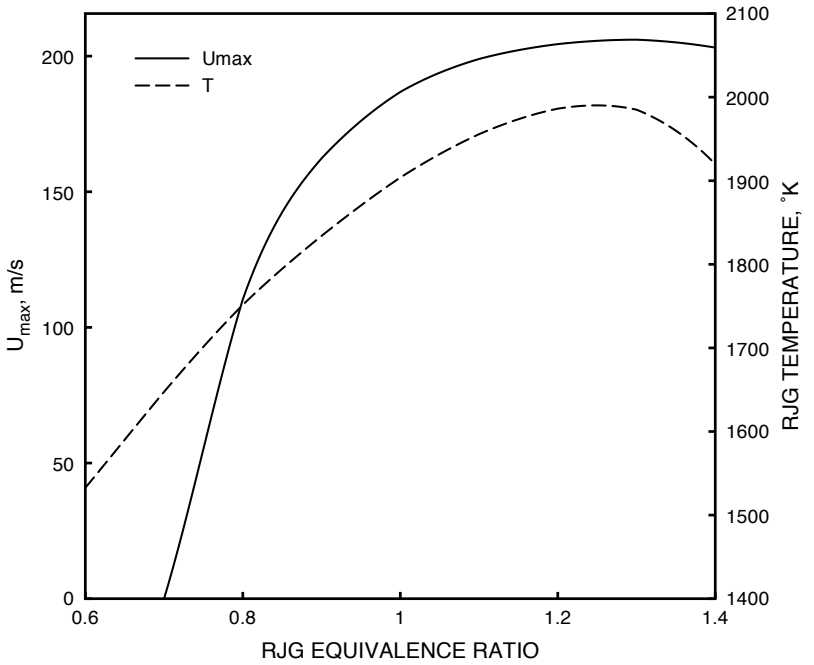

Figure 55: Variation of the maximum flame stabilization velocity with the RJG equivalence ratio; *m* is assumed to be 0.5 and main flow is stoichiometric

roughly divided into two sets based on the resulting degree of fluctuation of the main flame. Because recirculation increases with fluctuations, higher value of *m* must be used for the cases with stronger fluctuation. Because the precise amount of recirculating flow cannot be specified, two arbitrary values of *m* were assumed. Figure. 52 shows measured ignition distances compared with L_{ig} calculated using higher *m* for the cases in which the relatively strong fluctuation occurred in the main flame. This figure shows that the values estimated using the model are only slightly correlated with those obtained from the experiments. This large deviation may have been caused by using only two values of *m*, measurement errors due to the flame fluctuation, and the simplicity of this model, such as the use of a zero virtual origin. Provided that accurate ignition distance data are available, the value of *m* for various flow conditions can be estimated inversely using the data.

The solution of Eqn. (83) results in a value of η which corresponds to the ignition distance for given main and the radical jet velocities. A typical value of η is -0.35. This means that ignition occurs at very close to the radical jet as expected from Fig. 49. This,

in turn, means that the ignition distance is more dependent of the radical jet exit velocity than that of the main flow. However, increasing the radical jet velocity also increases the length of radical jet, so the net effect of the radical jet velocity on U_{max} is not large, see Fig. 53. In this calculation, the properties in the radical jet was assumed not to be changed by the inlet velocity of the RJG. In actual situation, radical jet strength, such as temperature, becomes weaker beyond a certain flow rate because of the limited spark power as described in Chapter 3. Thus U_{max} decreases again with increasing inlet velocity in a RJG, see Fig. 54 .

Figure 55 shows the variation of U_{max} with the equivalence ratio in the RJG. In these calculations the radical compositions and temperature are modeled by CHEMKIN in a flame, and the energies of ignition for the RJG at various equivalence ratios were calculated using those results. Because the temperature and the radical concentrations are relatively high in a rich jet, the maximum stabilization velocity is also higher in that case. The longer jet length in a rich radical jet also has a positive effect on U_{max}. This better performance on the flame stabilization by the rich radical jet agrees with the obtained experimental results, see Fig. 28.

CHAPTER VI

CONCLUSIONS AND RECOMENDATIONS

This chapter summarizes the major findings and conclusions presented in this thesis and provides recommendations for future studies.

It was demonstrated how a high frequency spark discharge successfully ignites and stabilizes a flame in a relatively low velocity flow. A spark convection process consisting of a series of low power sparks provides sufficient energy to ignite a flame kernel, which then propagates through a turbulent flow. The electrical energy consumption is much lower than the heat generated from the combustion process maintained by the plasma. A theoretical model was developed to predict the limits of flame ignition and stabilization. The results agree well with those obtained from experiments. The developed model also showed that the required discharge power increases rapidly with the flow velocity in the vicinity of the plasma. This restricts flame stabilization using an electrical discharge directly exposed to a combustible flow to applications with low flow rates.

High speed images obtained in a radical jet generator (RJG) showed unburnt mixture pocket between the flame kernels produced by the spark. The combustible mixture in these pockets burns as the flow convects downstream. The RJG, therefore, generates radicals throughout the jet, first by periodic ignition of flame kernels by the spark convection and then, during convection by the spread of the combustion process throughout the combustible mixture. The measurement of CH chemiluminescent light intensities confirmed that large quantities of active species exists in the jet even beyond the exit nozzle of RJG.

It was further shows that the radical jet, which is generated by the initialization process by the electrical discharge and then by the cascade process inside the RJG, can stabilize a flame in a main tube carrying a combustible gas at much higher flow rates. The CH*

chemiluminescence, temperatures, and the jet lengths were reported. Experiments showed that the ignition performance of the radical jet is much better than that of a high temperature, fully burnt product jet or of a the bluff body flame holder. The limits of equivalence ratio and flow velocity in the main flow, for which the flame can be stabilized by the radical jet were measured experimentally using a flame detector that was developed to quantify the "flammability." This flammability is defined as the fraction of time during which a fluctuating flame is ignited. This allows one that establishes flammability limits even in the presence of fluctuating combustion.

Finally, a simple ignition distance model was developed to predict the limits of flame stabilization by the radical jet. The results of this model suggested several reasons that could explain the better flame stabilization performance of the radical jet compared to that of bluff bodies. One possibility is that the RJG reduces the ignition delay time by providing additional active radicals in the ignition zone. Another is that it provides a longer ignition source; i.e., the radical jet is longer than the length of the recirculation zone produced by a bluff body. It was further demonstrated that the recirculation of products of combustion from the main flame affects the radical jet temperature. This, in turn, shortens the ignition delay time in the region where radical jet and main flow interact. Thus, recirculation can be an important parameter in flame stabilization, not only by bluff bodies, but also by radical jets.

In this study some interesting phenomena remain to be resolved. To better understand flame stabilization by the radical jet, and more accurate predict its limitation the following issues need to be resolved.

The electrical energy required to ignite the flame in the RJG was determined by measuring the output power of the spark generation system. However, those values may be significantly different from the actual energy deposited into the flow. The actual, transferred energy may vary with the current/voltage history and, therefore, the method used to generate the discharge, and the resulting discharge type. The predicted operating limits of flame

stabilization inside the RJG are then changed, which, in turn, affects the flame stabilization of the RJG. A more accurate prediction of the energy deposited into the flow would, therefore, results in a better prediction of the RJG's flame holding capabilities.

When the radical jet stabilizes a high velocity flame in a main combustor, combustion fluctuations were observed near the operating limits. In this work the mechanism responsible for those fluctuations were not addressed. Instead, a methodology was developed to define an upper flow velocity limit depending on one's tolerance to combustion unsteadiness based on the "flammability." Future work should address how these instabilities can be suppressed, and thus how the stable operating range can be broadened.

In an actual afterburner, the inlet mixture is vitiated and the temperature is very high. Therefore, this study needs to be repeated using a vitiated main flow at high temperature, and the variation of flame stabilization performance by the radical jet with temperature should be studied.

This study introduced a method to estimate average values for radical concentrations and jet temperature. The resulting values were not high enough to change the apparent energy of ignition significantly, and, therefore, underestimated the maximum flame stabilization velocity. The use of the ignition distance model to predict the maximum flame holding velocity in the radical jet flame stabilization may be improved by a more accurate determination of the temporal and spatial variations of the jet temperature and the level of radicals. In addition, the degree of the recirculation of the main flow needs to be studied to obtain a more clear understanding of its contribution to the flame stabilization process.

Finally, the heat transfer from the RJG wall to the main flow, especially for the coaxial RJG, may result in a more accurate prediction of the ignition delay time.

APPENDIX A

ELECTRICAL DISCHARGES

Electrical discharge was used to generate radical jet in this study. The detail knowledges about the plasma in the form of electrical discharge was not required for this study. However, a brief study about them may be very helpful for understanding the discharges in a RJG. Therefore,, terms and theories about the electrical discharges are briefly described and summarized below. For extensive explanation of this subject, see Refs [11, 18, 28, 75, 94, 118].

A.1 Townsend discharge

When the electric field is applied between two electrodes, cathode and anode, electrons emitted photoelectrically from the cathode moves towards the anode. As the voltage applied increases, this current increases. Over a certain value of voltage, current is not changed by increasing voltage. This situation is called *saturation*, in which all electrons emitted from cathode reaches to the anode. If the voltage increases further, electrons moving toward the anode gain sufficient energy to ionize a neutral gas particle, than the current increases again. The discharges in this region are called *Townsend discharge* named after J. S. Townsend. Mechanism of discharges in this region can be divided by two depending on the slope of increase of current with voltage.

Collision between electron and neutral gas

Relatively sight increase of current with voltage shown after saturation occurs when electrons emitted from the cathode traveling toward the anode gain energy sufficient to ionize the neutral particle by collision, current increase by additional produced electrons. In this

case current density is represented by

$$j = j_o e^{\alpha d}, \tag{89}$$

and this exponential growth of electrons is called *electron avalanche*. In equation above, j_o is a saturation current density, i.e., initial negative charge emitted from the cathode of unit area per second, and d is a distance between the cathode and the anode. α is the *first Townsend coefficient* which represents the number of ionizing collision per unit distance in the direction of the electric field, and is a function of electric field and mean free path. Because the mean free path is inversely proportional to the pressure, coefficient α has a relation with these parameter as [28],

$$\frac{\alpha}{p} = f\left(\frac{E}{p}\right) \tag{90}$$

If initial electrons are produced by ionizing radiation throughout the volume of gas, not by photoelectric process, then the current density becomes,

$$j(x) = j_o \frac{(e^{\alpha x} - 1)}{\alpha d}. \tag{91}$$

Collision between positive ion and neutral gas

When the voltage applied between the electrodes increase further, increase of current with voltage becomes larger, Townsend assumed that this is occurred when the positive ion which is produced by electron collision gains energy enough to produce electrons by colliding with neutral gas. In this case, current density at the arbitrary distance from the cathode is represented by

$$j = j_o \frac{(\alpha - \beta)e^{(\alpha-\beta)x}}{\alpha - \beta e^{(\alpha-\beta)x}}, \tag{92}$$

where β is the *second Townsend coefficient* and a function of electric field and pressure.

$$\frac{\beta}{p} = f\left(\frac{E}{p}\right) \tag{93}$$

Positive ion bombardment

More probable mechanism than positive ion collision to produce additional electron, which corresponds the large change of current with voltage in a relatively high voltage range, is the positive ion bombardment at the surface of cathode. In this case current density is represented by

$$j = j_o \frac{e^{\alpha d}}{1 - \gamma e^{\alpha d}}, \tag{94}$$

where γ is the number of electron emitted from the surface of cathode by a positive ion collision.

In addition to the mechanisms described above, electrons may be produced by the photoemission; i.e., electron emission at the surface of the cathode by photon emitted from ionizing process [28].

A.2 Spark breakdown

In Eqn. (92) or (94), when a denominator becomes zero, current increases rapidly and the spark breakdown occurs. After spark breakdown, discharge turns into different form of discharge, such as, arc discharge. The type of discharge formed after breakdown depends on the shape of the electrode, pressure, and the configuration of the discharge generating system, etc [28].

A.3 Corona discharge

Corona discharge appears in a non-uniform field, such as in the gap between wires, or sphere when the electrode curvature is relatively small to the gap distance. This is in the form of glow discharge, and is called corona at atmospheric pressure. Compared to theTownsend discharge, which is invisible and, thus, is called dark discharge, corona is a

visible and self-sustained discharge. This discharge is not treated as a breakdown in a typical engineering sense because the breakdown does not occurs through the entire gap between the electrode, but only near the surface of the electrode. Corona discharge precedes the spark breakdown, and thus, the surface breaks down at the lower voltage relative to the spark breakdown. Figure 2(a) showed the voltage-current range of the corona discharge. The increase of current in the corona discharge is not significant because of incomplete failure of the gap does [28].

A.4 Glow discharge

As voltage increases between electrodes beyond breakdown voltage, the transition from Townsend discharge to the glow discharge occurs. In this transition, the voltage drops while the current increases. The glow discharge is divided by two region. In one the current increase independent to the voltage drop. The discharge in this region is called *normal* glow discharge. In the other, the discharge voltage increases with increasing current, in which the discharge is called *abnormal* glow discharge. Glow discharge consists of a series of dark and light regions in the gap, which are called from the cathode to the anode, Aston dark space, cathode glow, cathode dark space, negative glow, Faraday dark space, positive column, anode glow, and anode dark space, respectively. Details about these region can be found in Ref [28]. The lengths of these regions depends on the gas pressure. Because most of the current is carried by the positive ions near the cathode, while there the electron density is very low. This produces the large voltage drop in a cathode dark space, which is called *cathode drop*. The net charge density is zero in plasma. Regions of the negative glow and the positive column are such regions in the glow discharge [28].

A.5 Arc discharge

A further increase in current from the glow discharge results in the transition to the arc discharge, which can be sustained in a very low electric field. Very large current can flow

through the arc discharge. The arc discharge can also be produced by separating contact. The temperature is very high in the core of arc discharge. For high pressure arc discharge, the gas temperature is of order of 6000°K. In this case, the gas in the discharge is in thermal equilibrium. On the other hand, for the low pressure arc discharge, the gas temperature is much lower than the electron temperature. In this case the latter increases up to 40000°K [28].

APPENDIX B

MODELING THE RJG EXIT TEMPERATURE

This chapter describes a model which is used to predict the variation of temperature at the RJG exit referred to in Section 4.1.3. The RJG is modeled as a straight pipe. It is also assumed that combustion is initiated by an electrical discharge in the inlet and propagates downstream as a one dimensional planar flame. The pressure is assumed to be constant throughout the RJG. The flame sheet propagates through the unburned mixture with the turbulent flame speed in both directions. At the same time the product gas between the two flame sheets convects downstream with the flow velocity. When the distance between the flame propagating upstream and the inlet becomes D_s, a new flame kernel is created at the inlet by the next short spark. Therefore, the period, τ_p in which a new flame kernel is created is $D_s/(U_{in}-S_t)$. Figure 56 shows the overall schematics of this model.

The velocity change of the flame sheets of the n-th kernel, k and l with respect to the inlet velocity can be represented as

$$V_{k,n} = U_n + S_t\left(2\frac{T_b}{T_u} - 1\right), \tag{95}$$

$$V_{l,n} = U_n - S_t, \tag{96}$$

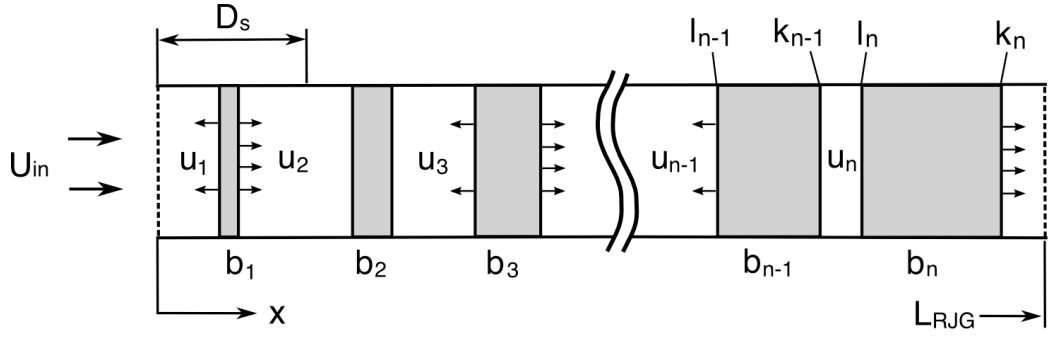

Figure 56: Schematics of a model for the gas temperature in the RJG exit

where the velocity of n is

$$U_n = U_{in} + 2S_t \left\lfloor \frac{t}{\tau_p} \right\rfloor \left(\frac{T_b}{T_u} - 1 \right). \tag{97}$$

Here $\lfloor\ \rfloor$ is a *floor function*; i.e., floor(x) is the largest integer not greater than x [43].

The location of the flame sheet of the n-th kernel, $x_{k,n}$ which propagates downstream, at time t is calculated as

$$x_{k,n} = \int_0^t V_{k,n}\, \mathrm{d}t \tag{98}$$

Integrating the floor function in Eqn. (97) results in

$$\int_0^t \left\lfloor \frac{t}{\tau_p} \right\rfloor \mathrm{d}t = (n-1)t^* + \tau_p \frac{(n-2)(n-1)}{2}, \tag{99}$$

where $t^* = t - (n-1)\tau_p$, $0 \leqslant t^* < \tau_p$, and $\lfloor t/\tau_p \rfloor = n-1$. Using Eqn. (99), $x_{k,n}$ can be solved in terms of t^* as,

$$\begin{aligned} x_{k,n} = {} & 2S_t(r-1)\left\{ (n-1)t^* + \tau_p \frac{(n-2)(n-1)}{2} \right\} \\ & + \left\{ U_{in} + S_t(2r-1) \right\} \left\{ t^* + (n-1)\tau_p \right\}, \end{aligned} \tag{100}$$

where $r = T_b/T_u$. Similarly the location of the upstream side flame sheet, $x_{l,n}$ is represented as

$$\begin{aligned} x_{l,n} = {} & 2S_t(r-1)\left\{ (n-1)t^* + \tau_p \frac{(n-2)(n-1)}{2} \right\} \\ & + (U_{in} - S_t) \left\{ t^* + (n-1)\tau_p \right\}, \end{aligned} \tag{101}$$

Without using a floor function, $x_{k,n}$ and $x_{l,n}$ can be obtained from total thickness of n unburned pockets

$$\begin{aligned} \sum_{i=1}^{n} u_i = {} & (U_{in} - S_t)t^* + D_s - 2S_t t^* + D_s - 2S_t(t^* + \tau_p) + \cdots \\ & + D_s - 2S_t\{t^* + (n-3)\} + D_s - 2S_t\{t^* + (n-2)\}, \end{aligned} \tag{102}$$

and total thickness of$n$ burnt regions at time t^*

$$\sum_{i=1}^{n} b_i = 2S_t r t^* + 2S_t r(r+\tau_p) + 2S_t r(r+2\tau_p) + \cdots + 2S_t r\{r+(n-2)\tau_p\} + 2S_t r\{r+(n-1)\tau_p\}. \tag{103}$$

The sum of Eqns. (102) and (103) results in the axial locations of the flame sheets of the n-th product zone, $x_{k,n}$ as

$$\begin{aligned} x_{k,n} &= \sum_{i=1}^{n}(b_i+u_i) \\ &= 2S_t r\left\{nt^* + \tau_p\frac{n(n-1)}{2}\right\} \\ &\quad + (U_{in}-S_t)t^* + (n-1)D_s - 2S_t\left\{(n-1)t^* + \tau_p\frac{(n-2)(n-1)}{2}\right\}, \end{aligned} \tag{104}$$

and $x_{l,n}$ as

$$\begin{aligned} x_{l,n} &= x_{k,n} - b_n \\ &= 2S_t r\left\{(n-1)t^* + \tau_p\frac{(n-2)(n-1)}{2}\right\} \\ &\quad + (U_{in}-S_t)t^* + (n-1)D_s - 2S_t\left\{(n-1)t^* + \tau_p\frac{(n-2)(n-1)}{2}\right\}. \end{aligned} \tag{105}$$

Since $\tau_p = D_s/(U_{in}-S_t)$, the result is the same as that obtained from Eqns. (100) and (101). Because t^* is measured just after b_1 is created, the residence time of the flame at $x_{k,n}$ inside the RJG are calculated by replacing $x_{k,n}$ by L_{RJG} and by solving Eqn. (104) for t^*. The residence time of the flame at $x_{l,n}$ is also solved similarly, and the results are represented as

$$t^*_{k,n} = \frac{L_{RJG} - \tau_p(n-1)\{S_t[(r-1)n+1]+U_{in}\}}{U_{in}+S_t\{2n(r-1)+1\}}, \tag{106}$$

$$t^*_{l,n} = \frac{L_{RJG} - \tau_p(n-1)\{S_t[(r-1)(n-2)-1]+U_{in}\}}{U_{in}+S_t\{2(n-1)(r-1)-1\}}, \tag{107}$$

where L_{RJG} is a distance from the electrode to the nozzle exit of the RJG.

If the RJG contains n burnt regions as $t^* \to 0$, the closest flame from the exit is located at $x_{k,n}$. Let t^*=0, and $x_{k,n} = L_{RJG}$ in Eqn. (104). This results in a quadratic equation in terms

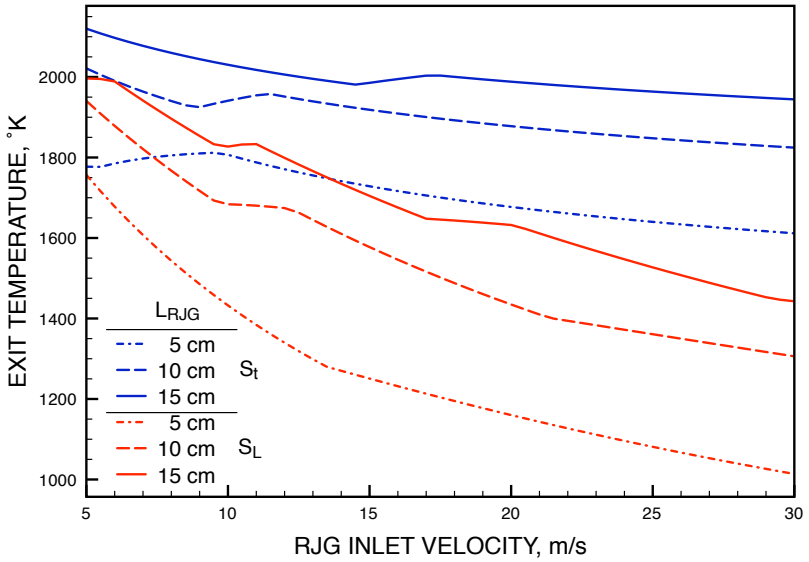

Figure 57: Variations of the temperature in the RJG exit with the length of RJG and the inlet velocity in the RJG.

of n. The desired value of n is then the integer that is obtained from truncating the decimal in the positive solution of the quadratic equation.

If the response time of the temperature measurement is assumed to be infinitely fast than that the average temperature of the gas at the exit can be simply calculated using the ratio of time difference, $t^*_{l,n} - t^*_{k,n}$, to τ_p, the time period of each flame sheet generation as

$$\overline{T}_{RJG,exit} = \theta T_b + (1-\theta) T_u \tag{108}$$

where

$$\theta = \frac{t^*_{l,n} - t^*_{k,n}}{\tau_p}. \tag{109}$$

Here, it should be noted that the values of $t^*_{k,n}$ and $t^*_{l,n}$ can be evaluated only when the corresponding flames are leaving the RJG in $t^* < \tau_p$. The above described method to calculate n guarantees that $x_{k,n}$ is larger than L_{RJG} at $t^* = \tau_p$. However, $x_{l,n}$ may or may not be larger than L_{RJG}. Therefore, when $x_{l,n}(\tau_p) < L_{RJG}$, the time difference in Eqn. (109) must be calculated by $t^*_{l,n+1} + (\tau_p - t^*_{k,n})$. This is because there are $n+1$ burnt gas zones in the RJG when the flame at $x_{l,n+1}$ is just exhausting.

Figure. 57 shows that the average temperature predicted using the above described

model decreases with increasing inlet flow velocity and decreasing length of the RJG. The growth of the burnt gas region depends on the burning velocity of the mixture. Therefore, the temperature drops faster when a laminar rather than a turbulent flame speed was used. Interestingly, the figure shows regions in which the gas temperature increase with increasing inlet velocity. This occurs over a velocity range over which the number of flame kernel inside RJG increases. However, this is not usually observed in the actual RJGs.

REFERENCES

[1] ABDEL-GAYED, R. and BRADLEY, D., "A two-eddy theory of premixed turbulent flame propagation," *Philosophical Transactions of the Royal Society of London. Series A, Mathematical and Physical Sciences*, vol. 301, pp. 1–25, 1981.

[2] ABDEL-GAYED, R. and BRADLEY, D., "Criteria for turbulent propagation limis of premixed flames," *Combustion and Flame*, vol. 62, pp. 61–68, 1985.

[3] ABDEL-GAYED, R., BRADLEY, D., and LUNG, F., "Combustion regimes and the straing of turbulent premixed flames," *Combustion and Flame*, vol. 76, pp. 213–218, 1989.

[4] AGOSTON, G. A., NOON, A. W., and WITHERLY, T. D., "Experimental study of a fiameholder reversed jet experimental study of a reversed jet flameholder," *Combustion and Flame*, vol. 2, pp. 333–347, 1958.

[5] ANDREWS, G. E. and BRADLEY, D., "The burning velocity of methane-air mixture," *Combustion and Flame*, vol. 19, pp. 275–288, 1972.

[6] ANIKIN, N., KUKAEV, E., STARIKOVSKAIA, S., and STARIKOVSKII, A., "Ignition of hydrogen-air and methane-air mixtures at low temperatures by nanosecond high voltage discharge," AIAA-2004-833, (Reno, Nevada), 42th AIAA Aerospace Meeting and Exhibit, 5-8 January 2004.

[7] ASABA, T., YONEDA, K., KAKIHARA, N., and HIKITA, T., "A shock tube study of ignition of methane-oxygen mixtures," *Ninth Symposium (International) on Combustion*, pp. 193–200, 1963.

[8] BALLAL, D. and LEFEBVRE, A., "The influence of flow parameters on minimum ignition energy and quenching distance," *Fifteenth Symposium (International) on Combustion*, pp. 1473–1480, 1974.

[9] BALLAL, D. and LEFEBVRE, A., "Ignition and flame quenching in flowing gaseous mixtures," *Proceedings of the Royal Society of London. Series A, Mathematical and Physical Sciences*, vol. 357, no. 1689, pp. 163–181, 1977.

[10] BATCHELOR, G. K., "The effect of homogeneous turbulence on material lines and surfaces," *Proceedings of the Royal Society of London. Series A, Mathematical and Physical Sciences*, vol. 213, pp. 349–366, 1952.

[11] BAZELYAN, E. and RAIZER, Y. P., *Spark Discharge*. Boca Raton, Fl,: CRC Press, 1998.

[12] BECKER, K. H., BRENIG, H. H., and TATARCZYK, T., "Lifetime measurements on electronically excited ch radicals," *Chemical Physics Letters*, vol. 71, pp. 242–245, 1980.

[13] BENSON, K., THORNTON, J. D., STRAUB, D. L., HUCKABY, E. D., and RICHARDS, G. A., "Flame ionization sensor integrated into a gas turbine fuel nozzle," *Journal of Engineering for Gas Turbines and Power*, vol. 127, pp. 42–48, 2005.

[14] BOZHENKOV, S., STARIKOVSKAIA, S., SECHENOV, V., STARIKOVSKII, A., and ZHUKOV, V., "Combustible mixtures ignition in a wide pressure range. nanosecond high-voltage discharge ignition," AIAA-2003-876, (Reno, Nevada), 41st Aerospace Sciences Meeting and Exhibit, Jan. 6-9 2003.

[15] BOZHENKOV, S., STARIKOVSKAIA, S., and STARIKOVSKII, A., "Nanosecond gas discharge ignition of H_2- and CH_4- containing mixtures," *Combustion and Flame*, vol. 133, pp. 133–146, 2003.

[16] BOZHENKOV, S., KYKAEV, E., KUKSIN, A., NUDNOVA, M., STARIKOVSKAIA, S., and STARIKOVSKII, A., "Plasma control of ignition of hydrogen-air and methane-air mixtures," AIAA 2003-5045, (Huntsville, Alabama), 39th AIAA/ASME/SAE/ASEE Joint Propulsion Conference and Exhibition, 20-23 July 2003.

[17] BRADLEY, D., LAU, A. K. C., and LAWES, M., "Flame stretch rate as a determinant of turbulent burning velocity," *Philosophical Transactions: Physical Sciences and Engineering*, vol. 338, no. 1650, pp. 359–387, 1992.

[18] BROWN, S., *Introduction to electrical discharges in gases*. New York: John Wiley and Sons, 1966.

[19] BROWN, S., *Basic Data of Plasma Physics: The Fundamental Data on Electrical Discharges in Gases*. Woodbury, New York: AIP Press, 1994.

[20] CALCOTE, H. F., "Mechanisms for the formation of ions in flames," *Combustion and Flame*, vol. 1, pp. 385–403, 1957.

[21] CARL, S. A., POPPEL, M. V., and PEETERS, J., "Identification of the CH + $O_2 \rightarrow$ OH(A) + CO reaction as the source of OH($a-x$) chemiluminescence in $C_2H_2/O/H/O_2$ atomic flames and determination of its absolute rate constant over the range T = 296 to 511 K," *The Journal of Physical Chemistry*, vol. 107, pp. 11001–11007, 2003.

[22] CETEGEN, B., TEICHMAN, K., WEINBERG, F., and OPPENHEIM, A., "Performance of a plasma jet," SAE Paper 800042, 1980.

[23] CHEN, J. H. and IM, H. G., "Correlation of flame speed with stretch in turbulent premixed methane/air flames," *Twenty-Seventh Sysposium (International) on Combustion*, pp. 819–826, 1998.

[24] CHENG, S. and KOVITZ, A., "Ignition in the laminar wake of a flat plate," *Sixth Symposium (International) on Combustion*, pp. 418–427, 1957.

[25] CHENG, W. K., SUMMERS, T., and COLLINGS, N., "The fast-response flame ionization detector," *Progress in Energy and Combustion Science*, vol. 24, pp. 89–124, 1998.

[26] CHINTALA, N., MEYER, R., HICKS, A., BYSTRICKY, B., RICH, J., LEMPERT, W., and ADAMOVICH, I., "Nonthermal ignition of premixed hydrocarbon-air and co-air flows by nonequilibrium rf plasma," (Reno, Nevada), 42th AIAA Aerospace Meeting and Exhibit, 5-8 January 2004.

[27] CHOI, W., NEUMEIER, Y., and JAGODA, J., "Stabilization of a combustion process near lean blow off by an electric discharge," in *42nd AIAA Aerospace Sciences Meeting and Exhibit*, AIAA-2004-982, (Reno, Nevada), 42nd AIAA Aerospace Sciences Meeting and Exhibit, Jan. 5-8 2004.

[28] COBINE, J. D., *Gaseous conductors: theory and engineering applications*. Dover Publications, New York, 1958.

[29] COX, G. and CURTIS, P. B., "An experimental study of natural ionization in hydrocarbon flames, using the negative electrostatic probe at atmospheric pressure i. a technique for measurement of ion density," *Journal of Physics D: Applied Physics*, vol. 3, pp. 1255–1262, 1970.

[30] DAHM, W. J. A., FRIELER, C. E., and TRYGGVASON, G., "Vortex structure and dynamics in the near field of a coaxial jet," *Journal of Fluid Mechanics*, vol. 241, pp. 371–402, 1992.

[31] DAKIN, T., LUXA, G., OPPERMANN, G., J.VIGREUX, WIND, G., and WINKELENKEMPER, H., "Breakdown of gases in uniform fields – paschen curves for nitrogen, air and sulfur hexafluoride," *Electra*, no. 32, pp. 61–82, 1974.

[32] DAVIS, M. G., MCGREGOR, W. K., and MASON, A. A., "OH chemiluminescent radiation from lean hydrogen-oxygen flames," *Journal of Chemical Physics*, vol. 61, pp. 1261–1606, 1974.

[33] DEVRIENDT, K., LOOK, H. V., CEURSTERS, B., and PEETERS, J., "Kinetics of formation of chemiluminescent ch(a) by the elementary reactions of C_2H with o and O_2: A pulse laser photolysis study," *Chemical Physics Letters*, vol. 261, pp. 450–456, 1996.

[34] DEZUBAY, E. A., "Characteristics of disk-controlled flame holders," *Aero. Digest*, vol. 61, no. 1, pp. 54–56; 102–104, 1950.

[35] DIMPFL, W. L. and KINSEY, J. L., "Radiative lifetimes of oh(a2sigma) and einstein coefficients for the a-x system of oh and od," *Journal of Quantitative Spectroscopy and Radiative Transfer*, vol. 21, pp. 233–241, 1979.

[36] EDELMAN, R. B. and HARSHA, P. T., "Laminar and turbulent gas dynamics in combustors—current statu," *Progress in Energy and Combustion Science*, vol. 4, no. 1, pp. 1–62, 1978.

[37] FETTING, F., CHOUDHURY, A., and WILHELM, R., "Turbulent flame blow-off stability, effect of auxiliary gas addition into separation zone," *Symposium (International) on Combustion*, vol. 7, pp. 621–632, 1958.

[38] FIALKOV, A. B., "Investigations on ions in flames," *Progress in Energy and Combustion Science*, vol. 23, pp. 399–528, 1997.

[39] GAYDON, A., *The Spectroscopy of Flames*. London: Champman and Hall, 1957.

[40] GLASS, G., KISTIAKOWSKY, G., MICHAEL, J., and NIKI, H., "The oxidation reactions of acetylene and methane," *Tenth Symposium (International) on Combustion*, pp. 513–522, 1963.

[41] GLASSMAN, I., *Combustion*. San Diego, CA: Academic Press, 3rd ed., 1996.

[42] GOLD, E., "The velocity of the negative ions in flames," *Proceedings of the Royal Society of London. Series A, Containing Papers of a Mathematical and Physical Character*, vol. 79, pp. 43–66, 1907.

[43] GRAHAM, R. L., KNUTH, D. E., and PATASHNIK, O., *Concrete Mathematics: A Foundation for Computer Science*. Addison-Wesley Publishing Co., 2nd edition ed., 1994.

[44] GREBE, J. and HOMANN, K. H. *Ber. Bunseng. Phys. Chem.*, vol. 86, pp. 581–587, 1982.

[45] GRILLO, A. and SLACK, M., "Shock tube study of ignition delay times in methane-oxygen-nitrogen-argon mixtures," *Combustion and Flame*, vol. 27, pp. 377–381, 1976.

[46] GUSSAK, L., "High chemical activity of incomplete combustion products and a method of prechamber torch ignition for avalanche activation of combustion in internal combustion engines," SAE paper 750890, (Detroit, Michigan), Automobile Engineering Meeting, October 13-17 1975.

[47] HADDOCK, G. H., "Flame-bolwoff studies of cylindrical flame holders in channeled flow," progress report 3-14, Jet Propulsion Laboratory, Pasadena, CA, May 14 1951.

[48] HAQ, M. Z., SHEPPARD, C. G. W., WOOLLEY, R., GREENHALGH, D. A., and LOCKETT, R. D., "Wrinkling and curvature of laminar and turbulent premixed flames," *Combustion and Flame*, vol. 131, pp. 1–15, 2002.

[49] HARRISON, A. and WEINBERG, F., "Flame stabilization by plasma jets," *Proceedings of the Royal Society of London. Series A, Mathematical and Physical Sciences*, vol. 321, no. 1544, pp. 95–103, 1971.

[50] HELMHOLTZ, H., "On discontinuous movements of fluids," *Philosophical Magazine*, vol. 36, pp. 337–346, 1868.

[51] HIDAKA, Y., TAKAHASHI, S., KAWANO, H., SUGA, M., and GARDINER, W. C., "Shock-tube measurement of the rate constant for excited hydroxyl(a2.sigma.+) formation in the hydrogen-oxygen reaction," *Journal of Physical Chemistry*, vol. 86, pp. 1429 – 1433, 1982.

[52] HIGGIN, R. and WILLIAMS, A., "A shock-tube investigation of the ignition of lean methane and n-butane mixtures with oxygen," *Twelfth Symposium (International) on Combustion*, pp. 579–590, 1969.

[53] HILL, B. J., "Measurement of local entrainment rate in the initial region of axisymmetric turbulent air jets," *Journal of Fluid Mechanics*, vol. 51, pp. 773–779, 1972.

[54] HOWARTH, L., "Concerning the effect of compressibility on laminar boundary layers and their separation," *Proceedings of the Royal Society of London. Series A, Mathematical and Physical Sciences*, vol. 194, pp. 16–42, 1948.

[55] JAGODA, I. and WEINBERG, F., "Optical studies of plasma jets," *Journal of Physics D: Applied Physics*, vol. 13, no. 4, pp. 551–561, 1980.

[56] KASKAN, W. E. *Journal of Chemical Physics*, vol. 31, pp. 944–956, 1959.

[57] KEE, R. J., GRCAR, J. F., SMOOKE, M. D., and MILLER, J. A., "A fortran program for modeling steady a fortran program for modeling steady laminar one-dimensional premixed flames," *Sandia National Laboratories Report No. SAND85-8240*, 1985.

[58] KEE, R. J., RUPLEY, F. M., MILLER, J. A., COLTRIN, M. E., GRCAR, J. F., MEEKS, E., MOFFAT, H. K., LUTZ, A. E., DIXON-LEWIS, G., SMOOKE, M. D., WARZATZ, J., EVANS, G. H., LARSON, R. S., MITCHELL, R. E., PETZOLD, L. R., REYNOLDS, W. C., CARACOTSIOS, M., STEWART, W. E., GLARBORG, P., WANG, C., MCLELLAN, C. L., ADIGUN, O., HOUF, W. G., CHOU, C. P., MILLER, S. F., HO, P., YOUNG, P. D., YOUNG, D. J., HODGSON, D. W., PETROVA, M. V., and PUDUPPAKKAM, K. V., *CHEMKIN Release 4.1*. Reaction Design, San Diego, CA, 2006.

[59] KIM, J., CHOI, W., NEUMEIER, Y., and JAGODA, J., "Combustion instabilities in plasma driven flame holders for afterburners," AIAA-2009-1175, (Orlando, Florida), 47th AIAA Aerospace Sciences Meeting including The New Horizons Forum and Aerospace Exposition, Jan. 5-8 2009.

[60] KIM, W., DO, H., MUNGAL, M., and CAPPELLI, M., "Flame stabilization enhancement and nox production using ultra short repetitively pulsed plasma discharges," AIAA-2006-560, (Reno, Nevada), 44th AIAA Aerospace Sciences Meeting and Exhibit, Jan. 9-12 2006.

[61] KISTIAKOWSKY, G. B. and RICHARDS, L. W., "Emission of vacuum ultraviolet radiation from the acetylene-oxygen and the methane-oxygen reactions in shock waves," *Journal of Chemical Physics*, vol. 36, pp. 1707–1714, 1962.

[62] KLIMOV, A., BYTURIN, V., BROVKIN, V., VINOGRADOV, V., and WIE, D. M. V., "Plasma assisted combustion," AIAA-2001-491, (Reno, NV), 39th Aerospace Sciences Meeting and Exhibit, 39th Aerospace Sciences Meeting and Exhibit, Jan. 8-11 2001.

[63] KONO, M., KUMAGAI, S., and SAKAI, T., "The optimum condition for ignition of. gases by composite sparks," *Sixteenth Symposium (International) on Combustion*, pp. 757–766, 1976.

[64] KUMAR, R. K., "A method of estimating pressure loss across flame holders in high velocity streams," *Combustion Science and Technology*, vol. 21, pp. 199–203, 1980.

[65] LANGMUIR, I. and MOTT-SMITH, JR., H. M. *General Electrical Review*, vol. 27, pp. 449, 538, 616, 762, 810, 1924.

[66] LAW, C. K., *Combustion Physics*. New York: Cambridge University Press, 2006.

[67] LAWTON, J. and WEINBERG, F. J., *Electrical Aspects of Combustion*. Oxford: Clarendon Press, 1969.

[68] LEO, M. D., SAVELIEV, A., KENNEDY, L. A., and ZELEPOUGA, S. A., "OH and CH luminescence in opposed flow methane oxy-flames," *Combustion and Flame*, vol. 149, pp. 435–447, June 2007.

[69] LEONOV, S., YARANTSEV, D., NAPARTOVICH, A., and KOCHETOV, I., "Plasma-assisted ignition and flameholding in high-speed flow," AIAA-2006-563, (Reno, Nevada), 44th AIAA Aerospace Sciences Meeting and Exhibit, 44th AIAA Aerospace Sciences Meeting and Exhibit, Jan. 9-12 2006.

[70] LEWIS, B. and VON ELBE, G., *Combustion, Flames and Explosions of Gases*. Academic Press, 3rd ed., 1987.

[71] LIEPMANN, D. and GHARIB, M., "The role of streamwise vorticity in the near-field entrainment of round jets," *Journal of Fluid Mechanics*, vol. 245, pp. 643–668, 1992.

[72] LIFSHITZ, A., SCHELLER, K., BURCAT, A., and SKINNER, G. B., "Shock-tube investigation of ignition in methane-oxygen-argon mixtures," *Combustion and Flame*, vol. 16, pp. 311–321, 1971.

[73] LIU, J., WANG, F., LEE, L., THEISS, N., RONNEY, P., , and GUNDERSEN, M., "Effect of discharge energy and cavity geometry on flame ignition by transient plasma," AIAA-2004-1011, (Reno, Nevada), 42nd AIAA Aerospace Sciences Meeting and Exhibit, Jan. 5-8 2004.

[74] LIU, J., WANG, F., LEE, L., THEISS, N., RONNEY, P., and GUNDERSEN, M., "Effect of fuel type on flame ignition by transient plasma discharges," AIAA-2004-837, (Reno, Nevada), 42nd AIAA Aerospace Sciences Meeting and Exhibit, Jan. 5-8 2004.

[75] LOEB, L. B., *Fundamental processes of electrical discharge in gases*. NY: Wiley, 1939.

[76] LONGWELL, J. P., FROST, E. E., and WEISS, M. A., "Flame stability in bluff body recirculation zones," *Industrial and engineering chemistry*, vol. 45, pp. 1629–1633, 1953.

[77] LONGWELL, J., CHENEVEY, J., CLARK, W., and FROST, E., "Flame stabilization by baffles in a high velocity gas stream," *Third Symposium on Combustion and Flame and Explosion Phenomena*, vol. 3, pp. 40–44, 1949.

[78] LUTZ, A. E. and KEE, R. J., "A fortran program for computing opposed-flow diffusion flames," *Sandia National Laboratories Report No. SAND96-8243*, 1996.

[79] MALY, R. and VOGEL, M., "Initation and propagation of flame fronts in lean ch4-air mixtures by the three modes of the ignition spark," *Seventeenth Symposium (Internaional) on Combustion*, p. 821, 1978.

[80] MARBLE, F. and ADAMSON JR., T., "Ignition and combustion in a laminar mixing region," *Jet Propulsion*, vol. 24, p. 85, 1954.

[81] MARGASON, R. J., "Fifty years of jet in cross flow research," *AGARD-CP*, vol. 534, 1993.

[82] MARSHALL, R. L., CANUEL, G. E., and SULLIVAN, D. J., *Augmentation systems for turbofan engines*, vol. 10 of *Cranfield international symposium series*. OXFORD: PERGAMON PRESS, LTD., 1968.

[83] MCWILLIAM, I. G. and DEWAR, R. A., "Flame ionization detector for gas chromatography," *Nature*, vol. 181, p. 760, 1958.

[84] MINTOUSSOV, E., NIKIPELOV, A., STARIKOVSKAIA, S., and STARIKOVSKII, A., "Rapid combsution achievement by nanosecond barrier discharge," (Reno, Nevada), 44th AIAA Aerospace Meeting and Exhibit, 9-12 January 2006.

[85] MINTOUSSOV, E., PANCHESHNYI, S., and STARIKOVSKII, A., "Propane-air flame control by non-equilibrium low-temperature pulsed nanosecond barrier discharge," AIAA-2004-1013, (Reno, Nevada), 42nd AIAA Aerospace Sciences Meeting and Exhibit, Jan. 5-8 2004.

[86] MIYAMA, H. and TAKEYAMA, T., "Mechanism of methane oxidation in shock waves," *Journal of Chemical Physics*, vol. 40, pp. 2049–2050, 1964.

[87] MOHR, P. J., TAYLOR, B. N., and NEWELL, D. B., "Codata recommended values of the fundamental physical constants: 2006," (Gaithersburg, ML, USA), NIST, December 28, 2007.

[88] ORRIN, J., VINCE, I., and WEINBERG, F., "Ignition by radiation from plasmas," *Combustion and Flame*, vol. 37, pp. 91–93, 1980.

[89] PASCHEN, F. *Wied. Ann. 37, 69*.

[90] PETER, N., *Turbulent combustion*. Cambridge University Press, 2000.

[91] POPE, S. B., *Turblent Flows*. Cambridge, UK: Cambridge University Press, 2000.

[92] PORTER, R. P., CLARK, A. H., KASKAN, W. E., and BROWNE, W. E. *Proceedings of the Combustion Institute*, vol. 11, pp. 907–917, 1966.

[93] POTTER, JR, A. E. and WONG, E. L., "Effect of pressure and duct geometry on bluff-body flame stabilization," *NACA TN 4381*, 1958.

[94] RAJU, G., *Gaseous electronics : theory and practice*. Boca Raton, FL: Taylor and Francis, 2006.

[95] REFAEL, S. and SHER, E., "A theoritical study of the ignition of a reactive medium by means of an electrical discharge," *Combustion and Flame*, vol. 59, pp. 17–30, 1985.

[96] REHAB, H., VILLERMAUX, E., and HOPFINGER, E. J., "Flow regimes of large-velocity-ratio coaxial jets," *Journal of Fluid Mechanic*, vol. 345, pp. 357–381, 1997.

[97] RICOU, F. P. and SPALDING, D. B., "Measurements of entrainment by axisymmetrical turbulent jets," *Journal of Fluid Mechanics*, vol. 11, pp. 21–32, 1961.

[98] SEERY, D. J. and BOWMAN, C. T., "An experimental and analytical study of methane oxidation behind shock waves," *Combustion and Flame*, vol. 14, pp. 37–47, 1970.

[99] SHER, E. and KECK, J., "Spark ignition of combustible gas mixtures," *Combustion and Flame*, vol. 66, pp. 17–25, 1986.

[100] SKINNER, G. B. and RUEHRWEIN, R. A., "Shock tube studies on the pyrolysis and oxidation of methane," *Journal of Physical Chemistry*, vol. 63, pp. 1736–1742, 1959.

[101] SMITH, G. P., GOLDEN, D. M., FRENKLACH, M., MORIARTY, N. W., EITENEER, B., GOLDENBERG, M., BOWMAN, C. T., HANSON, R. K., SONG, S., GARDINER, JR., W. C., LISSIANSKI, V. V., and QIN, Z., *GRI-Mech 3.0*.

[102] SMITH, G. P., LUQUE, J., PARK, C., JEFFRIES, J. B., and CROSLEY, D. R., "Low pressure flame determinations of rate constants for oh(a) and ch(a) chemiluminescence," *Combustion and Flame*, vol. 131, pp. 59–69, 2002.

[103] SMITH, S. H. and MUNGAL, M. G., "Mixing, structure and scaling of the jet in crossflow," *Journal of Fluid Mechanics*, vol. 357, pp. 83–122, 1998.

[104] SOLOUKHIN, R., "Quasi-stationary reaction zone in gaseous detonation," *Eleventh Symposium (International) on Combustion*, pp. 671–676, 1967.

[105] SPADACCINI, L. and III, M. C., "Ignition delay characteristics of methane fuels," *Progress in Energy and Combustion Science*, vol. 20, pp. 431–460, 1994.

[106] SPALDING, D. B., *Some fundamentals of combustion*. New York, Academic Press, 1955.

[107] SPALDING, D. B., "Development of the eddy-break-up model of turbulent combustion," *Sixteenth Symposium (International) on Combustion*, pp. 1657–1663, 1977.

[108] SWETT, JR., C., "Spark ignition of flowing gases," *NACA Report 1287*, 1956.

[109] TAKITA, K., "Ignition and flame-holding by oxygen, nitrogen and argon plasma troches in supersonic airflow," *Combustion and Flame*, vol. 128, pp. 301–313, 2002.

[110] TAKITA, K., MORIWAKI, A., KITAGAWA, T., and MASUYA, G., "Ignition and flame-holding of h2 and ch4 in high temperature airflow by a plasma torch," *Combustion and Flame*, vol. 132, pp. 679–689, 2003.

[111] TAMURA, M., BERG, P. A., HARRINGTON, J. E., LUQUE, J., JEFFRIES, J. B., SMITH, G. P., and CROSLEY, D. R., "Collisional quenching of ch(a), oh(a), and no(a) in low pressure hydrocarbon flames," *Combustion and Flame*, vol. 114, pp. 502–514, 1998.

[112] TERAO, K., "Selbstzündung von kohlenwasserstoff-luftgemischen in stosswellen," *Journal of the physical Society of Japan*, vol. 15, pp. 2086–2092, 1960.

[113] TESAŘ, V., "Similarity solutions of jet development mixing layers using algebraic and 1−equation turbulence models," *Acta Ploytechnica*, vol. 46, pp. 40–56.

[114] THIELE, M., WARNATZ, J., and MAAS, U., "Geometrical study of spark ignition in two dimension," *Combustion Theory and Modeling*, vol. 4, pp. 413–434, 2000.

[115] THOMSON (LORD KELVIN), W., "Hydrokinetic solutions and observations," *Philosophical Magazine*, vol. 42, pp. 362–377, 1871.

[116] THRING, M. and NEWBY, M., "Combustion length of enclosed turbulent jet flames," *Fourth Symposium (International) on Combustion*, pp. 789–796, 1953.

[117] TOPHAM, D., CLEMENTS, R., and SMY, P., "Turbulent mixing in a pulsed plasma-jet exhaust," *Journal of Fluid Mechanics*, vol. 148, pp. 207–224, 1984.

[118] TOWNSEND, J. S., *Electricity in gases*. Oxford University Press, 1915.

[119] TSUBOI, T. and WAGNER, H., "Homogeneous thermal oxidation of methane in reflected shock waves," *Fifteenth Symposium (International) on Combustion*, pp. 883–890, 1975.

[120] VAN TIGGELEN, A., *Ionization in High Temperature Gases*. New York-London: Academic Press, 1963.

[121] VEYNANTE, D. and VERVISCH, L., "Turbulent combustion modeling," *Progress in Energy and Combustion Science*, vol. 28, pp. 193–266, 2002.

[122] VILLERMAUX, E. and REHAB, H., "Mixing in coaxial jets," *Journal of Fluid Mechanics*, vol. 425, pp. 161–185, 2000.

[123] VILLERMAUX, E., REHAB, H., and HOPFINGER, E. J., "Breakup regimes and self-sustained pulsations in coaxial jets," *Meccanica*, vol. 29, pp. 393–401, 1994.

[124] VINCE, I. and WEINBERG, F., "Hydrogen atom distribution in pulsed plasma jet igniters," *Combustion and Flame*, vol. 67, pp. 259–264, 1987.

[125] WALKER, D. W., DIEHL, L. H., STRAUSS, W. A., and LOSE, R., "Investigation of the ignition properties of flowing combustible gas mixtures," *USAF Report A FA PL- TR-69-82*, 1969.

[126] WEINBERG, F., HOM, K., OPPENHEIM, A., and TEICHMAN, K., "Ignition by plasma jet," *Nature*, vol. 272, pp. 341–343, 1978.

[127] WEINBERG, F. and WARRIS, A., "Ignition and flame stabilization by plasma. jets in fast gas streams," *Twentieth Symposium (International) on Combustion*, pp. 1825–1831, 1984.

[128] WHITE, D. R. *Contract AF 33(615)-5772 Rep. S-70-1054 OARS WPAFB Ohio*.

[129] WILLAMS, F. A., *Combustion Theory*. Combustion Science and Engineering Series, Menlo Park, CA: The Benjamin/Cummings, second edition ed., 1985.

[130] WILLIAMS, G., HOTTEL, H., and SCURLOCK, A., "Flame stabilization and propagation in high velocity gas streams," *Third Symposium on Combustion and Flame and Explosion Phenomena*, pp. 21–40, 1949.

[131] WRIGHT, F., "Bluff-body flame stabilization: Blockage effects," *Combustion and Flame*, vol. 3, pp. 319–337, 1959.

[132] YAMAGUCHI, S., OHIWA, N., and HASEGAWA, T., "Structure and blow-off mechanism of rod-stabilized premixed structure and blow-off mechanism of rod-stabilized premixed flame," *Combustion and Flame*, vol. 62, pp. 31–41, 1985.

[133] YANG, J.-T., YEN, C.-W., and TSAI, G.-L., "Flame stabilization in the wake flow behind a slit v-gutter," *Combustion and Flame*, vol. 99, pp. 288–294, 1994.

[134] YEUNG, P. K., GIRIMAJI, S. S., and POPE, S. B., "Straining and scalar dissipation on material surfaces in turbulence: Implications for flamelets," *Combustion and Flame*, vol. 79, pp. 340–365, 1990.

[135] ZHANG, J., CLEMENTS, R., and SMY, P., "An experimental investigateion of the effect of a plasma jet on a freely expanding methane-air flame," *Combustion and Flame*, vol. 50, pp. 99–106, 1983.

[136] ZUKOSKI, E. E., *Flame Stabilization on Bluff Bodies at Low and Intermediate Reynolds Numbers*. PhD thesis, California Institute of Technology, 1954.

[137] ZUKOSKI, E. E. and MARBLE, F. E., *Combustion Research and Review*. 1955.

[138] ZUKOSKI, E., *Aerothermodyanamics of Aircraft Engine Componests*, ch. 2, pp. 59–84. AIAA Education series, New York, NY: AIAA, 1985.

[139] ZUKOSKI, E. and MARBLE, F., "Experiments concerning the mechanism of flame blow off from bluff bodies," *Proc. Gas-Dynamics Symposium on Aerothermochemistry*, pp. 205–210, 1956.

VITA

Woong-Sik Choi was born in Anyang, Korea on January 7, 1974, the son of Youngjae Choi and Bok-im Cho. He received his Bachelor Degree in Mechanical Engineering from Kyung Hee University (Suwon, Korea) in 2000 and his Master of Science Degree in Aerospace Engineering from Georgia Institute of Technology (Atlanta, GA) in 2002. He is married to Chowoon Lee.